Doctoral Dissertation

Investigation on high-temperature growth of single-walled carbon nanotubes from solid carbon nanoparticle seeds

Mengyue Wang

Department of Applied Physics

Graduate School of Engineering

Osaka University

December 2022

Supervisor: Prof. Yoshihiro Kobayashi

Abstract

Carbon nanotubes (CNTs), a kind of one-dimensional carbon material benefiting from their extraordinary properties, have been applied in several areas, including sensors, field-effect transistors (FETs), and batteries. Related to the application in the electronic industry, CNTs with high crystallinity have attracted more attention for decades because of their excellent electrical transportation, especially for single-walled carbon nanotubes (SWCNTs). The defects formed on SWCNTs will likely reduce the crystallinity and extinguish the mechanical and electrical characteristics of SWCNTs. These years, high temperature treatment has been proven to be one of efficient methods for defect healing in both CNT growth process and post-treatment process. However, high temperature growth produced SWCNTs with a lower yield than those grown at the lower temperature. Besides, another problem needed to be solved is the formation of impurity, amorphous carbon (a-C), which covers the surface of growth seeds and prevents the growth of CNTs. Moreover, in the post-treatment process, high temperature annealing exhibited a limitation in the efficiency of defect healing on SWCNTs.

In this dissertation, aimed on the yield increase of highly crystalline SWCNTs, I divided the research into two areas: high temperature CNT growth process and post-treatment process. In the CNT synthesis, nanodiamonds (NDs), structured by sp^3 carbon bound, are used as the growth seeds because of their high thermal suitability and containing no metal impurity. Based on study of growth driving force, I developed the high temperature growth process to a cap formation engineered two-step growth process. Further, to prevent a-C deposition during the growth process, I systematically analyzed the effects of growth enhancers, which were introduced into the carbon solid seeds-based SWCNTs growth system. Moreover, in the thermal post-treatment process, we experimentally investigated the effect of carbon-containing reactants (C_2H_2).

To increase the growth yield of CNTs synthesized at high temperature, a two-stage growth process was built. The growth process was divided into initial and secondary growth steps and the growth temperature was adjusted in different growth steps. In this work, the two-step growth process was further developed. Combining with the study of the growth driving force, I illustrated the influence of partial pressure of carbon feedstock and growth temperature on the efficient initial growth of SWCNTs. It has been found that the yield of cap structure was increased at low growth temperature and high partial pressure of carbon source, which provided a high growth driving force for CNT nucleation. After achieving a higher density of the cap structures, stationary elongation of SWCNTs was conducted by a secondary growth step. Compared to the classical high temperature growth process, the cap formation engineered two-step growth process efficiently increased the yield of SWCNTs with high crystallinity. Through the two-step growth process, however, we still cannot avoid the formation of a-C. Therefore, I introduced growth enhancers in the two-step growth process and analyzed their effects.

In the metal catalyst-based CNTs growth process, growth enhancers have been added to etch the a-C formed with the promotion of metal catalysts. Thus, in this ND-based SWCNTs growth process, I injected the growth enhancers (H_2O and CO_2) and investigated their enhancing roles when different carbon sources (C_2H_2 and C_2H_4) were supplied. Using H_2O as the growth enhancer, we found that the a-C deposition is efficiently limited when a low partial pressure of C_2H_2 was injected. However, in a high partial pressure C_2H_4-supplied growth, H_2O with high concentration damaged SWCNTs structure because of its strong oxidizing ability. In addition to H_2O, CO_2 exhibited a better a-C formation-preventing role in C_2H_4-supplied growth. Notability, in the C_2H_2-supplied growth, rather than removing a-C in the other combinations, CO_2 injection dramatically increased a-C deposition while the yield of SWCNTs was also increased. This phenomenon indicated the dehydration reaction between CO_2 and C_2H_2, which could be referred from the previous research about the pyrolysis reaction happening at high temperature. The present findings lead to a promoted growth of high-quality SWCNTs from non-metallic growth seeds with growth enhancers injection.

When discussing about the application, however, we found that the publication of SWCNTs directly grown through high-temperature process is still not enough in some cases. Thus, in the next research, I studied the post-treatment method for the defect healing of the massive SWCNTs grown at low temperature. Recently, among the thermal treatment processes for high crystallinity SWCNTs formation, the injected carbon-containing reactants exhibited a positive tendency in defect healing. Thus, combining with previous theoretical research, we experimentally confirmed the healing behavior of carbon-containing reactant (C_2H_2) in the high temperature (1100 ^oC) annealing process. Compared with the SWCNTs healed only in Ar gas, the SWCNTs healed with C_2H_2 presented higher crystallinity. Further, we found that the healing effect of C_2H_2 injection was more evident in the thin SWCNTs (<1.1 nm).

In the non-metallic growth seed-based SWCNT synthesis, we increased the yield of high quality SWCNTs by building a cap formation engineered two-step growth process with the participation of growth enhancers. The healing role of carbon-containing reactant (C_2H_2) in the post-treatment process was also experimentally revealed.

Based on such studies, in the future, I would like to study the nucleation behavior of SWCNTs on the surface of solid carbon growth seeds and modify the growth condition to achieve SWCNTs with high chirality purity. I also would like to apply this high temperature growth system into the formation of horizontally well-aligned SWCNTs arrays and study the related properties. In the thermal annealing post-treatment with the injection of carbon-containing reactants, finding method to prevent the formation of a-C would be the next step to be finish.

Table of Contents

Chapter 1: Introduction

1.1 Structure of carbon nanotubes

1.1.1 Single-walled carbon nanotubes and multi-walled carbon nanotubes

Nanostructured carbon materials, including fullerenes [1, 2], graphene [3], and carbon nanotubes (CNTs) [4, 5] et al., have attracted broad interest for several decades because of their unique properties. As a one-dimensional material, CNTs are structured by the rolled-up sheets of graphene, which are consisted of sp^2 carbon atoms. According to the layers of the sidewall, CNTs could be divided into single-walled carbon nanotubes (SWCNTs) [4] and multi-walled carbon nanotubes (MWCNTs) [5] with diameters ranging from 0.8 to 2 nm (Figure 1.1 (a)) and 5 to 20 nm (Figure 1.1 (b)), respectively. Recently, single-walled carbon nanotubes (SWCNTs) are going to be attractive recently due to their excellent electrical transportation [6], mechanical strength [7, 8], and thermal transportation [9, 10], which brings applications in the area of sensor [11, 12], batteries [13], and capacitors [14, 15]. These properties have been proven to relate to the structure of SWCNTs.

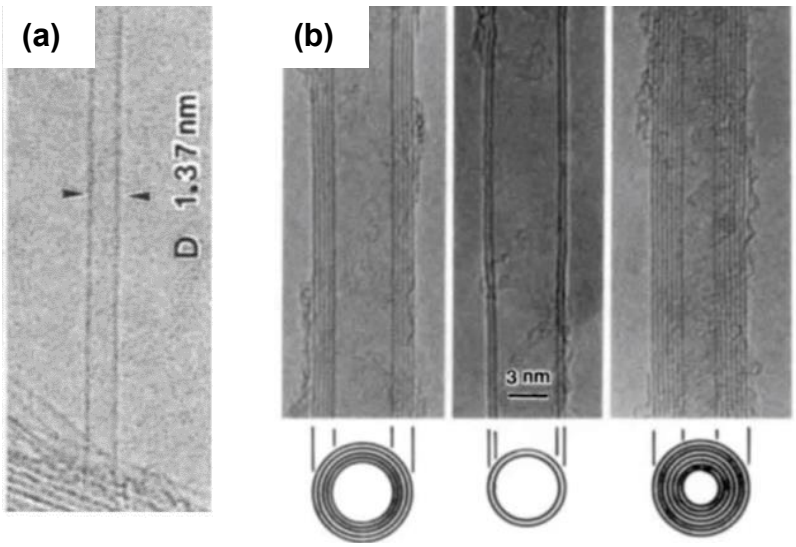

Figure 1.1 TEM images of the (a) SWCNTs [4] and (b) MWCNTs [5].

1.1.2 Chirality and crystallinity of SWCNTs

When mentioning the structure of SWCNTs, many parameters should be considered, including the diameter, length, purity, and so on. One of the important structure factors is chirality (helicity). As Figure 1.2 (a) [16, 17] shows, a vector called as

the chiral vector, connects the centers of the two hexagons. In determining the atomic structure of a single-walled carbon nanotube, the chiral vector C can be written as

$$C = na_1 + ma_2$$

where a_1 and a_2 are the unit cell base vectors of the graphene sheet. The pair of integers (n, m) is called the chiral index or just chirality, and $n \geq m$ [18]. According to the chirality, CNTs could be divided into three types—armchair (n=m), zig–zag (n=0 or m=0), and chiral structure (any other n and m). Generally, the armchair structure has electrical properties similar to a conductor, whereas the zig–zag structure has semiconductor-like properties. In the case of the chiral structure, it has the characteristics of a semiconductor or metallic by the chiral index. Here, a general rule is supported to distinguish the electronic properties of SWCNTs. If $(n-m)$ is a multiple of 3, the SWCNTs show metallic properties. Otherwise, the SWCNTs present a behavior of semiconducting [19, 20].

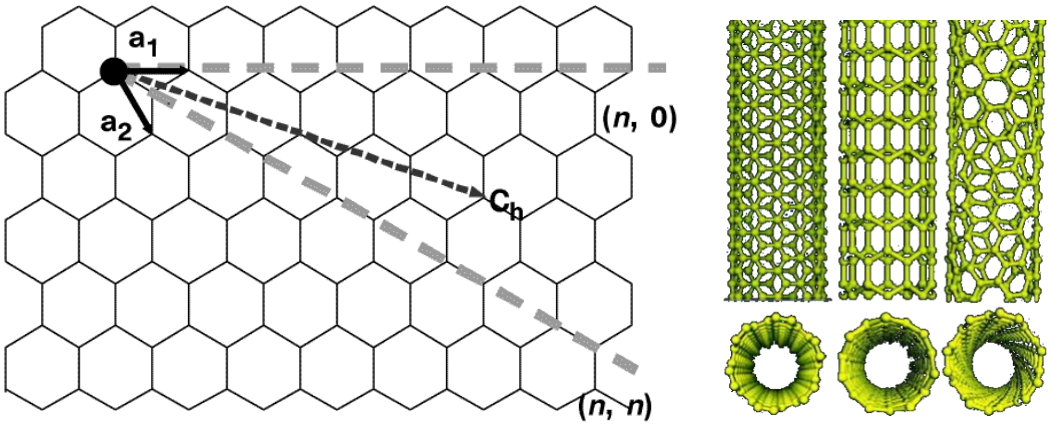

Figure 1.2 (a) Schematic of a carbon nanotube in a two-dimensional graphene sheet with lattice vectors a1 and a2, and the roll-up vector. [16] (b) armchair, zig–zag, and chiral structure of SWCNTs [17].

Another important factor that affected the properties of SWCNTs is crystallinity. Perfect SWCNTs own a well-defined lattice that is structured by six-membered rings. However, with the practical process of synthesis and chemical post-treatment, defects usually form in the SWCNTs structure. The appearance of defects, as shown in Figure 1.3 [21], including pentagonal, heptagonal defects, and pentagon-heptagon (5|7) pairs [21, 22] or even line defects [23], significantly changed the properties of SWCNTs.

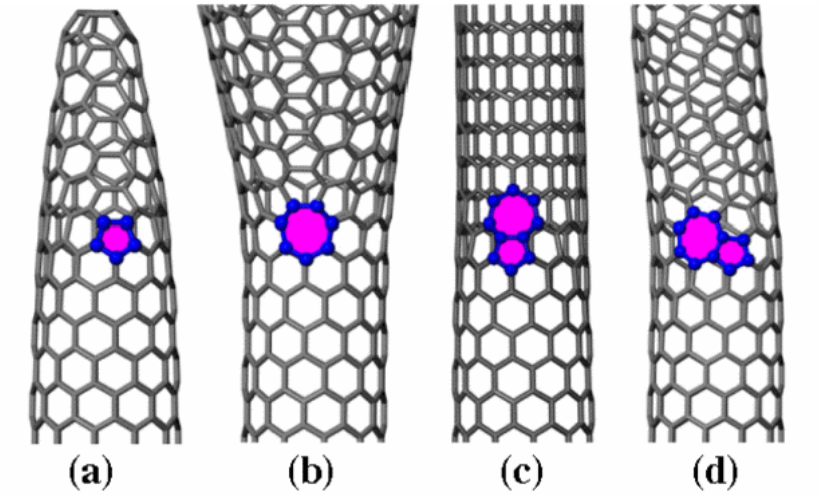

Figure 1.3 A SWCNT with (a) an isolated pentagon defect, (b) a heptagon defect and (c, d) a 5|7 pair defect [21].

With the formation of defects, the number of anchor points in SWCNTs increases, which enhances the charge injection, chemical functionalization and benefits the relevant applications [24, 25]. On the other hand, SWCNTs' electronic and transport properties drastically decreased by the appearance of such non-hexagonal rings. A variety of theoretical and experimental studies proved the SWCNTs' remarkable mechanical properties, including high Young's modulus values (~1 TPa) [7, 8] and high tensile strength (~100 GPa) [26]. However, it has been concluded that single defects can bring a 0~25 % reduction in tensile strength [27]. When the number of defects increases to three, the tensile strength of SWCNTs will appear to have a 50 % reduction [27]. Similarly, the experimentally synthesized SWCNTs usually presented lower transportation properties compared with the theoretically calculated electrical (10^9 A/cm^2) [6] and thermal (3500 W/m K) transportation values [9, 10]. Moreover, defects can be the edge dislocation core in SWCNTs, which change the chirality of the tube [28, 29].

Until now, we still need efforts to control the crystallinity and chirality of SWCNTs during the synthesis and post-treatment process.

1.1.3 Structure characterization of SWCNTs

As aforementioned, the structure of SWCNTs is highly related to the properties, which further affects the applications. Therefore, details of the SWCNT structure should be precisely evaluated.

Scanning electron microscopy (SEM) is a convenient and recommended tool to directly observe the morphology of CNTs on a large-scale (Figure 1.4) [18, 30]. In SEM characterization, CNT sample is irradiated by an accelerated electron beam and signals are emitted from the sample through electron-sample interaction, including the secondary electrons (SE), backscattered electrons (BSE), and diffracted backscattered electrons (EBSD). Among these signals, SE and BSE are mainly used to image samples, which are more efficient in reflecting the morphology and composition of samples respectively.

However, the usage of SEM is limited by the resolution ratio. Thus, it is difficult to confirm the atomic structure in CNTs. As shown in Figure 1.5, compared with SEM, transmission electronic microscopy (TEM) is preferred to characterize the details of CNTs, especially for the length, diameters, purity, and chirality of SWCNTs [31-33]. High resolution TEM (HR-TEM) can measure atomic structure of CNTs directly and even see the structure of defects [34]. Recently, in-situ TEM was used as an effective approach to characterize the real time growth behavior of CNTs, which supports the study of CNT growth mechanism [35]. However, TEM measurement exhibits a difficulty in quantitative analysis.

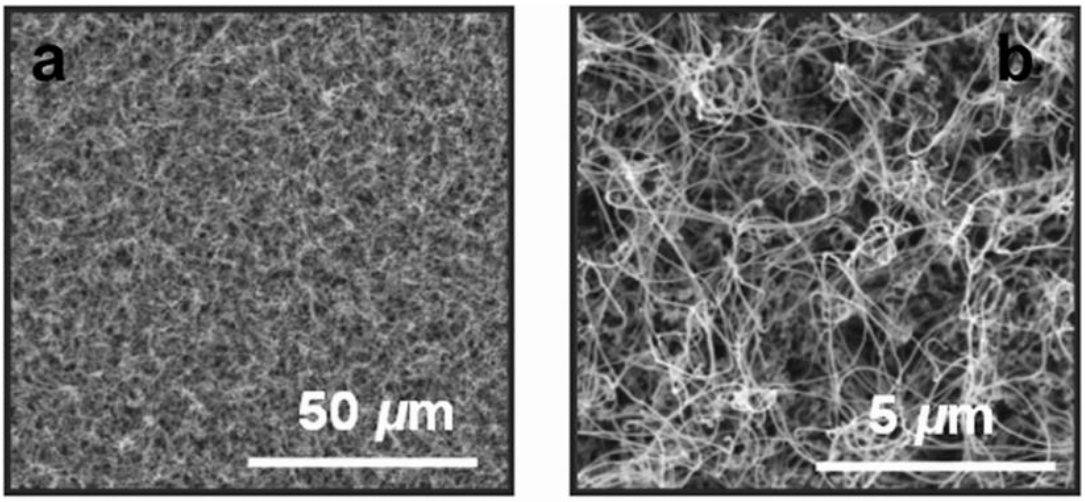

Figure 1.4 SEM images of CNTs with low magnification (a) and high magnification (b) [30].

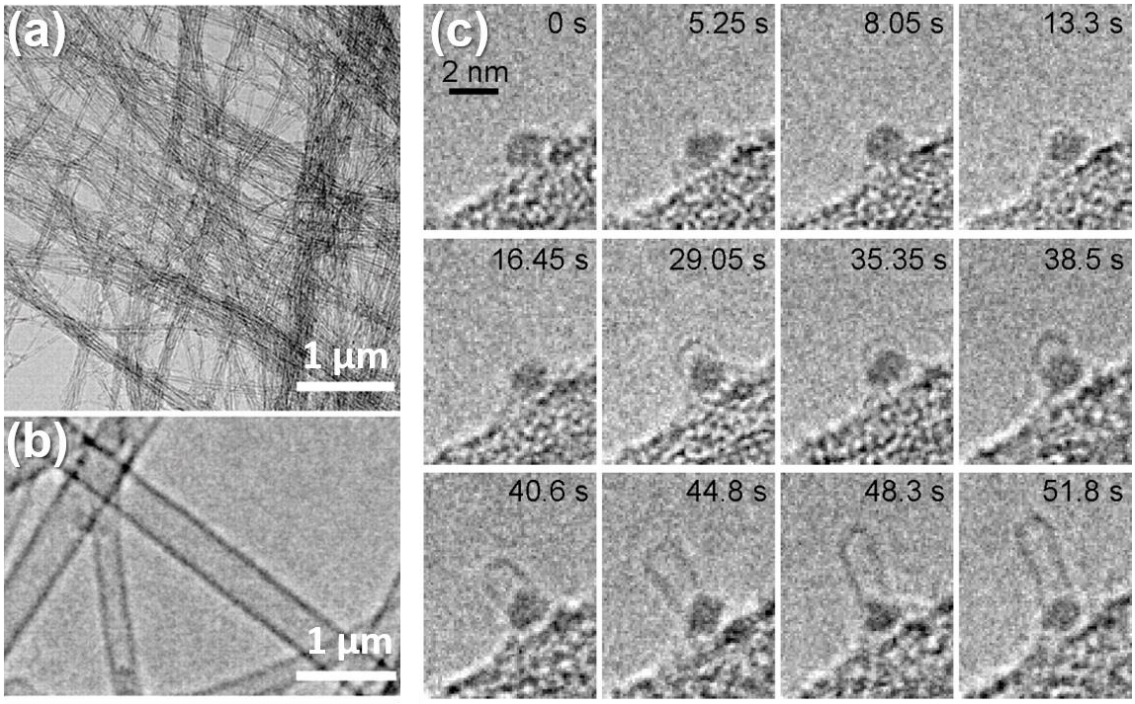

Figure 1.5 TEM images of SWCNTs with low magnification (a) and high magnification (b) [33], (c) in situ TEM images of a SWNT growth in nucleation and elongation process from a nanoparticle catalyst on a substrate [35].

Another method used to mainly measure the morphology of CNTs is the atomic force microscopy (AFM). Through recording the relative height of the probe, a three-dimensional shape (topography) of CNTs is exhibited in an image (Figure 1.6) [36].

Moreover, because of the high resolution, AFM is also widely applied to revel the surface of CNTs which are modified with dispersants.

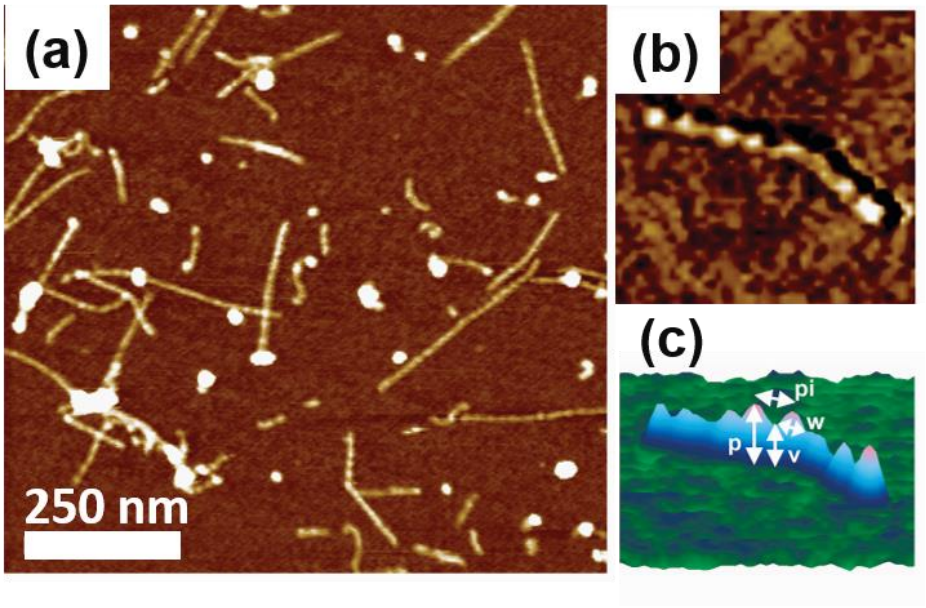

Figure 1.6 AFM height image (a) and phase image (b) of CNTs wrapped with single-stranded DNA, (c) a three-dimensional representation of the height of modified CNTs [36].

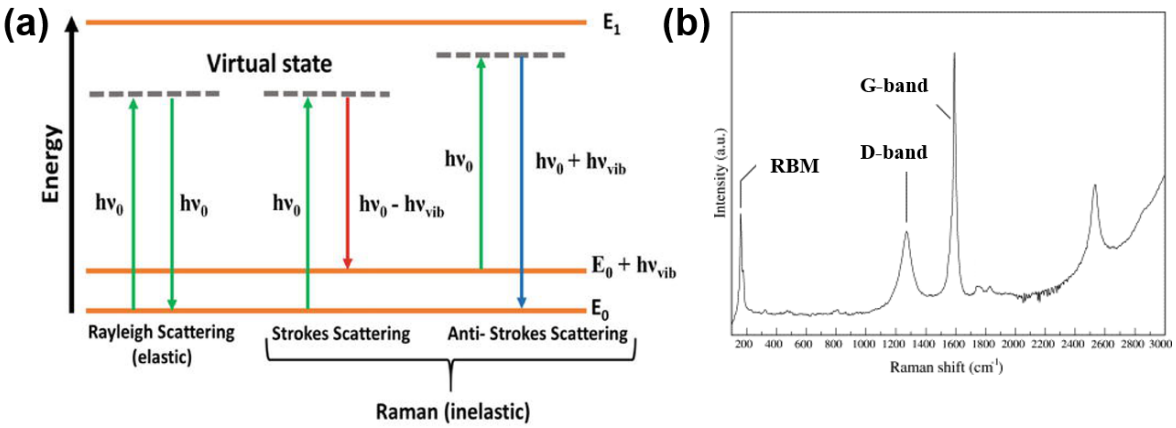

Figure 1.7 (a) Energy level diagram for Rayleigh and Raman scattering, where radiation having an energy hv_0 incident on a molecule and hv_{vib} represents a difference in the vibrational or rotational energy levels of that molecule [37] (b) Raman spectrum showing the most characteristic features of CNTs: radial breathing mode (RBM), the D-band, and G-band [38].

Besides SEM, TEM, and AFM measurement, Raman spectroscopy is another widely used tool to detect the details of CNT structure on a large-scale. The detection result could be achieved rapidly by providing a few samples. Raman spectroscopy is a

light scattering technique. As Figure 1.7 (a) shows [37], when high-intensity incident light from a laser source is scattered by molecules, most of the scattered light has the same wavelength as the incident laser, and this scattering is called Rayleigh scattering. Noticeably, there is a very small fraction of the scattered light, called Stokes and Anti-Stokes scattering, which has a wavelength different from the incident light. Such fraction is called Raman scattering, and the change in wavelength reflects the chemical structure of the test sample. In addition, when the wavelength of the incident light is close to the wavelength needed for an electronic transition of the specific compound, the resonance effect appears and the intensity of the scattering peak from such compound could be increased by several times.

The representative Raman active peaks in SWCNTs are the radial breathing modes (RBM), D-band and G-band, which are shown in Figure 1.7 (b) [38]. The G-band at ~1590 cm^{-1} represents the graphite (sp^2 carbon) structure and the D-band at 1330~1360 cm^{-1} reflects all carbon allotropes (amorphous sp^2 and sp^3 carbon), including defect structure. The RBM frequency at 100~300 cm^{-1} (ω_{RBM}) is proved to be inversely proportional to the diameter of tube (d_t) according to the equation [39]:

$$\omega_{RBM}\ (cm^{-1}) = 223.5\ /d_t\ (nm) + 12.5$$

This relationship between the RBM frequency and tube diameter is reliable for SWCNTs with diameter small than 2 nm.

The resonance energy of SWCNTs is determined by their chirality, and the chirality of the resonance varies depending on the laser wavelength used. The chirality distribution of CNTs can be analyzed in detail by comparing the Raman spectra measured at several laser wavelengths with the Kataura plot (Figure 1.8), which plots the energy between van Hobe singularities for each chirality and diameter [40]. The round and square dots in Figure 1.8 represent the chirality of semiconducting and metallic CNTs, respectively. The chirality connected by a line is called a family and indicates that $2n+m$ calculated from the chiral exponents (n, m) are equal.

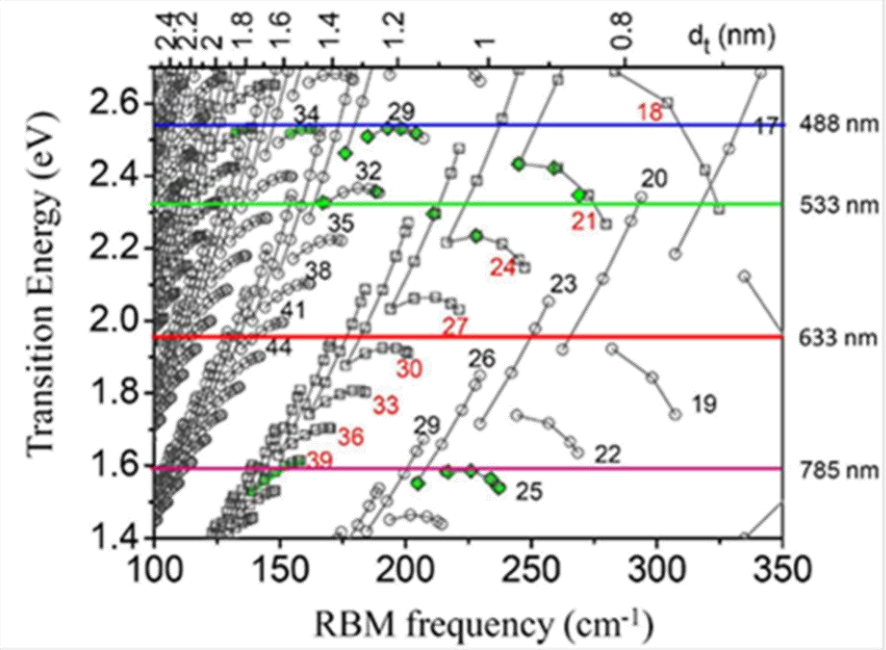

Figure 1.8 The figure of Kataura plot, which exhibits the information of chirality and diameter of CNTs [40].

The Raman scattering intensity becomes weaker as the resonance energy and excitation energy move away from each other. Specifically, when CNTs form a bundle, the resonance energy decreases, and the amount of change is about 0.05-0.15 eV, depending on the chirality.

Through above characterization methods, the structure and morphology of SWCNTs could be clearly detected.

1.2 Synthesis of SWCNTs and the relevant growth mechanism

1.2.1 Chemical vapor deposition

Until now, several methods have been developed to synthesize SWCNTs, including arc discharge [41], laser ablation [42], and chemical vapor deposition (CVD) [43]. Among these methods. CVD is one of the most investigated and widely used techniques, which requires simpler equipment and milder conditions in terms of temperature and pressure [44]. Based on such advantages, CVD synthesis tends to be more suitable for the large-scale production of CNTs. As shown in Figure 1.9, in CVD synthesis, carbon-containing reactants, such as carbon monoxide (CO) [45], methane

(CH_4) [46-48], ethylene (C_2H_4) [49-51], acetylene (C_2H_2) [52, 53], and ethanol (C_2H_5OH) [54, 55], are used as the carbon source. Metal or non-metallic nanoparticles are usually employed as catalysts or growth seeds, and carbon feedstocks could adsorb on their surface and form CNTs. Through controlling the temperature and pressure in the tubular reactor, the injected carbon source processes decomposition reactions and reconstructs to CNTs on the surface of catalysts or growth seeds, which are deposited on kinds of substrates.

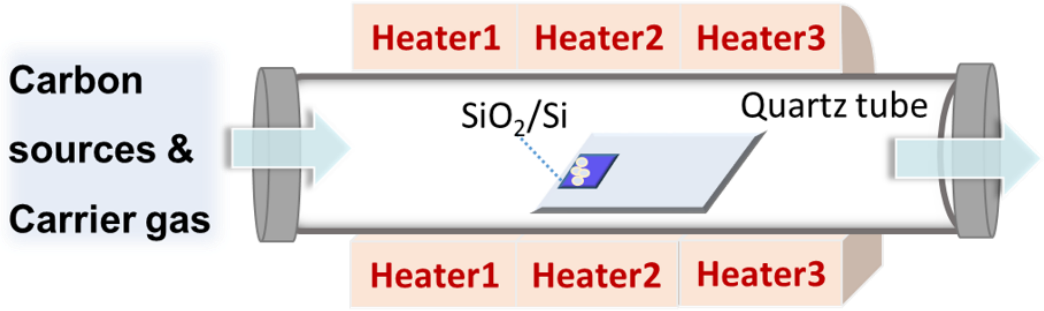

Figure 1.9 Schematic diagram of CNT growth through CVD method happened in a tubular reactor.

1.2.2 Metal catalyst-based SWCNTs growth

In the synthesis of CNTs, metal nanoparticles are usually applied as catalysts to promote growth. Through adsorbing on the active sites of the metal catalyst surface, the decomposition of the carbon sources could be speeded up at a lower temperature than the temperature needed for spontaneous decomposition. Since the reports of the catalytic formation of nanotubular carbon filaments in the 1950s [56] and the seminal research about the metal nanoparticle-based synthesis of the SWCNTs and MWCNTs in the early 1990s [4, 5], significant progress has been made in terms of synthesis yield, nanotube alignment, and sample purity.

Over the years, nickel (Ni), iron (Fe), and cobalt (Co) are the widely used as catalysts for high activity in SWCNT growth [57-60]. Besides, the use of other transition metals and noble metals has been reported recently, including palladium (Pd) [61], platinum (Pt) [61], chromium (Cr) [62], and so on. Considering the thermal stability of the metal catalysts during the CNT growth process, weakly active elements, such as ruthenium (Ru) [63] and molybdenum (Mo) [64], are used in some cases to form alloys for preventing or controlling the coarsening of catalysts.

Based on the reaction conditions and post-deposition product analyses, the widely-accepted metal catalyst-based CNT growth mechanism can be outlined as follows. When injected into the tubular reactor, carbon source vapor adsorbs on the surface of metal nanoparticles. Under the promotion effect of the catalyst, the carbon source decomposes into carbon atoms that get dissolved into the metal. When the carbon atoms reach the limit of carbon-solubility in the metal, such dissolved carbon precipitates out and crystallizes in the form of a cylindrical network, which finally constructs CNTs. As shown in Figure 1.10, this growth process is defined as the vapor-liquid-solid (VLS) growth [65-68].

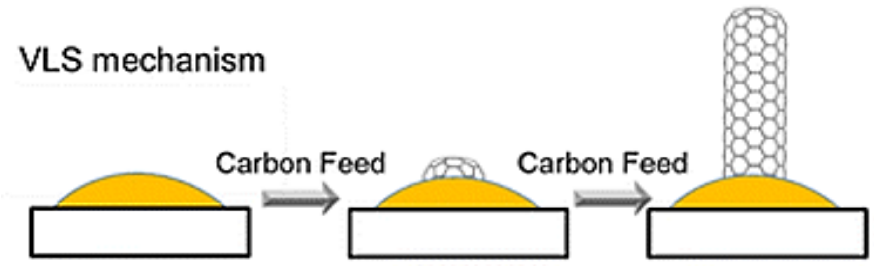

Figure 1.10 Schematic diagram of SWCNT synthesis through VLS growth mode [68].

1.2.3 Solid carbon nanoparticle-based SWCNTs growth

Recently, as Figure 1.11 shows, nanodiamonds (NDs) (~5 nm), produced by detonation of carbon-containing explosions, were successfully used as a growth seed in CNT synthesis [69]. In the ND-based CNT growth process, the adsorption step of the carbon source is similar to the metal nanoparticle-based growth case. However, different from the metal catalyst, the adsorbed carbon source will not proceed a catalytic effect promoted decomposition process and will not dissolve into NDs, which remain solid during the growth process. By diffusing on the surface of the growth seeds, the carbon source decomposed and constructed into CNTs. This growth process is called the vapor-solid surface-solid (VSSS) growth [69, 70]. In this growth mode, the diameter of CNTs is directly related to the size of growth seeds.

As one of the solid carbon nanoparticles, NDs will not fuse and change into large nanoparticles during the high temperature treatments (1000–1500 ^{o}C) because of the high thermal stability. Especially, with high temperature annealing treatment, the surface of

NDs gradually transforms sp^3 to sp^2 carbon structure (graphite sheets), which further increase their morphology stability at high temperature. This property makes NDs suitable to be employed as a growth seed in the high-temperature CVD growth process, especially in the synthesis of SWCNTs, which need growth seeds with small size. Besides, NDs bring fewer metal impurities during CNT growth than the CNTs synthesized with metal nanoparticles. In the VSSS growth mode, NDs are supposed to be a template for the nucleation of CNTs and the cap structure of CNTs can be modified by the morphology of NDs. Therefore, NDs exhibit high potential in CNT chirality control by engineering the nucleation step, which is supposed to have further study in future.

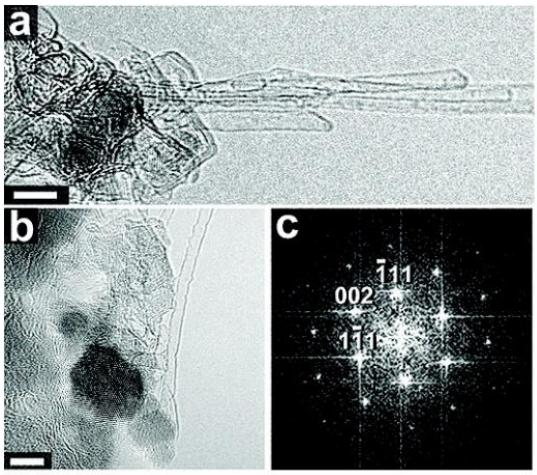

Figure 1.11 (a), (b) TEM image of SWCNTs grown from NDs and (c) Fourier transform pattern obtained from (b), where the diffraction spots represent the ($\bar{1}\bar{1}1$), (002), and ($1\bar{1}\bar{1}$) surfaces of diamond crystal. The scale bars in (a) and (b) are 5 nm [69].

1.3 Thermodynamic analysis for the growth of SWCNTs with high crystallinity

1.3.1 High temperature treatment for the achievement of SWCNTs with high crystallinity

As mentioned in section 1.1.2, crystallinity is a significant factor that decide the properties of SWCNTs. Due to the high mechanical strength and transportation properties, there grows the need for SWCNTs with low density of defects, which can be applied to logic circuits, batteries, and so on.

Aimed to prevent or heal the defects formed in SWCNTs, as Figure 1.12 shows, high temperature is suggested during the SWCNT growth or the annealing after synthesis [71]. According to previous research, types of defects formed on the edges or tubular structure of SWCNTs, and healing such defects needs to overcome the relevant activation energy [21]. The use of high temperature brings energy for the defect healing and makes it more effective, thus leading to a lower overall density of defects.

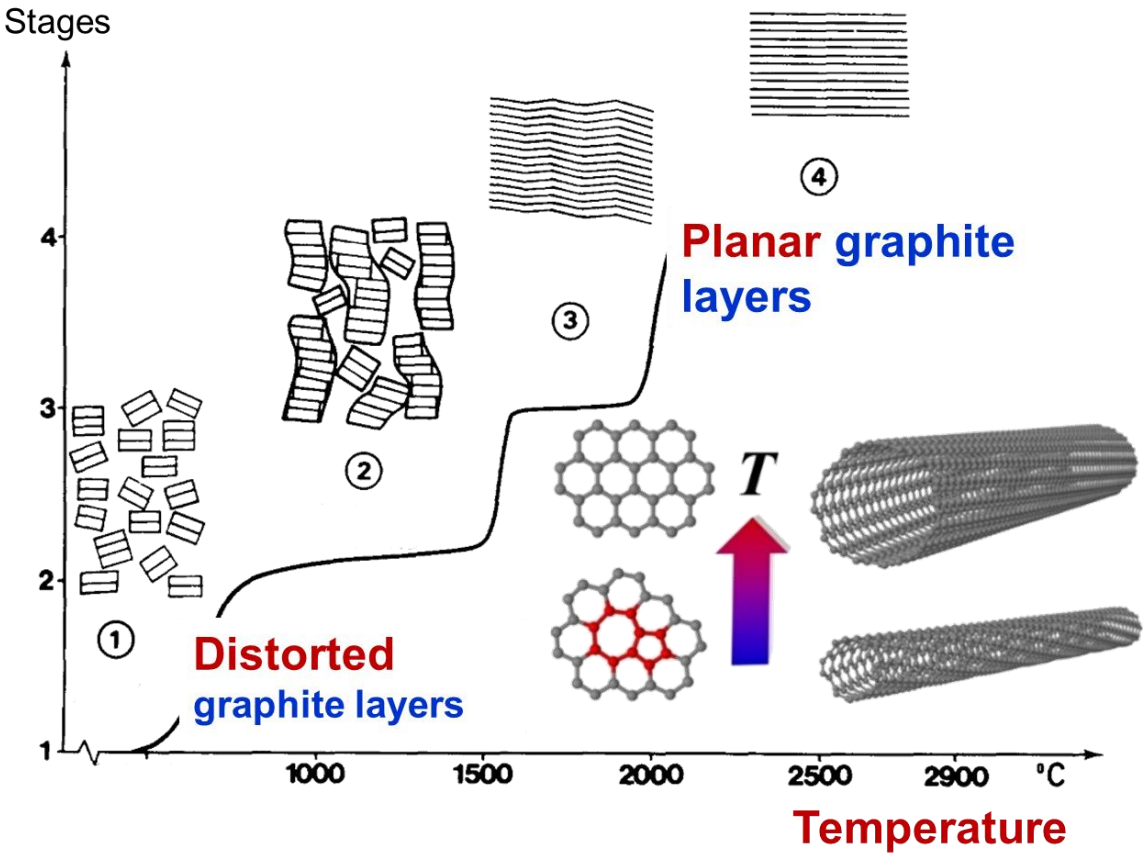

Figure 1.12 Schematic diagram of the temperature influenced graphitization process [71, 72].

On the other hand, in the high-temperature growth process, it has been found that the yield of SWCNTs tends to be lower than that of SWCNTs synthesized at the lower growth temperature. Therefore, the growth mechanism of SWCNTs should be further discussed to analyze the influence of growth conditions.

1.3.2 The influence of growth driving force during SWCNTs synthesis

In order to further understand the mechanism of SWCNTs grown from growth seeds, it is necessary to understand the concept of growth driving force ($\Delta\mu$) [73]. The growth driving force represents the energy shift from the equilibrium state, and is a concept widely used in the field of crystal growth. Applying this to SWCNT growth by CVD, as shown in Figure 1.13, the growth driving force is determined by the difference between the chemical potential of carbon atoms in carbon feedstock molecules in the gas phase $\mu_{C(gas)}$ and that of carbon atoms in SWCNTs in the solid phase $\mu_{C(solid)}$, which is expressed as $\Delta\mu = \mu_{C(gas)} - \mu_{C(solid)}$.

The growth driving force $\Delta\mu$ can be controlled by the growth conditions, the growth temperature and the carbon source partial pressure [74]. Since the chemical potential μ is equal to the partial molar Gibbs energy, keeping pressure p constant with changing temperature T, the variation of μ is proportional to the partial molar entropy S_m according to the equation $\left(\frac{\partial \mu}{\partial T}\right)_p = -S_m$, where S_m in the gas phase is higher than that in the solid phase. When the growth temperature increases, the decrease of $\mu_{C(gas)}$ is more drastic than $\mu_{C(solid)}$, these result in a reduction of $\Delta\mu$ at higher temperature (Figure 1.13 (c)). As another influential factor, the change in the carbon source partial pressure mainly affects $\mu_{C(gas)}$. A higher carbon source partial pressure increases $\mu_{C(gas)}$, which increases $\Delta\mu$ (Figure 1.13 (d)).

Based on the above study of growth driving force, it could be found that high growth temperature decreases the growth driving force in the synthesis process, which increases the difficulty of SWCNTs growth and finally reduces the yield of high crystallinity SWCNTs.

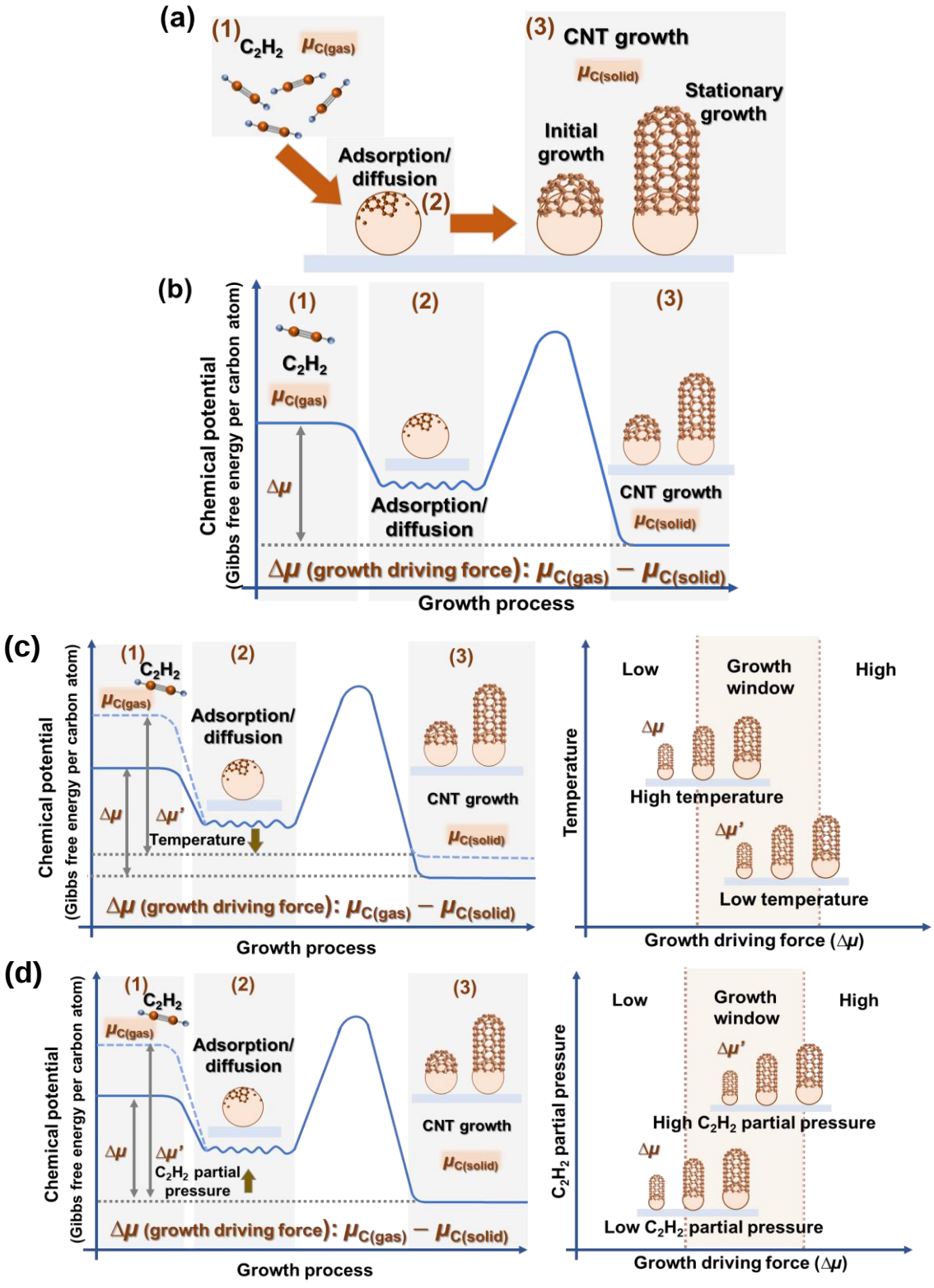

Figure 1.13 (a) Schematic model of the CVD growth process of SWCNTs from solid carbon nanoparticles. (b) Reaction coordinate in the nucleation and growth of SWCNT. (c) Reaction coordinate and growth driving force variations when the temperature changes at a fixed carbon

source partial pressure (solid line for high temperature and dotted line for low temperature). As the temperature decreases, the growth driving force at higher growth temperature Δμ increases to Δμ'. (d) Reaction coordinate and growth driving force variations when the carbon source partial pressure changes at a fixed temperature (solid line for low pressure and dotted line for high pressure). As the carbon source partial pressure increases, growth driving force Δμ increases to Δμ'.

1.4 Motivation and challenges

Highly crystalline SWCNTs are preferred to be achieved through high temperature treatment [71]. However, limitations appear with the usage of high temperature. In the metal nanoparticle-based synthesis process, supplying high temperature makes metal catalysts easy to fuse and aggregate into particles with large size, which will decrease the activity of growth catalysts and increase the size of CNTs [75]. Besides, the deformation of metal nanoparticles at high temperature will trigger the formation of defects in CNTs [76]. Compared with metal nanoparticles, as shown in Figure 1.14, the solid carbon nanoparticles, NDs, were proved to be one of the expected growth seeds because of their advantage of thermal stability, and they will not fuse in high temperature growth process. Moreover, when used as growth seeds, solid carbon nanoparticles bring fewer metal impurities to SWCNTs, which helps to avoid the chemical post-treatment for impurity removal.

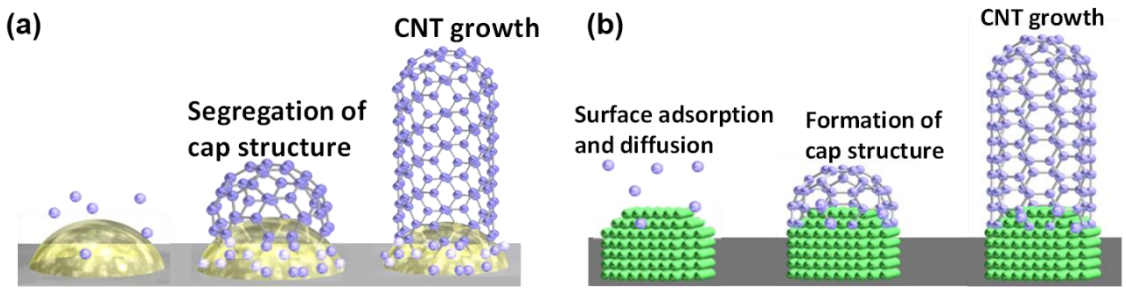

Figure 1.14 (a) Schematic mode of CNT grown from metal nanoparticles (a) and solid carbon nanoparticles

Even in the solid carbon nanoparticle-based growth process, the problem of low yield of SWCNTs synthesized at high temperature is still unsolved. In previous research, the flow rate of the carbon source for the initial growth of SWCNTs was adjusted to

increase the growth yield [77]. Combined with the relevant research about the growth driving force, the growth conditions for high crystallinity SWCNTs growth could still be adjusted to provide more suitable driving force for higher growth yield.

Another influence is the formation of amorphous carbon (a-C), structured by the hybrid of sp^2 and sp^3 carbon with low crystallinity. The formed a-C becomes another impurity in SWCNTs, and the lifetime of growth seeds would be shortened if a-C is covered on their surface. Until now, in the metal catalyst-based growth process, some reactants (H_2O, CO_2, and H_2) have been proven to remove a-C by reacting with carbon atoms [78-87]. In the solid carbon nanoparticle-based growth process, there are few discussions about employing reactants to prevent the deposition of a-C in the high temperature growth process, and the effects of the reactants also need to be illustrated.

Not only helps to decrease defects during the formation step, the high temperature was also proved to heal the defects which are already structured and diffused from the edge of CNTs into tubular structure. However, high temperature treatment has been proven to be challenging to heal some kinds of defects perfectly, such as vacancy defects. Recently, several theoretical studies supported that, with the participation of carbon-containing reactants, vacancy defects can be healed [88-91]. Therefore, it is necessary to be further proved this by combining it with experimental results.

1.5 Organization of the thesis

In previous works, high temperature growth process has been applied to achieve high crystallinity SWCNTs. However, high temperature growth produced SWCNTs with a limitation in yield. Besides in such high temperature growth process, a-C forms as the impurity and prevents the growth of CNTs. Moreover, when use the post-treatment process as another method to increase the quality of massive SWCNTs, high temperature annealing exhibited a limitation in the efficiency of defect healing on SWCNTs.

Therefore, in this dissertation, I developed the high temperature growth process to a cap formation engineered two-step growth process to solve the issues of low yield. Further, to prevent a-C deposition at high temperature, according to previous works about growth enhancers, I applied them into the carbon solid seeds-based SWCNTs growth

system and illustrated the effects of enhancers. Finally, to increase the healing efficiency of high temperature, I injected carbon-containing reactants in the post-treatment and experimentally investigated the effect of such reactants.

This thesis consists of six chapters. Chapter one includes the introduction of CNTs structure, structure measurement methods, synthesis methods of CNTs, and the growth mechanism studied recently.

In chapter two, experimental methods were expressed, including the preparation of growth seeds (NDs), the process of SWCNTs synthesis in the CVD equipment, and the methods mainly used for the structural characterization of synthesized SWCNTs in this thesis.

Chapter three describes work about building a new two-step growth process, the cap engineered two-step growth process. According to the research about thermodynamic considerations of growth driving force required for different growth stages, the growth temperature and partial pressure of carbon source was mainly analyzed and adjusted to increase the growth efficiency. Besides, a strong etchant, water vapor, was employed in this growth process to decrease the amount of deposited a-C. Through the characterization results of SWCNTs, we found that the yield of high crystallinity SWCNTs was increased by using the cap engineered two-step growth process.

Chapter four discusses the enhancing roles of water (H_2O) and carbon dioxide (CO_2) in the non-metallic nanoparticle-based SWCNT growth at high temperature. In this research, different carbon source was used during the classic high temperature growth process and the two-step growth process. Through analysis, in the non-metallic nanoparticle-based growth process, the etching ability of H_2O was found. Besides, CO_2 presents roles in preventing a-C deposition and/or enhancing carbon source supply, depending on the injected carbon feedstocks.

Chapter five experimentally investigated the effect of carbon-containing reactants (C_2H_2) in the high temperature annealing process. In this study, grown from NDs, the defective SWCNTs were healed with or without the injection of C_2H_2. Using the healing process in Ar ambient as a comparison, the SWCNTs healed with C_2H_2 injection presented higher crystallinity, and a partial pressure dependent healing effect was

revealed. Moreover, the C_2H_2-injected high temperature annealing exhibited higher healing efficiency in thinner SWCNTs compared with the thicker tubes.

Finally, chapter six states a conclusion of the aforementioned research works and provides a future perspective based on the achieved results.

Chapter 2: Experiments

2.1 Preparation of substrate and growth seeds

500-μm-thick Si substrates with a 300-nm-thick SiO_2 were cut into a ~10 mm square. An ultrasonic cleaner was used to clean the substrate in the following order: acetone (99.5%), ethanol (99.5%), and ultrapure water (99.5%). Each step lasts for 5 minutes. Dried by N_2 gas, the ultrasonic cleaned substrate was treated by an ozone cleaning process (L-UV253, Japan Electronics Industry) by flowing 6 L/min oxygen for 5 min under ultraviolet light for 60 min followed by exhausting with 6 L/min nitrogen for 5 min. Within the above-mentioned cleaning process, the impurities like metal particles and organic matter can be removed from the surface of the substrate.

In this study, we used high-purity NDs (provided by Nippon Kayaku, impurity concentrations of 80 ppm for Fe, 2100 ppm for Zr, and 6–20 ppm for Pd) produced by the detonation method. The ND is purified to remove impurities mixed in during the manufacturing process and is dispersed in ethanol (2.0 wt %). After ultrasonic dispersion, 20 μl of the ND solution was dropped on the surface of the thermally oxidized Si substrates (~300 nm-SiO_2, ~500 μm-Si) by using a micropipette. Additionally, the Si substrates treated with the same cleaning process but without any growth seeds were used as a reference to examine the amount of a-C deposited directly on substrates (hereafter called blank samples). The substrate dropped with 20 μl-NDs is shown in Figure 2.1

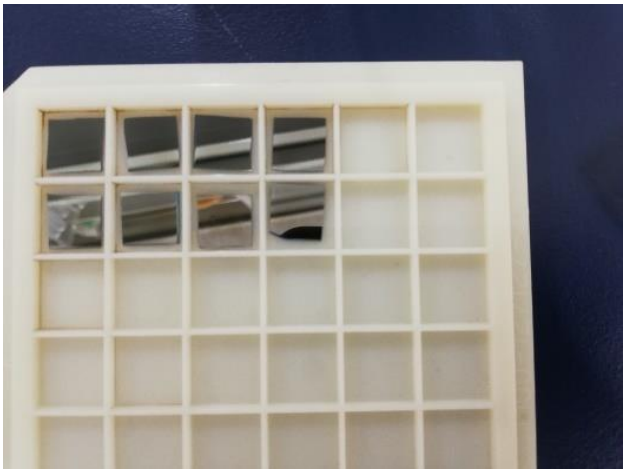

Figure 2.1 The photo of cleaned SiO_2/Si substrate (~10 mm square) uniformly dropped with 20 μl-NDs.

2.2 Synthesis of SWCNTs in the CVD equipment

Figure 2.2 shows an external view of the CVD equipment and the relevant schematic diagram used for SWCNT growth. Figure 2.3 shows the diagram of the pipeline in the CVD system.

According to Figure 2.2, the feature of this equipment is that the temperatures in the pyrolysis area of the carbon source gas and the growth area of CNTs can be controlled independently. When using NDs as the growth seeds, the decomposition of the injected carbon source occurs only by high temperature heating. Therefore, it is effective to keep the pyrolysis zone at a high temperature to ensure the decomposition of the carbon source during the growth process. The multi-temperature CVD system used in this study is described below.

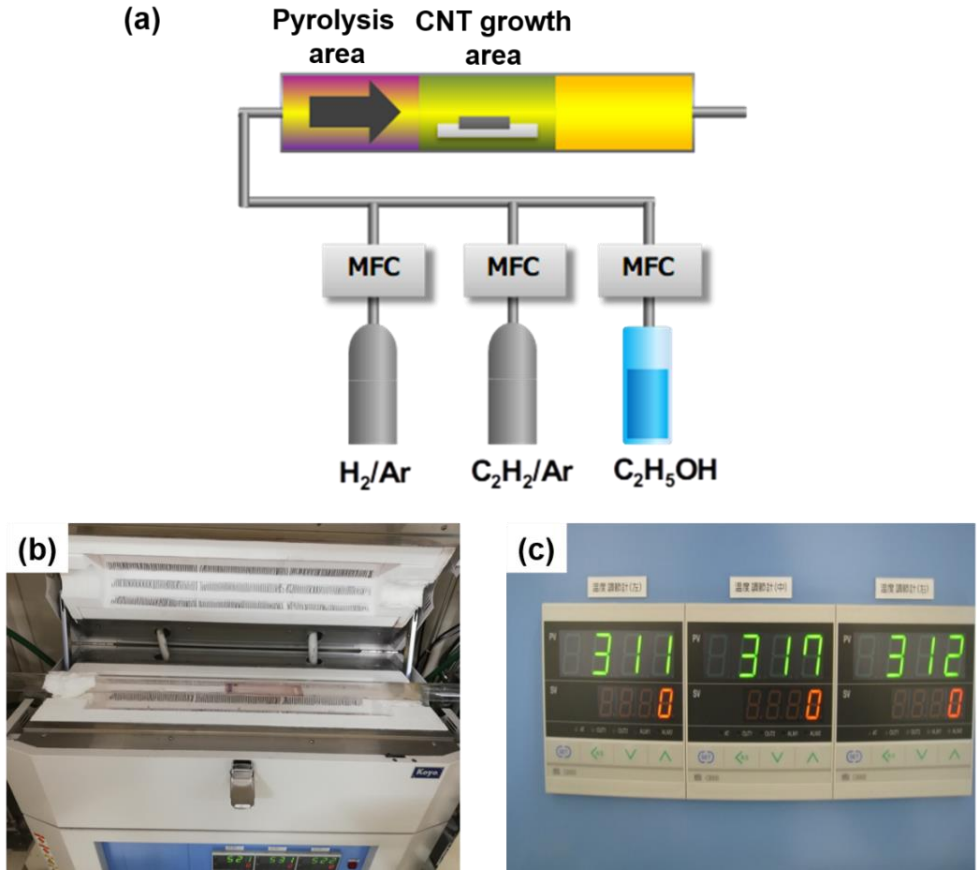

Figure 2.2 (a) Schematic diagram of CVD system with multi-temperature zone, (b) the inside of the growth furnace and (c) the temperature controller to adjust the heat temperature in different area.

As shown in Figure 2.2 (b) and (c), temperature controllers are provided upstream, midstream, and downstream. Therefore, the temperature can be controlled in each area, and the temperature can be raised up to 1100 °C. However, because each area is equipped with a thermocouple, the temperature in each area is affected by the temperature in the adjacent area, limiting the temperature setting in each area. Therefore, the maximum temperature difference between the upstream and midstream is ~100 °C and is ~50 °C between the midstream and downstream.

As shown in Figure 2.3, argon, argon diluted hydrogen gas, hydrocarbon gas, water vapor (H_2O), and carbon dioxide (CO_2) could be introduced in this system. The features of the H_2O and CO_2 gas lines are described in detail.

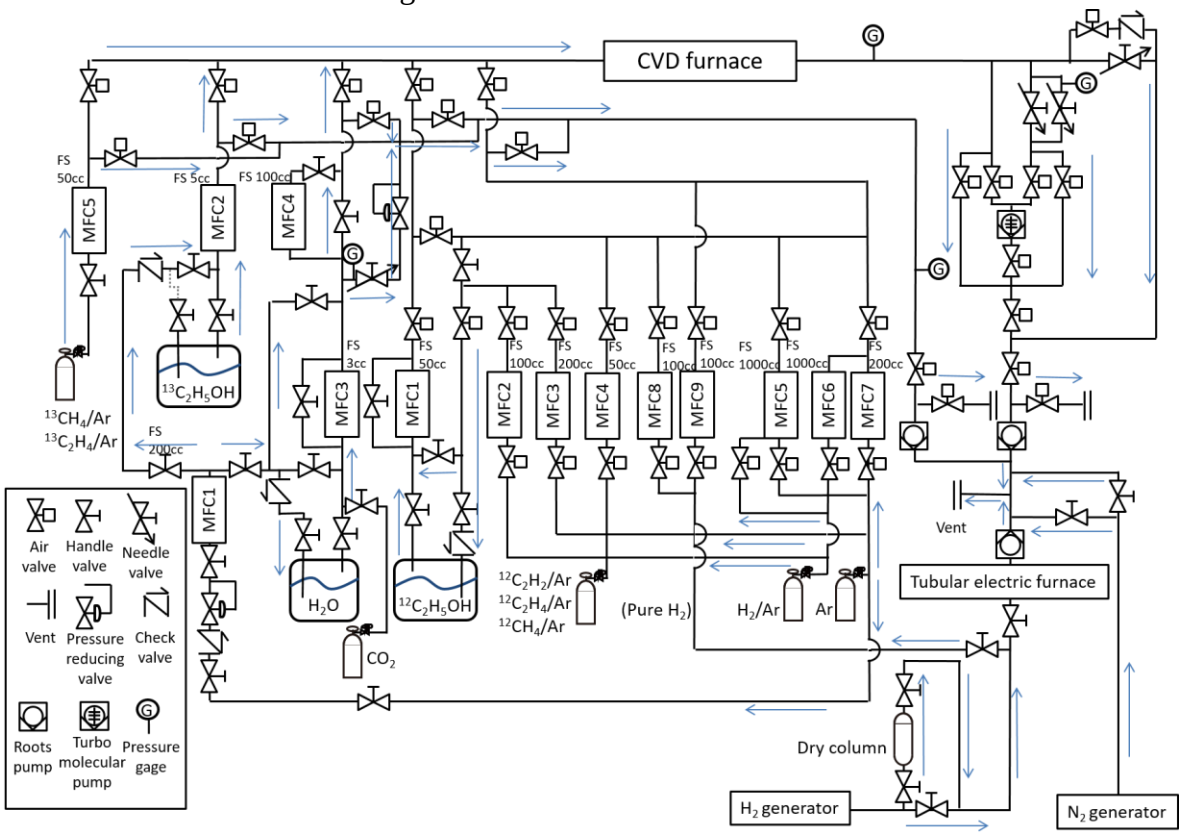

Figure 2.3 The diagram of gas lines connected to CVD system.

An external view is shown in Figure 2.4. The gas line used for H_2O and CO_2 is branched into two lines: a vent line and a main line leading to the tubular reactor. The injected H_2O or CO_2, diluted with argon gas, can be controlled at an extremely low concentration to participate in the growth process. Especially for H_2O, the piping can be heated by a heater to prevent water coagulation.

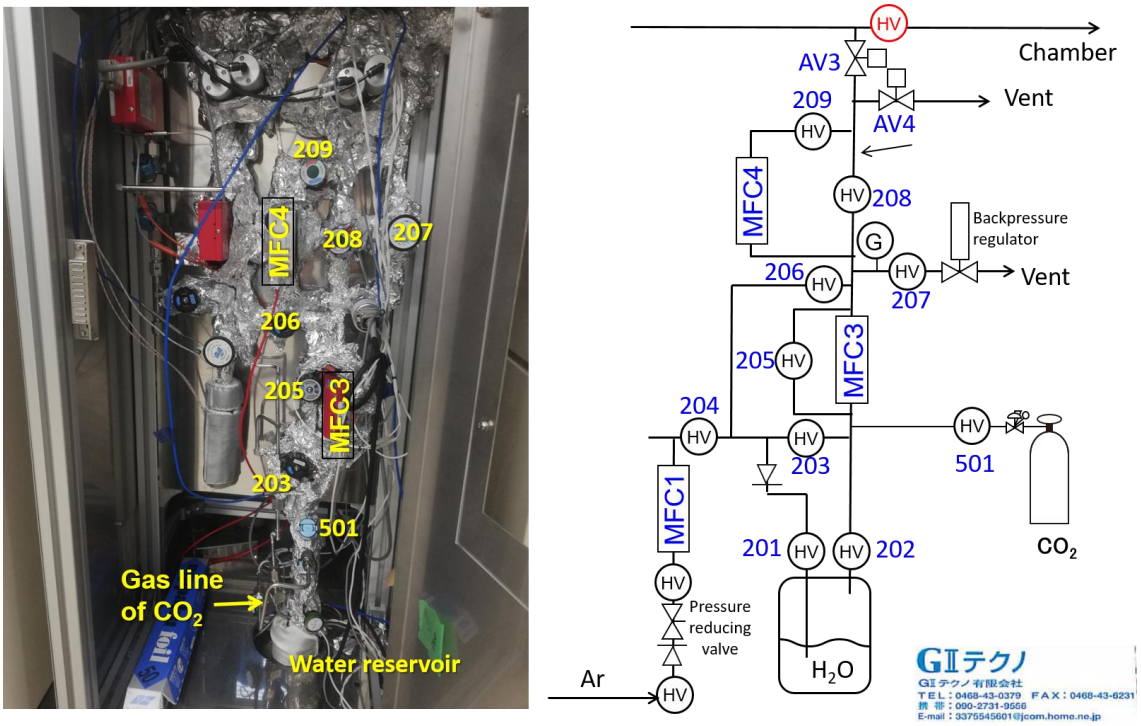

Figure 2.4 The appearance of H_2O and CO_2 introduction gas line.

2.3 Raman measurement of SWCNTs

In this study, the Raman spectra was observed using LabRAM HR800, HORIBA Jovin Yvon with a laser wavelength of 633 nm was used. When evaluating the obtained SWCNT growth yield, the I_G/I_{Si} ratio was used as an index, which is the peak intensity ratio of the peak from the Si substrate (~520 cm^{-1}) and the G-band (~1590 cm^{-1}) from the in-plane vibration of graphite. As shown in Figure 2.5, the magnitude of I_G/I_{Si} ratio corresponds to the growth amount estimated from the SEM image, confirming the validity of this index.

The I_G/I_{Si} ratio can be used when CNTs are growing on the entire surface of the substrate, as shown in Figure 2.5 [92]. Noticeably, in the case of random growth on the substrate, the G band observation frequency is used as a method to evaluate the growth amount.

When evaluating the density of defects in the obtained SWCNTs, the I_G/I_D ratio was used as an indicator [93], which is the intensity ratio of the G-band and the D-band (1300 cm^{-1}), which is derived from the defect structure.

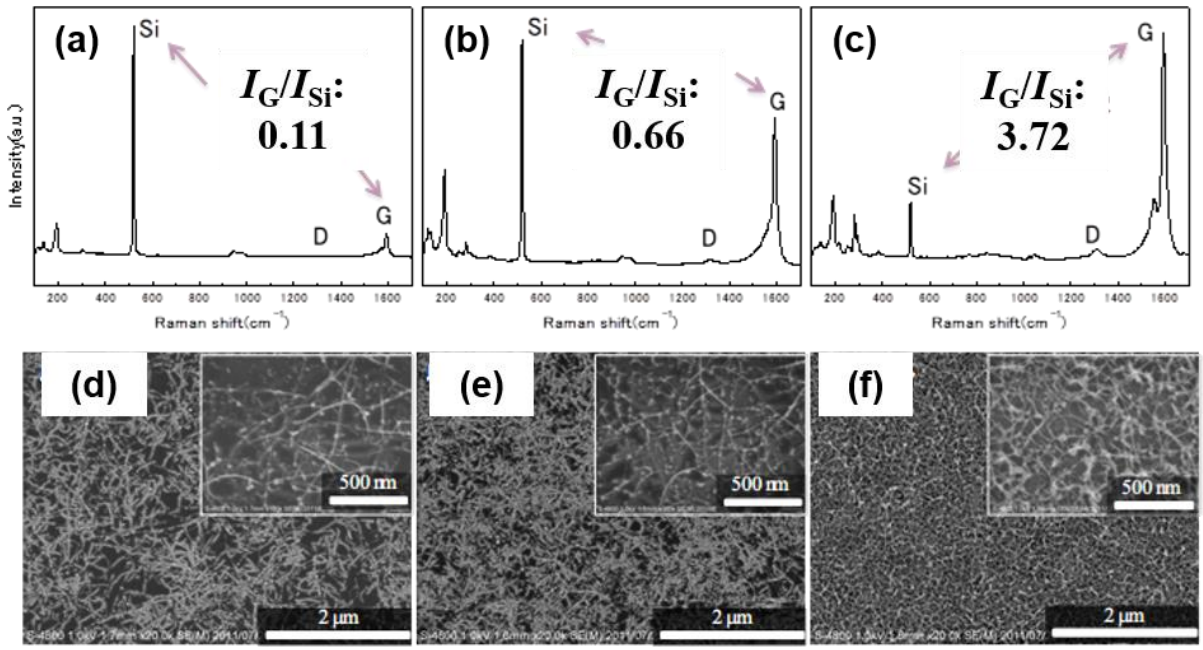

Figure 2.5 (a-c) Raman spectra of CNTs samples and (d-f) the relevant SEM images, where I_G/I_{Si} ratio corresponds to the yield of CNTs [92].

2.4 Scanning electron microscope (SEM) and atomic force microscope (AFM) measurement

SEM detection is a system in which the secondary and backscattered electrons are collected from the electron irradiated sample to form an image. Contrast is added by the difference in the amount of detected signal at each scanned point. In this study, the growth morphology of SWCNTs was observed using NVision, Carl Zeiss, and S-4800, Hitachi.

Atomic force microscopy (AFM) detection is a system used to evaluate the surface texture of a sample by tracing the sample surface. Through the sharp tip attached to a cantilever, the sample surface is scanned with a distance between the tip and the sample surface. The distance is fixed by controlling the vertical displacement of the cantilever. This scanning becomes precious with the usage of piezoelectric elements, which brings accurate movements on the command and enable precise scanning. Thus, the AFM image

provides three-dimensional (3D) shape (topography) of a sample surface with high resolution. In this study, the morphology of NDs was observed using. In this study, the size of NDs was analyzed using AFM5000, Hitachi.

Chapter 3: Single-walled carbon nanotube growth by two-step process with water injection

Growth of single-walled carbon nanotubes from solid carbon nanoparticle seeds via cap formation engineering with a two-step growth process and water vapor supply

3.1 Background

Single-walled CNTs (SWCNTs) [4] have received increasing attention toward logic circuits [94], chemical sensors [95], and quantum light sources [96] because of their excellent performances and chirality-dependent optoelectronic properties [97]. During the growth of SWCNTs, carbon atoms decomposed from carbon source molecules are bonded together on a suitable growth seed, which is a nanoparticle that acts as a template and initially forms a hemispherical graphitic structure, which is referred to as a cap structure. After the cap structure lifts off from the growth seed, a tube structure gradually elongates as the carbon atoms attach at the interface between the edge of the tube and the growth seed [35]. The CVD process has been extensively investigated for the structural control and high yield synthesis of SWCNTs due to the high degree of freedom of growth parameters and good compatibility with large-scale production [33, 98-100].

Unfortunately, there are still significant differences between experimentally synthesized SWCNTs and ideal SWCNTs, which are required for applications in terms of crystallinity, chirality, and length. The crystallinity of SWCNTs is one of the most important aspects, since the structural defects formed on SWCNTs significantly alter the electronic structure [101, 102] and deteriorate their superior properties, including electrical transport [101, 103, 104], thermal transport [105], and mechanical strength [106]. To achieve highly crystalline SWCNTs, high-temperature CVD processes are effective because the activation barrier of healing defects must be overcome [21, 71]. For high growth temperature, the growth seeds for SWCNTs require high temperature stability to prevent aggregation phenomena. Catalytic metal nanoparticles, including iron [107, 108], nickel [109], cobalt [110], and relevant alloys [111], are widely used as growth seeds. However, due to their moderate melting points, metal catalysts usually suffer from

deactivation caused by aggregation, limiting the yield of SWCNTs at high temperatures [75]. Also, post-treatment is required in some applications to exclude metallic impurities from the grown SWCNTs, but it can induce the formation of additional defects [112].

Recently, non-metallic nanoparticles with higher melting points have been utilized as growth seeds of SWCNTs [70, 113-116]. Among them, nanodiamonds (NDs) [69] are promising growth seeds because of their nonfusion properties that prevent aggregation or sintering of nanoparticles even at high growth temperatures. In addition, as-grown SWCNTs from ND nanoparticles are highly pure in terms of elemental composition, alleviating the need for post-growth purification. One study successfully synthesized highly crystalline SWCNTs at 1000 °C using solid carbon nanoparticles derived from NDs as growth seeds [117]. However, the yield of high-quality SWCNTs remained low at high growth temperatures. Increasing the growth temperature has been reported to make the organization of SWCNTs more difficult.

As discussed in section 1.3.2 regarding thermodynamic considerations [118], a reduction of $\Delta\mu$ occurs at higher temperature (Figure 1.13 (c)). This reduction in $\Delta\mu$ at high temperature makes the formation of SWCNTs difficult, especially for cap structures with higher strain energies above $\mu_{C(solid)}$ [119].

Since the growth of SWCNTs starts from the cap formation process, optimizing the cap formation condition to obtain higher nucleation efficiency is necessary to increase the growth yield of SWCNTs. Therefore, increasing the partial pressure of the carbon feedstock or decreasing the growth temperature only at the beginning of SWCNT growth should compensate for the high driving force required for the nucleation of the cap structure. After the effective formation of the cap structures, a moderate driving force should be provided for the subsequent growth of the nanotube sidewalls by controlling the growth conditions. Details of the required driving forces for the different growth stages are explained in section 3.3.2. A two-step growth approach using conventional metal nanoparticles at moderate temperatures has been used in the synthesis of SWCNTs [120]. However, the effectiveness of two-step growth has hardly been investigated so far because of the unique vapor-solid-surface-solid (VSSS) growth mechanism that occurs in solid seed-supported SWCNTs growth systems [69, 70], rather than the vapor-liquid-solid (VLS) model based on metal catalyst growth [65, 66]. Although our previous study

reported a preliminary results of two-step growth from solid carbon seeds by temporally changing the carbon feeding rate [77], a more in-depth investigation of the cap formation process should enable efficient synthesis of highly crystalline SWCNTs and elucidate the unconventional mechanism for growing SWCNTs from solid carbon nanoparticles.

Another factor that hinders the growth of SWCNTs is the deposition of amorphous carbon (a-C), which is easily formed at high temperatures and high carbon feed rates. In metal catalyst-based CNT growth, with the introduction of water vapor, it has been reported that the activity and lifetime of metal catalyst was improved by selective etching of a-C. During growth, the improved catalyst performance resulted in high efficiency of CNT synthesis and massive or ultra-long CNT growth from metal nanoparticles [33, 87, 121-124]. Therefore, water-induced etching of a-C could potentially be exploited for the growth of SWCNTs from solid carbon seeds.

In this work, a two-step approach is developed to efficiently synthesize high-quality SWCNTs using ND-based solid carbon nanoparticles as growth seeds at high temperatures. The effects of growth temperature, partial pressure of carbon feedstock, and growth time in the initial growth step on the nucleation of SWCNT caps is investigated to enhance the synthesis from non-metallic nanoparticles. After an efficient cap formation stage, the carbon supply was reduced in the secondary growth step at high temperature to adjust the growth drive. The stationary elongation of tubes in the secondary growth step increased the growth yield of SWCNTs with high crystallinity. In addition, by introducing water vapor as etchant, just after the formation of SWCNT cap structure, impurity-free SWCNTs with high crystallinity were obtained and the growth yield was increased.

3.2 Experimental Section

3.2.1 Growth seed preparation

Figure 3.1 depicts the entire process, including the pretreatment step for growth seeds and the two-step growth process with and without water injection. Purified ND particles (provided by Nippon Kayaku, impurity concentrations of 80 ppm for Fe, 2100 ppm for Zr, and 6–20 ppm for Pd) prepared by the detonation method [125, 126] were

dispersed in ethanol (2.0 wt%) and used as the starting material of the seeds for SWCNT growth.

The silicon (Si) substrates with a 300-nm-thick thermal oxide layer were cut into approximately 10 mm squares and cleaned by an ozone treatment process (L-UV253, Japan Electronics Industry) by flowing 6 L/min oxygen for 5 min under ultraviolet light for 60 min followed by exhausting with 6 L/min nitrogen for 5 min. After ultrasonic dispersion, 20 μl of the ND solution was dropped on the surface of the Si substrates. In addition, the same Si substrates without any growth seeds were used as a reference to examine the amount of a-C deposited directly on substrates (hereafter referred to as blank samples).

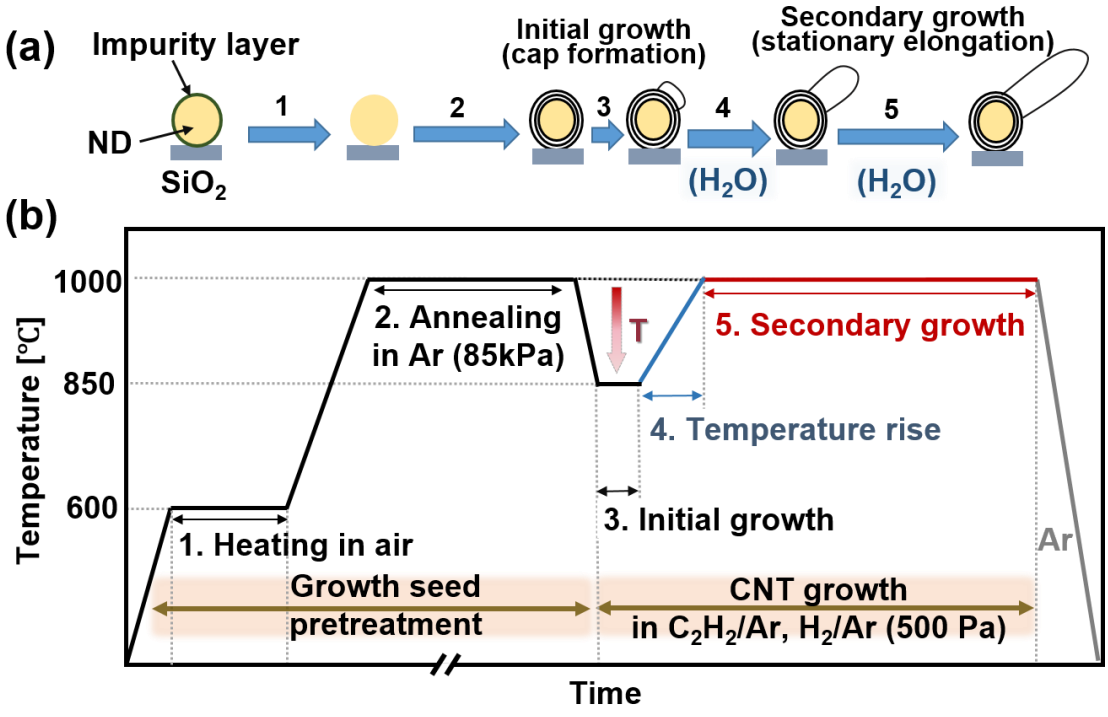

Figure 3.1: (a) Schematic diagram of the growth seed pre-treatment and the two-step growth process of SWCNTs from solid carbon nanoparticles. (b) Temperature profile of the reaction furnace as a function of processing time.

3.2.2 Two-step growth process without water vapor injection

A tubular CVD furnace (GE-1000, GII Techno) The substrate was placed in the center of a quartz tube chamber with a semicircular cross-section, a diameter of 43.6 mm,

and a heating zone length of 890 mm, and heated in air at 600 °C for 10 min to remove various impurities from the surface of the substrate and ND (Figure 3.1 (b), process 1). During this process, the diameter of ND was reduced to the appropriate size for SWCNT growth [69], and the size variation is shown in Figure 3.2. Further processing was performed by gradually increasing the furnace temperature to 1000 °C under argon at 85 kPa and keeping it at 1000 °C for 1 h as an annealing procedure (Figure 3.1 (b), process 2). This step should turn the surface of ND (sp^3 carbon) into a more stable graphitic shell (sp^2 carbon), which is called as the carbon nano-onion structure [127, 128].

To adjust the growth conditions suitable for the initial growth step of forming the cap structures, the growth temperature was set to 850 °C or 900 °C after the annealing process of 1000 °C described above (Figure 3.1 (b), process 3). Once the temperature dropped to the set value, which was determined based on the previous high temperature SWCNT synthesis condition [129], the pressure was dropped to 500 Pa while argon was continuously injected at 20 sccm and held for 3 min to stabilize the environment. Afterwards, the gas condition was converted to a mass flow mixture of 20 sccm of C_2H_2 (2%)/Ar (1–10 sccm) and H_2 (3%)/Ar (10–19 sccm) while the total pressure was maintained at 500 Pa, corresponding to a C_2H_2 partial pressure of 0.5–5 Pa. The typical flow rates for C_2H_2/Ar and H_2/Ar were 2 sccm and 18 sccm, respectively, corresponding to a C_2H_2 partial pressure of 1 Pa. The process lasted for 1 or 2 min as the cap growth stage. Before entering the secondary growth step, the growth temperature was raised to 1000 °C while the control gas mixture was 1 sccm C_2H_2 (2%)/Ar and 19 sccm of H_2 (3%)/Ar, where the partial pressure of C_2H_2 was 0.5 Pa (Figure 3.1 (b), process 4). The secondary growth step, where stationary elongation of SWCNTs should occur, started when the growth temperature reached 1000 °C and lasting 30 min while maintaining the same gas phase mixture and pressure conditions (Figure 3.1 (b), process 5). In some experiments, only the initial growth step was performed, and after 1 or 2 min of the initial growth at 850 ºC or 900 ºC, the temperature was decreased and no secondary growth step was performed.

3.2.3 Two-step growth process with water vapor injection

Water vapor was added as a growth enhancer in some experiments because water vapor may prevent the deposition of a-C. According to the two-step growth process described above, water vapor at 0.15 Pa is usually injected into the gas phase environment. We started the water vapor supply at two different timings: from the beginning of the temperature rising step and from the beginning of the secondary growth step. The details are explained in section 3.3.5.

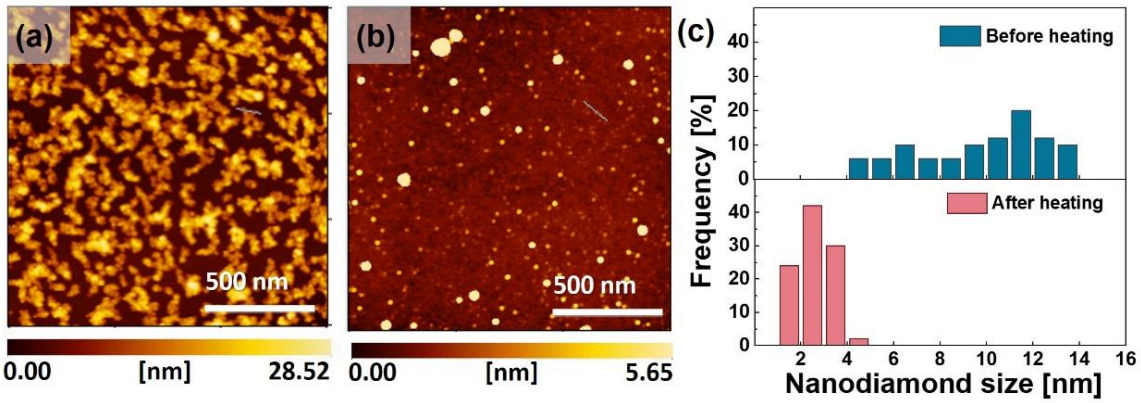

Figure 3.2: (a) AFM image and particle size distribution histogram (c, blue column) of the samples obtained from purified ND before heating in air. (b) AFM image and particle size distribution histogram (c, red column) of the samples obtained from purified ND after heating in air at 600 °C for 10 min. The ND particle size was evaluated by height profiles of the AFM images.

3.2.4 Structure characterization and yield evaluation of synthesized SWCNTs

We analyzed the structure of the synthesized SWCNTs by Raman spectroscopy. A Raman spectrometer (LabRAM HR800, HORIBA Jovin Yvon) was used with an excitation wavelength λ_{ex} of 633 nm. The size of the laser spot was about 0.9 μm, and the laser power of the measurement spot was about 7 mW. The exposure time for each measurement spot was 1 second and cycled 5 times. Raman spectra were collected from 30 randomly selected spots on each sample, and the average spectra were used for further analysis. The quality of the formed SWCNTs was discussed by comparing the intensity ratio of the G-band (~1590 cm^{-1}) to the D-band (1330–1360 cm^{-1}), which was denoted as I_G/I_D [93]. The density of SWCNTs was low, and in the case of high temperature

synthesis, the G-band was occasionally not observed. Therefore, the growth yield of SWCNTs was assessed by the G-band observation frequency (the number of times the G-band appears in the measured spectrum divided by the total number of measurements). Typically, 100 spots of Raman spectra were collected to assess the G-band observation frequency. Note that more measurement spots were used to determine the G-band observation frequency than that for averaging Raman spectra to ensure the accuracy of the G-band observation frequency, even for samples with low-density SWCNTs. Scanning electron microscopy (SEM) (NVision, Carl Zeiss) was used for morphological observation of SWCNTs with an acceleration voltage of 1–5 kV. Atomic force microscopy (AFM) (AFM5000, Hitachi) was used to analyze the morphology of NDs.

3.3 Results and Discussion

3.3.1 Investigation of possible SWCNT growth from impurity in ND

We conducted a separate experiment to examine whether SWCNTs grow from metallic impurities contained in NDs. We prepared purified and unpurified ND samples whose Zr impurity concentrations were evaluated as 2100 ppm and 10000–20000 ppm, respectively, by inductively coupled plasma mass spectrometry. By heating the ND in air at 900 ^{o}C for 30 minute, the NDs was burned off, leaving only the metallic impurities on the substrate, and then we performed a two-step SWCNT growth. The purified and unpurified ND samples after the burning and growth processes were examined by Raman spectroscopy, SEM, and AFM (Figure 3.3). Raman measurements were performed on randomly selected 30 spots on each sample. While the G-bands were detected on some measurement points of the unpurified ND samples, the purified ND samples did not show any G-bands in their Raman spectra. SEM observation also confirmed that SWCNTs with low-density was grown from unpurified ND, while no tubular structures were present in the purified ND samples. This result proves that the impurity concentration in the purified NDs is low enough not to grow SWCNTs and that SWCNTs obtained in this study which did not undergo ND burning were grown from solid carbon nanoparticles transformed from NDs.

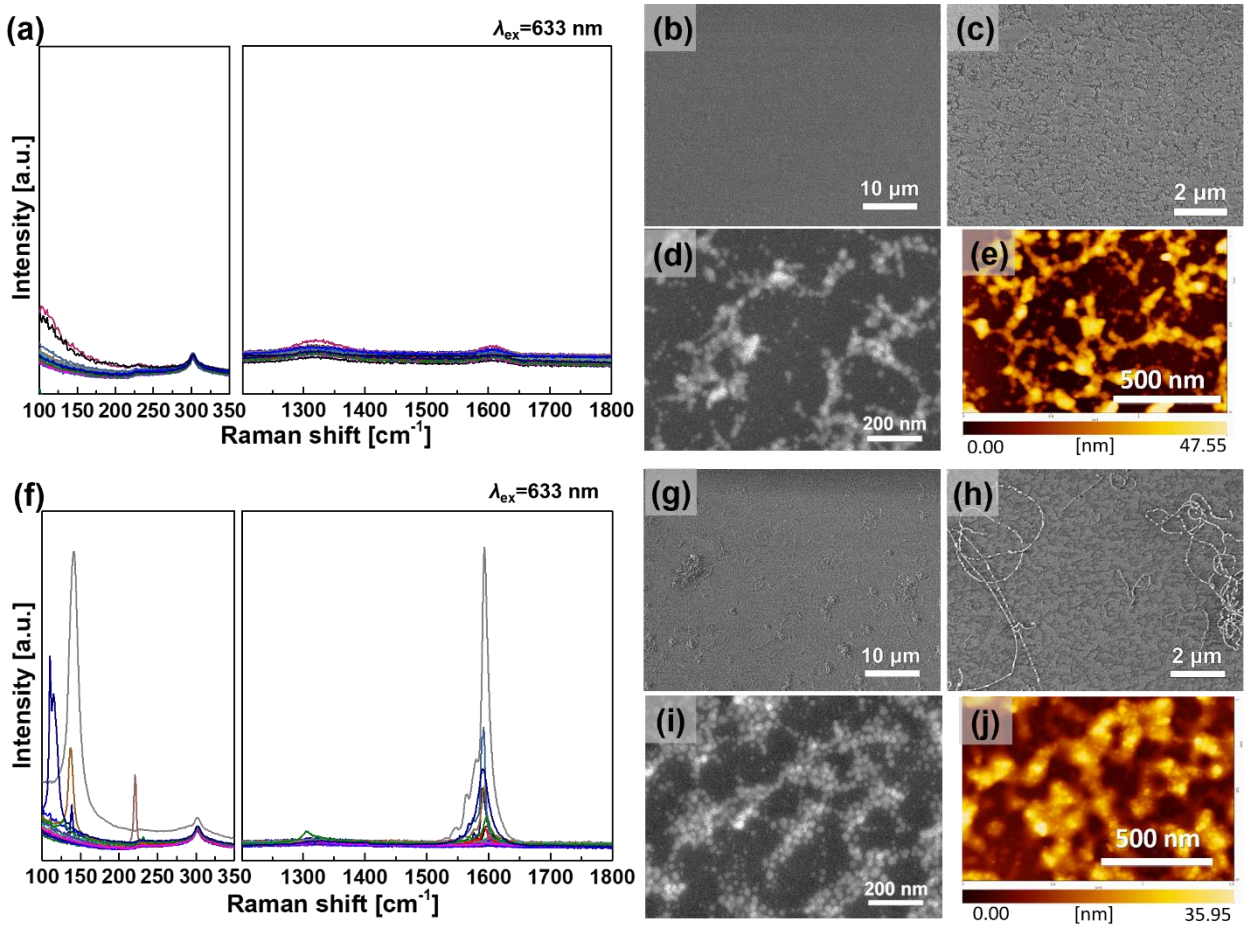

Figure 3.3: Growth results from (a–e) purified and (f–i) unpurified ND after burning in air at 900 °C for 30 min. (a, f) Raman spectra, (b–d, g–i) SEM images, and (e, j) AFM images of the samples. The SEM images were taken at (b, g) low and (c, h) high magnifications and also at (d, i) high magnification with a higher acceleration voltage (5 kV).

Note that some structures with deeper contrast than SWCNTs were observed by SEM (Figure 3.3 (h)). Referring to the literature, SEM observations were carried out at a higher magnification and a higher accelerating voltage (5 kV). [130]. The observation reveals that there are particle-like structures (Figure 3.3 (d, i)). The height of the particles was evaluated to be several tens of nanometers by AFM (Figure 3.3 (e, j)). We believe that these structures are aggregated particles composed of impurities, mainly Zr, with a-C deposition.

3.3.2 Effects of temperature and C_2H_2 partial pressure in the initial growth step

In order to improve the growth efficiency of cap structures with solid carbon nanoparticles as the growth seeds, SWCNT growth was performed under different initial growth conditions while omitting the secondary growth step. To amplify the difference of the growth results, the growth time of the initial growth step was preliminarily set to 2 min. Figure 3.4 presents the effect of the growth temperature and the partial pressure of carbon feedstock in the initial growth step.

The Raman spectra in Figure 3.4 (a) show the variations of the SWCNT growth results in the initial growth step at temperatures of 850 °C and 900 °C only. For the same carbon source partial pressure (1 Pa) and growth time (2 min), the sample synthesized at 900 °C shows a higher intensity of the G band than the sample synthesized at 850 °C. Since the G-band intensity reflects the amount of SWCNTs in the measurement region, its increase suggests that the initial growth efficiency of SWCNTs increases as the temperature increases from 850 °C to 900 °C. A peak in the D-band, which originate from structural defects formed on SWCNTs and/or a-C deposited on the surface of SWCNTs and substrates, are observed in both samples. On the other hand, no the D-band was observed in the spectra from the control samples without ND deposition (blank samples, Figure 3.4 (a), dotted lines). The absence of D-band in the blank samples indicates that the D-band of the SWCNT samples mainly originates from the defects formed on SWCNTs rather than a-C, which can also be deposited on the blank samples. The samples synthesized at 900 °C have higher G-band and D-band intensities, which implies that the stationary growth of SWCNTs may start with a higher growth efficiency even in the initial growth step. The earlier start of stationary growth may be the reason for the decrease in quality of SWCNTs obtained at 900 °C, which will be discussed in section 3.3.4.

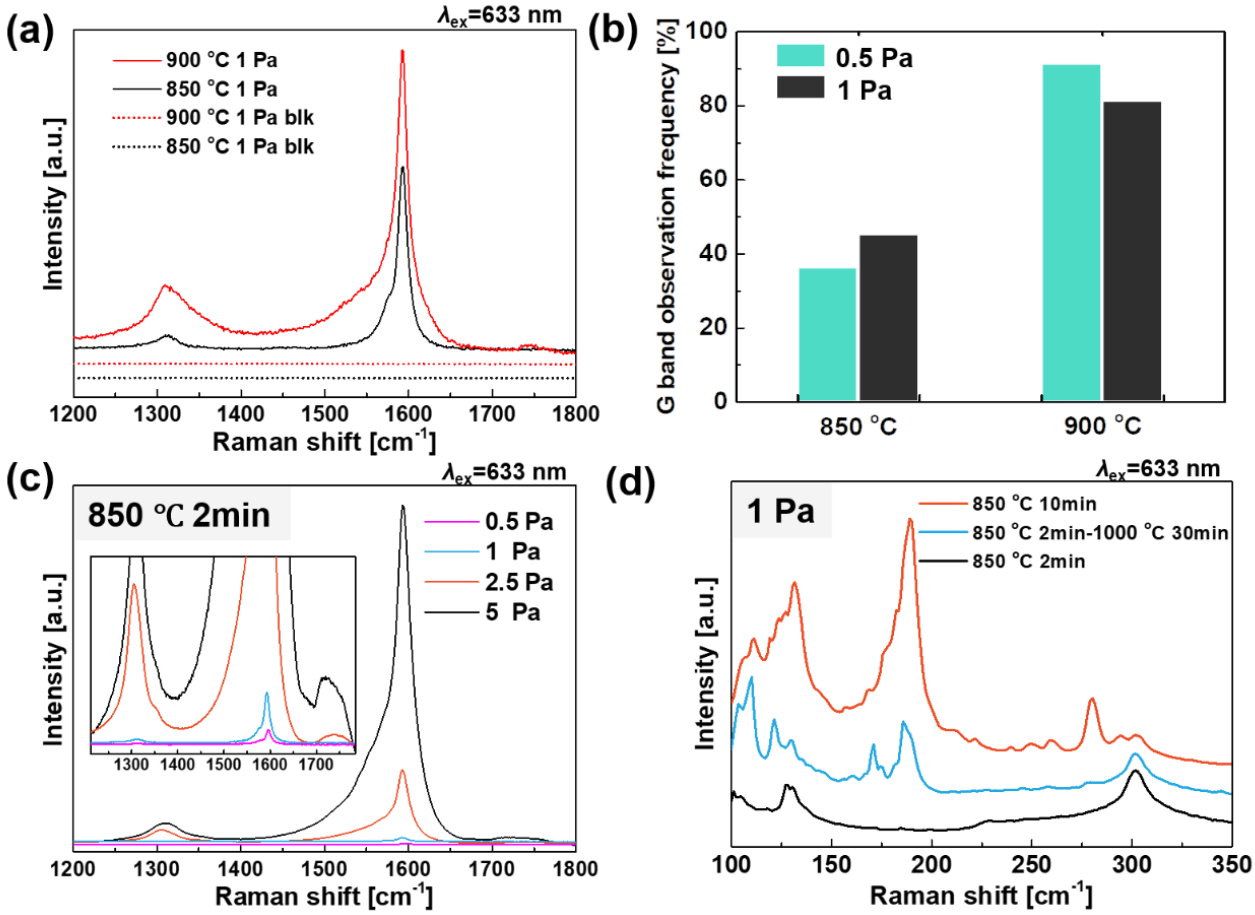

Figure 3.4: Dependence of the initial growth conditions on the structure and yield of SWCNTs. (a) Raman spectra of SWCNTs grown at 850 °C and 900 °C with C_2H_2 partial pressure of 1 Pa for 2 min. Dotted lines denote Raman spectra of the blank samples obtained under the same conditions. (b) G band observation frequency of SWCNTs synthesized at 850 °C and 900 °C with a carbon source partial pressure of 0.5 Pa and 1 Pa for 2 min, which represents the growth yield of SWCNTs. (c) Raman spectra of SWCNTs grown at different carbon source partial pressures: 0.5 Pa, 1 Pa, 2.5 Pa, and 5 Pa. Growth temperature is 850 °C and growth time is 2 min. Inset shows magnified spectra. (d) RBM peaks in Raman spectra of SWCNTs synthesized through only the initial growth step of 850 °C, 1 Pa, and 2 min (denoted as 850 °C 2 min) and 850 °C, 1 Pa, and 10 min (850 °C 10 min) as well as through the initial growth step of 850 °C, 1 Pa, and 2 min followed by the secondary growth step of 1000 °C, 0.5 Pa, and 30 min (850 °C 2min-1000 °C 30 min).

As shown in Figure 3.4 (b), the effect of the growth temperature and the carbon source partial pressure on the growth yield of SWCNTs were investigated by recording the G-band observation frequencies of the samples grown at 850 °C and 900 °C and at 0.5 Pa and 1 Pa. The increase in the growth temperature from 850 °C to 900 °C led to a significant improvement in the growth yield. It should be noted that the yield of SWCNTs grown at 900 °C decreases when the partial pressure of C_2H_2 is slightly increased from 0.5 Pa to 1 Pa. At high temperature, the decrease in the growth efficiency with increasing the carbon supply may be related to the deposition of a-C around the growth seeds. Because the growth seed nanoparticles should have a higher surface energy compared to flat SiO_2/Si substrate, a-C is more easily adsorbed on SWCNT growth samples with growth seeds than on blank samples. This explains why almost no D-band appears on the blank samples but a small amount of a-C is deposited on the SWCNT samples (Figure 3.4 (a), dotted line). The increase in partial pressure of the carbon source at the higher temperature of cap formation contributes to the enhanced growth drive, which makes it easier to overcome the activation barrier of SWCNT cap nucleation. Since the higher growth driving force also makes it easier to meet the growth threshold of a-C, a higher temperature accelerates the deposition of a-C. The faster formation of a-C on the growth surface reduces the growth efficiency of the cap structure and hinders its lift-off from the nanoparticle. In the case of growth at higher temperatures above 900 °C, the increase in the carbon source partial pressure enhances the deposition rate of a-C on the surface of the growth seeds. As a result, even if the initial growth was not completed, a part of the growth seeds was inactivated early, which led to a decrease in growth yield.

The effect of the carbon source partial pressure during the initial growth step was examined over a wider range from 0.5 Pa to 5 Pa at 850 °C for 2 min. Figure 3.4 (c) shows the Raman spectra of the samples. At partial pressure of 0.5 and 1 Pa of C_2H_2, weak G band intensities of the samples were observed, indicating that the initial nucleation of SWCNT caps has occurred, but very little SWCNT goes to the next growth stage where the nanotubes fixedly elongate. The intensity of the G- and D-band increased significantly when the partial pressure of C_2H_2 is increased to 2.5 Pa or 5 Pa. The cap structure of SWCNTs is a hemispherical carbon cage, similar to one half of a C_{60} molecule, and no detectable Raman signal is expected to exhibit in the same wavenumber region as the G-

and D-band [131]. Thus, the stronger G- and D-band intensities indicate that most of SWCNTs have already entered into the stationary elongation stage in the case of 2.5 Pa or 5 Pa. Unlike the growth at 900 °C, the surface of the growth seeds remains clean at a slower a-C deposition rate of 850 °C, which allows enough time to complete the nucleation process (Figure 3.4 (a)). At the same time, the increased partial pressure of carbon source oversupplies carbon atoms to the growth seeds during the initial growth step, which leads to an early start of stationary growth even at the lower growth temperature and the formation of defective SWCNTs (Figure 3.4 (c), 2.5 Pa and 5 Pa).

The experimental results on the growth temperature and partial pressure of the carbon source suggest that the initial growth step should be well controlled to achieve a high nucleation efficiency of cap structures, while further stationary growth of SWCNTs should be avoided in this step. Therefore, the initial growth process performed at 850 °C and 1 Pa-C_2H_2 is suitable for further improving the yield of high quality SWCNTs, and is employed in the later experiments. It should be noted that the solid carbon nanoparticles employed as growth seeds in this study do not possess a high catalytic activity, which is quite different from conventional metal catalysts. Hence, the concentration of carbon feedstock has to be controlled with high precision to achieve efficient growth of SWCNTs, especially in the cap nucleation stage.

3.3.3 Two-step growth of SWCNTs and diameter variations

During the SWCNT growth process, the diameter of SWCNTs is mainly determined by the formed cap structure. Therefore, different nucleation rates of SWCNTs with various diameters were indirectly investigated by characterizing the diameter of SWCNT tubes through the radial breathing modes (RBMs) in the Raman spectra (Figure 3.4 (d)). Samples were synthesized only in the initial growth step at 850 °C for 2 min or 10 min. A sample grown with the secondary growth step at 1000 °C for 30 min after initial growth at 850 °C for 2 min was also examined. Comparison of the samples synthesized at 850 °C for 2 min and 10 min indicates that the RBM peaks mainly appear at ~130 cm^{-1}, ~180 cm^{-1}, and ~270 cm^{-1} in the case of 10 min, but the RBM peak appears only at ~130 cm^{-1} in the case of 2 min. This difference represents the growth behavior of

SWCNTs as a function of diameter. The thicker SWCNTs, which showed the RBM peak at 130 cm^{-1}, completed their nucleation and gradually entered into stationary growth within the first two minutes.

About the above mentioned diameter dependence of cap nucleation, we explain it by the regulation of $\Delta\mu$, which is the difference between $\mu_{C(gas)}$ and $\mu_{C(solid)}$. As mentioned in Figure 1.13, the variation of $\mu_{C(gas)}$ and $\mu_{C(solid)}$ is related to growth conditions, including the growth temperature and the partial pressure carbon source. Moreover, the thermodynamic parameters need to be adjusted for different crystal structures of SWCNTs, such as the cap structures and the tube structures with different diameters, which own different strain energy. As reported previously [71], in an actual reaction, reactants in gas phase are not in their standard state, and also strain energy should be considered. Thus, when the temperature is constant, the growth driving force ($\Delta\mu$) for carbon feedstock (for example, C_2H_2) converting into an SWCNT (cap and tube) can be expressed as

$$\Delta\mu = \Delta\mu^{\circ} + \frac{1}{2} k_B T \, ln\left(\frac{P_{C_2H_2}}{P_{H_2}}\right) - \frac{A}{d^2} \qquad (1)$$

where " ° ", k_B, d, $P_{C_2H_2}$, P_{H_2}, and $\frac{A}{d^2}$ represent the standard state, Boltzmann constant, diameter, partial pressure of C_2H_2, partial pressure of H_2, and strain energy, respectively. As a factor partly depended on the SWCNT (cap and tube structures) and the diameter, the strain energy influenced the chemical potential $\mu_{C(solid)}$ of SWCNT. The constant A differs depending on the cap or the tube structure.

Due to the higher strain energy, the cap structure of SWCNTs presents higher $\mu_{C(solid)}$ than the tube structure, which is similar to the higher $\mu_{C(solid)}$ for thinner SWCNTs than thicker SWCNTs. Therefore, under the same growth conditions (temperature and partial pressure of C_2H_2), the $\Delta\mu$ during the stationary elongation of the tube structure is higher than that in cap formation process, and that for thicker SWCNT formation is higher than that for thinner SWCNT formation (Figure 3.5). According to the above discussion, for the initial growth step, $\Delta\mu$ provided by the growth condition must meet the threshold of the driving force required for nucleation of the cap structures. The initial growth step at 850 °C for 2 min, because of the higher $\Delta\mu$, a higher growth efficiency exhibited on

thicker SWCNTs (Figure 3.4 (d), black line). In the case of the only initial growth step, once the nucleation stage is finished, the reduction of $\mu_{C(solid)}$ for the tube increases $\Delta\mu$ for stationary elongation under the same growth condition (Figure 3.6 (a)). Such an increase makes $\Delta\mu$ fit the threshold for elongation of thinner SWCNTs. On the other hand, this increase can also result in a slight excess of $\Delta\mu$ for elongation of thicker SWCNTs, which is above the growth window (Figure 3.6 (b)). This leads to the increased possibility of a-C formation, resulting in a decrease in the efficiency of stationary elongation. This growth mechanism explains the result of the stationary elongation stage after the cap formation stage only with the initial growth step for the longer time (10 min), which shows a delayed formation of thinner SWCNTs with RBM peak at ~270 cm^{-1} and the appearance of stronger RBM peak at ~180 cm^{-1} than that at ~130 cm^{-1} (Figure 3.4 (d), red line). If we consider the two-step growth process, after the initial growth, both the increase in the growth temperature and the decrease in the carbon source partial pressure cause the decrease of $\mu_{C(gas)}$ (Figure 3.6 (c)). Additionally, $\mu_{C(solid)}$ also decreases due to the structural change from a cap to a tube. These decreases make $\Delta\mu$ for stationary elongation during the secondary growth step similar to or lower than that for cap formation during the initial growth step (Figure 3.6 (d)). Such variation of the growth driving force contributes to the stronger RBM peak at ~130 cm^{-1} and almost no RBM peak at ~270 cm^{-1} (Figure 3.4 (d), blue line).

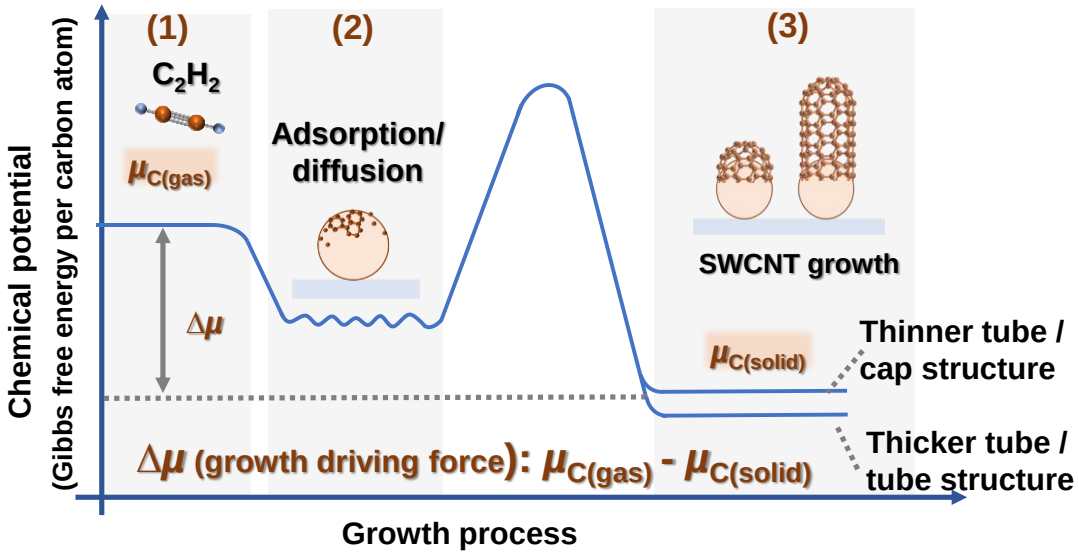

Figure 3.5: Reaction coordinate in the nucleation and growth of SWCNTs for different growth stages and diameters.

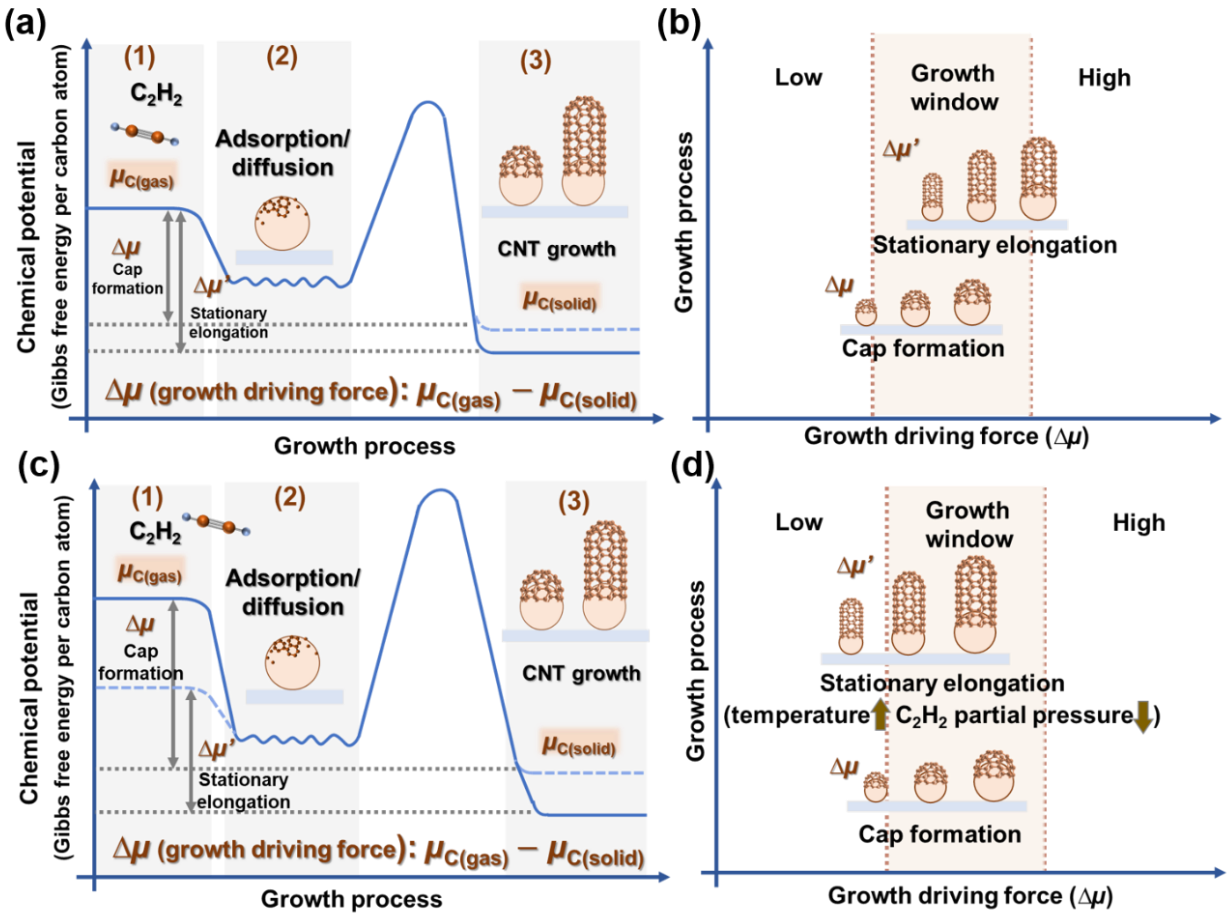

Figure 3.6: (a) Reaction coordinate and different growth driving force for the cap formation ($\Delta\mu$, solid line) and the stationary elongation ($\Delta\mu'$, dotted line) by only initial growth step (fixed growth condition). (b) Schematic of growth driving force variation for the cap formation and the stationary elongation with different diameters by only initial growth step. (c) Reaction coordinate and different growth driving force by the two-step growth. Growth driving force for the cap formation in the initial growth step ($\Delta\mu$, solid line) and the stationary elongation in the secondary growth step ($\Delta\mu'$, dotted line) is shown. (d) Schematic of growth driving force variation for the cap formation and the stationary elongation with different diameters by the two-step growth.

3.3.4 Effect of growth time in the initial growth step

The growth behavior of SWCNTs was also studied by changing the initial growth time. Figure 3.7 (a) and (b) show the Raman spectra of the samples synthesized at 850 °C with the initial growth step of 1 min and 2 min with and without the secondary growth

step of 30 min, respectively. In the case of only initial growth, a small D band appears from the 2 min sample, whereas the D band from the 1 min sample is negligible. Considering that the blank sample does not show a D band (Figure 3.4 (a), black dotted line), a-C deposition does not occur even with 2 min. These results indicate that the D-band from the 2 min sample originates from the defects and that the formation of defects begins after the initial growth of 1 min.

Furthermore, the RBM peaks of the samples synthesized with the secondary growth step at a high temperature exhibit information on the temporal evolution of SWCNTs with different diameters. By conducting the secondary growth step after the initial growth step of 1 min or 2 min, a stronger RBM peak around ~180 cm^{-1} emerges, which represents the extra formation of thinner SWCNTs (Figures 3.7 (a) and (b)). Since SWCNTs are grown from solid nanoparticles which keep stable morphology at high temperature, diameters of SWCNTs are defined at the stage of cap structure formation and should remain unchanged during the later growth stage. Thus, such extra formation of thinner SWCNTs reflects that the higher amount of smaller size cap structures is formed while prolong initial growth time. Compared with the 1-min initial growth, the higher RBM peak intensity at ~180 cm^{-1} for the 2-min initial growth indicates a delay in thinner SWCNT growth. The results confirm the diameter dependence of the nucleation timing of SWCNTs in the cap formation stage, which was discussed for Figure 3.4 (d) previously.

Besides, growth rate of SWCNTs with different thickness can be discussed. As shown in Figures 3.7 (a) and (b), RBM peak around ~130 cm^{-1} appears in 1 min and 2 min initial growth step when there is no thinner SWCNT formed. This growth delay indicates the slower growth rate of thinner SWCNTs than that of thicker SWCNTs from carbon solid nanoparticles.

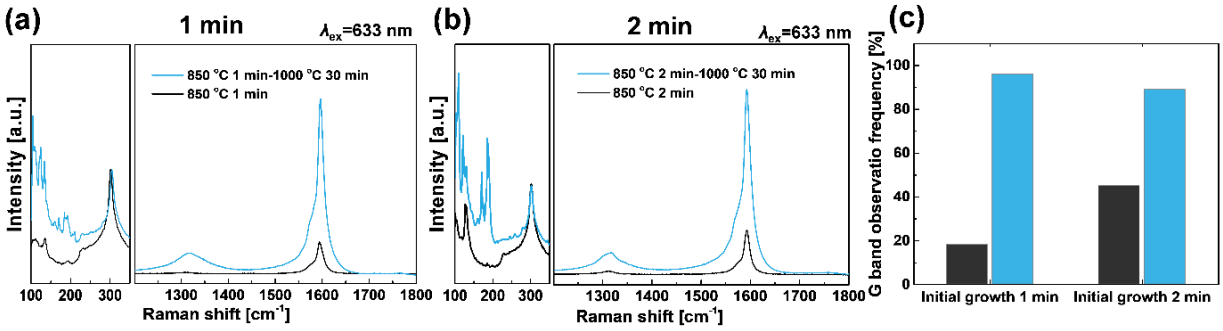

Figure 3.7: (a, b) Raman spectra of SWCNTs grown with different initial growth times of (a) 1 min and (b) 2 min at 850 °C and 1 Pa, with (blue line) and without (black line) the secondary growth step at 1000 °C and 0.5 Pa for 30 min. (c) G band observation frequency of the four samples with (blue bar) and without (black bar) the secondary growth step.

The growth yield variation upon adjusting initial growth time is displayed in Figure 3.7 (c). Compared with the 1-min initial growth, a smaller increase in the G band observation frequency before and after the secondary growth step is observed for the initial growth of 2 min. This is presumably because the initial growth of SWCNTs for 2 min induces some deposition of a-C around ND particles, reducing the growth efficiency in the subsequent growth step.

3.3.5 Water vapor injection during two-step growth

As the growth temperature increases, it becomes more difficult to avoid the formation of a-C on the surface of growth seeds. The formation of a-C hinders further growth of SWCNTs just by adjusting the supply rate of carbon feedstock. To prevent the deposition of a-C, water vapor [33, 121] was used to eliminate such deposition via an oxidization reaction. The etching result was analyzed while controlling the injection time and partial pressure of water vapor. As schematically shown in Figure 3.8 (a), the etchant injection time was divided into three cases: the addition of water vapor at the beginning of the initial growth step (Figure 3.8 (a), process 1), the addition of the etchant at the beginning of the temperature rising step (process 2), and the water vapor addition at the beginning of the secondary growth step (process 3). Additionally, the etchant concentration was separately controlled during the temperature rising step and the

secondary growth step. Here, samples are named according to the three values of the water vapor pressure for processes 1, 2, and 3. For example, a sample grown without water vapor during processes 1 and 2 and with the addition of water vapor at 0.15 Pa during process 3 is represented by 0-0-0.15 Pa. As for the other growth parameters, the optimized conditions in the previous section were employed for the initial growth strep (850 °C with 1 Pa C_2H_2 for 1 min) and the secondary growth step (1000 °C with 0.5 Pa C_2H_2 for 30 min).

The decrease in the D band intensity with the injection of etchant demonstrates that water vapor helps prevent the formation of a-C, although the timing of water vapor injection affects the quality (I_G/I_D ratio in Figure 3.8 (b)) and quantity (G band observation frequency in Figure 3.8 (c)) of SWCNTs. Compared with the case in which water vapor is injected from the secondary growth step (0-0-0.15 Pa), the case in which the injection time is set at the beginning of the temperature rising step (0-0.15-0.15 Pa) exhibits a higher purity of SWCNTs with a smaller a-C deposition, as indicated by the lower D band intensity. It should be noted that the effect of the water vapor concentration was separately examined for the case of water vapor injection from the secondary growth step (Figure 3.9). As Figure 3.9 shows, even when varying the concentration, water vapor cannot etch all the deposited a-C. a-C may be partly formed before the water vapor injection time during the period where temperature rises to 1000 °C.

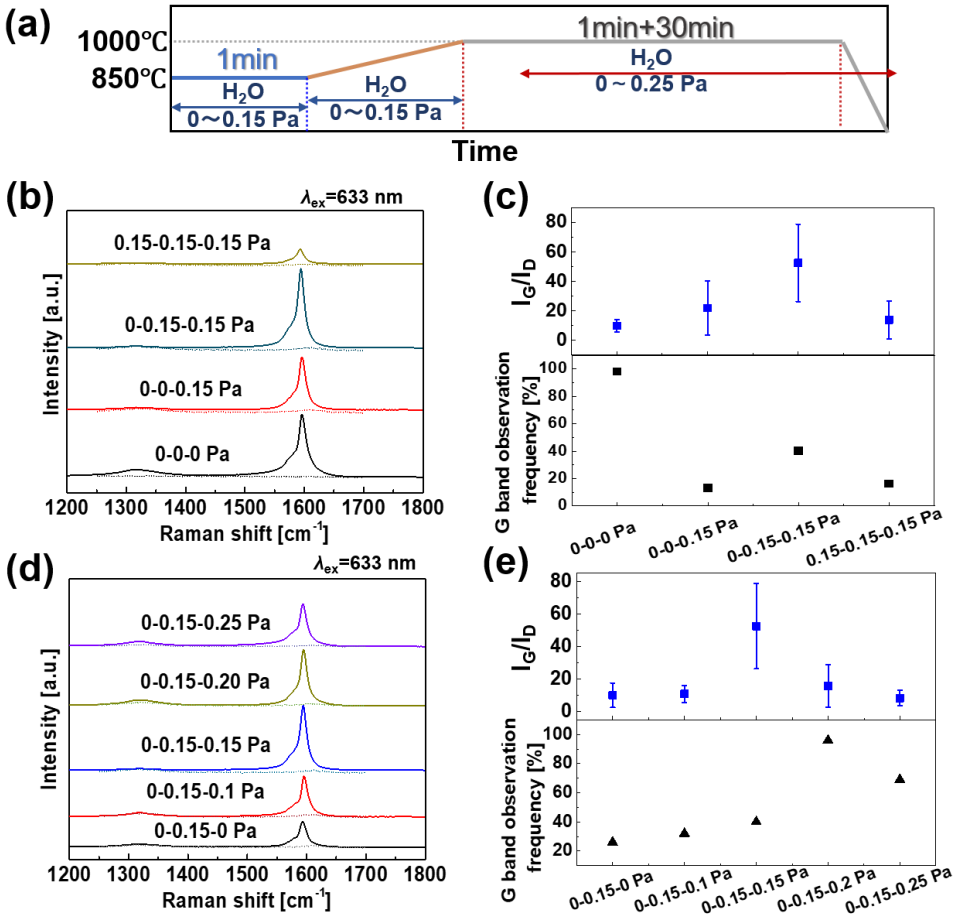

Figure 3.8: (a) Profiles of temperature and water vapor partial pressure for the SWCNT two-step growth process with water vapor injection. (b) Raman spectra of SWCNTs grown with different timings of water vapor supply: without water vapor throughout the processes (0-0-0 Pa), without water vapor during the temperature rising step and supplying it during the secondary growth step at 0.15 Pa (0-0-0.15 Pa), supplying water vapor both during the temperature rising step and the secondary growth step at 0.15 Pa (0-0.15-0.15 Pa), and supplying water vapor during whole process at 0.15 Pa (0.15-0.15-0.15 Pa). Growth temperature, partial pressure of C_2H_2, and growth time for the initial growth step are fixed at 850 °C, 1 Pa, and 1 min, respectively, while those for the secondary growth step are 1000 °C, 0.5 Pa, and 30 min, respectively. Dotted lines denote Raman spectra of the blank samples. (c) G band observation frequency and I_G/I_D ratio of the same samples as (b), which reflect the SWCNT yield and quality, respectively. Standard deviation was also calculated and presented as the error bar of averaged I_G/I_D. (d) Raman spectra of SWCNTs grown with different partial pressures of water vapor for both the temperature rising step and the secondary growth step. Dotted lines denote Raman spectra of blank samples. (e) Corresponding G band observation frequency and I_G/I_D, which reflect the SWCNT yield and quality, respectively. Standard deviation was also calculated and presented as the error bar of averaged I_G/I_D

Water vapor was also injected from the beginning of the initial growth step (0.15-0.15-0.15 Pa). Compared with water vapor injection from the end of the initial growth step, the case where water vapor participated in the whole growth process exhibits an obvious decrease in the growth yield according to the G band observation frequency and the G band intensity. Such a reduction of the growth yield reflects the negative effect of water vapor on SWCNT nucleation. It has been reported that the cap of SWCNTs is more easily oxidized and consequently destroyed than the sidewall due to the strain and the pentagonal rings of the cap structure [132]. These results indicate that the starting time of etchant injection should begin as soon as possible once the formation of cap structures is finished when etchant is employed in a solid carbon seed-based growth system to prevent a-C deposition and to enhance growth yield.

The I_G/I_D ratio in Figure 3.8 (d) and the G band observation frequency in Figure 3.8 (e) show the effect of water vapor etching as a function of partial pressures on the quality and quantity of SWCNTs. While the partial pressure of water vapor during the temperature rising step was fixed at 0.15 Pa, that during the secondary growth step at 1000 °C was varied from 0 Pa to 0.25 Pa. From 0 Pa to 0.15 Pa (0-0.15-0 Pa, 0-0.15-0.1 Pa, and 0-0.15-0.15 Pa), both I_G/I_D and the G band observation frequency show a rising tendency with the partial pressure, indicating efficient etching of a-C induced by the participation of water vapor. On the other hand, increasing the partial pressure to 0.2 Pa (0-0.15-0.2 Pa), even though growth yield is further increased, the quality of SWCNTs decreases considerably, and both the quality and the yield decrease when the partial pressure continues to increase to 0.25 Pa (0-0.15-0.25 Pa)). Since no obvious D band appears in the Raman spectra of the relevant blank samples, the D band of the SWCNTs grown with water vapor of 0.2 and 0.25 Pa is attributed not to a-C but to the formation of structural defects of SWCNTs. Similar to a previous study using metal nanoparticles [133], this result suggests that an excess of water vapor damages the SWCNT structures during the growth process but it keeps the surface of growth seeds free from a-C and enhances the SWCNT yield. In addition, as mentioned earlier, a further increase of SWCNT yield appeared in the case of excessive water injection concentration (0-0.15-0.2 Pa), in which the quality of SWCNTs decreased. This phenomenon in the VSSS growth mode brings the possibility to discuss the etching site by water vapor; that is a-C

on carbon growth seeds or the edges of SWCNTs. If we assume the edge of newly-grown SWCNTs is preferentially etched by water, the growth rate would be sensitive to etchant concentration and more likely to decrease once the partial pressure of water vapor is increased to more than 0.15 Pa. However, the experiment provided an opposite result, an increased yield of SWCNTs. Thus, we speculate that water vapor tends to etch a-C randomly on the growth seeds surface. Further study is needed to elucidate the atomistic mechanism of water in the VSSS mode in future.

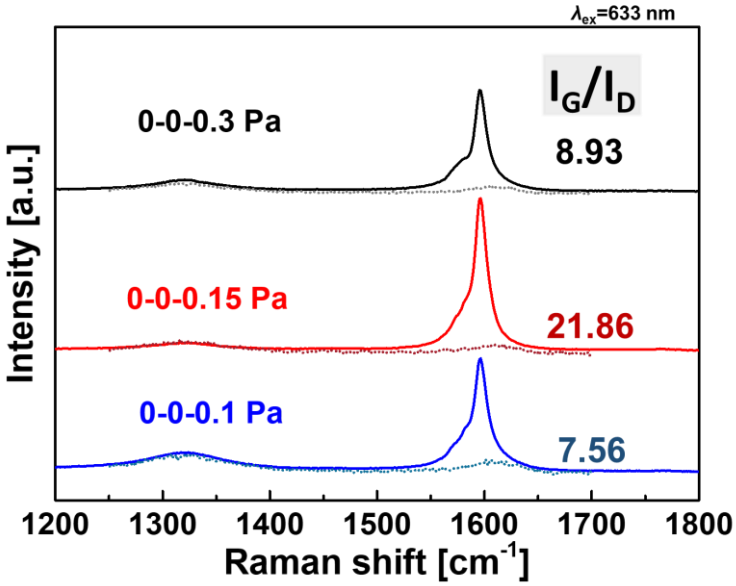

Figure 3.9**:** Raman spectra of SWCNTs grown with different partial pressures of water vapor added at the beginning of the secondary growth step. Dotted lines represent the Raman spectra of blank samples.

The interpretation of the growth results with the water vapor addition provides a practical direction for efficient growth of SWCNTs from solid growth seeds. Through the reaction between water vapor and a-C, excessive deposition of carbon source on the growth seed surface is controlled, which therefore enhanced the lifetime of growth seeds. The addition of water vapor just after the formation of cap structures and the precise adjustment of the concentration of etchant are keys to obtain high-quality SWCNTs with a high yield.

3.3.6. Yield and quality of SWCNTs synthesized under different growth conditions

Figure 3.10 (a) compares the yield and the quality of SWCNTs grown under various conditions from solid carbon particles as growth seeds. Compared with previous research on one-step growth at 1000 °C [129], cap engineering using the two-step growth process developed in this study significantly improves the growth yield, although the deposition of a-C, which reduces I_G/I_D, remains. To solve this impurity problem, water vapor was employed as an etchant to keep the surface of growth seeds clean. We successfully obtained highly crystalline SWCNTs with a higher growth yield, which have I_G/I_D of ~52 and a G band observation frequency of 40%. The value of the G band observation frequency demonstrates a significant improvement from the previous work of 4% [129]. This result demonstrates the effectiveness of the two-step growth process combined with water vapor addition.

Figures 3.10 (b) shows SEM image of SWCNTs grown by the two-step growth process with water vapor injection. Supported by carbon nanoparticle seeds (light gray particles in Figs. 3.9 (b)), SWCNTs with a length of a few micrometers are observed. The SWCNT density of the samples well corresponds to the values of the G band observation frequency. It should be noted that the length of SWCNTs is limited by the relatively low efficiency of SWCNT growth at a high temperature. Based on the present achievement to enhance the cap formation, future studies on prolonging growth lifetime of SWCNTs from solid carbon nanoparticles should further improve the length and the yield of high-crystallinity SWCNTs.

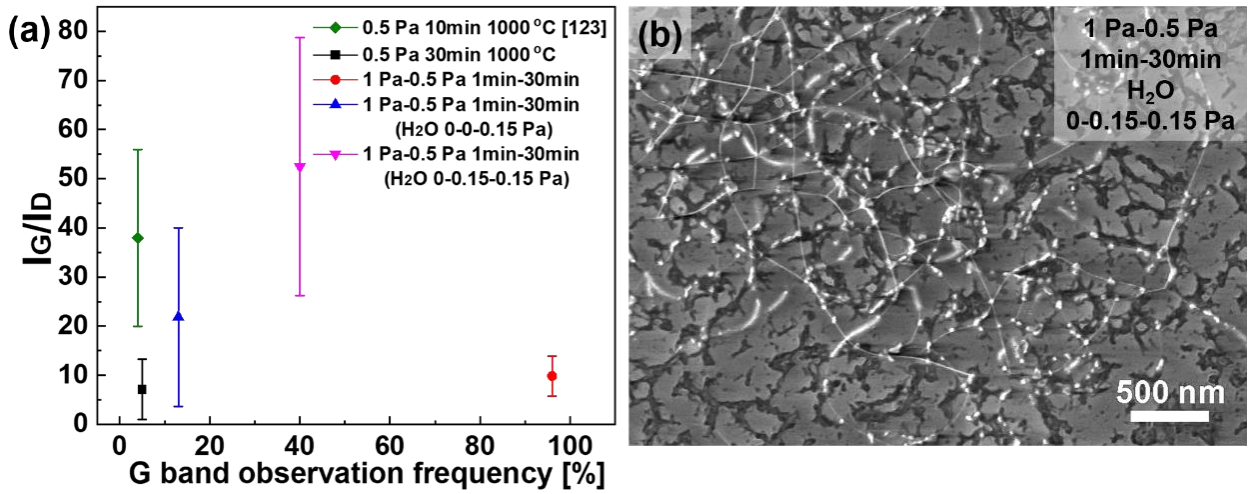

Figure 3.10: (a) Variations of the growth yield (G band observation frequency) and quality (I_G/I_D ratio) of SWCNTs according to the control of the initial growth conditions and the addition of water vapor in the high temperature synthesis procedure. Standard deviation was also calculated and presented as the error bar of averaged I_G/I_D. (b) SEM image (acceleration voltage: 5 kV) of SWCNTs grown from two-step growth with water vapor injection, where the initial growth step is conducted at 850 °C and 1 Pa for 1 min followed by the secondary growth step at 1000 °C and 0.5 Pa for 30 min. Water vapor was injected with 0.15 Pa from the beginning in the temperature rising step.

3.4. Conclusion

In conclusion, we developed a cap formation-engineered two-step growth process of SWCNTs from solid carbon nanoparticles at a high temperature by considering the growth driving forces in different growth stages. We successfully grew highly crystalline SWCNTs with improved yields. In this growth system, we mainly concentrated on the initial growth efficiency, which significantly influences the quality and quantity of the resulting SWCNTs. To fit the higher growth driving force needed for cap structure formation, a higher partial pressure of carbon source was selected for the initial growth step. The effects of growth temperature and time for the initial growth step were also systematically examined to prevent the deposition of a-C and to control the formation of SWCNT caps. After achieving a higher nucleation density of the cap structures, stationary elongation of SWCNTs was conducted by a secondary growth step. Furthermore, the

deposition of a-C at high temperatures was eliminated by supplying an etchant, water vapor, to the growth system. By investigating the injection time and the concentration of water vapor, we optimized the condition for efficiently removing a-C while preserving the nucleation of the cap structures. We significantly improved the growth yield, as evidenced by the increase of the G band observation frequency from 4% to 40% while maintaining a high I_G/I_D ratio of 52. Our results provide a rational guideline to synthesize high quality SWCNTs using high temperature-stable solid carbon nanoparticles as growth seeds, and will enable various high-end applications based on SWCNTs that are free from defects and a-C.

In this research, as one of the growth etchants, H_2O was applied in the catalyst-free high temperature growth process and expressed its high efficient in a-C etching. However, the strong etching ability of H_2O also brings a shortage to the H_2O-injected growth process. As shown in section 3.3.5, the concentration of H2O should be kept in ppm level carefully to prevent the defect formation on SWCNTs by the existence of excess H_2O. Therefore, in the next research, we further studied the growth enhancers which could be used in such high temperature system to prevent a-C deposition and achieve high yield SWCNTs with high purity.

Chapter 4: Growth enhancers injection in single-walled carbon nanotube growth process

Combination effect of growth enhancers and carbon sources on synthesis of single-walled carbon nanotubes from solid carbon growth seeds

4.1 Background

To achieve highly crystalline SWCNTs, a high temperature has been recommended for the CVD process because it assists SWCNTs in overcoming the activation energy of defect healing during growth [21, 71]. Along with the increase in growth temperature, the selection of growth seeds that possess high-temperature stability is a necessary factor for the synthesis of highly crystalline SWCNTs. Unfortunately, traditional metal catalysts, such as iron [107, 108], nickel [109], cobalt [110], and related alloys [111], cannot avoid aggregation because of their low melting point [75, 134]. Moreover, even though they could be used as solid catalysts, e.g., W [135], Mo [135], Re [135], and TiC [136], metal nanoparticles are regarded as an impurity in some applications and must be removed through post-treatment procedures, which causes damage to the as-grown SWCNTs [112]. Non-metallic nanoparticles, such as Si [113], SiC [113], Ge [113], and nanodiamond (ND) [69, 70], which possess desirable high melting points, have gradually attracted attention as alternative growth seeds of CNTs. Among these growth seeds, ND [69] possesses the notable advantage of avoiding the introduction of unnecessary elements owing to its composition, i.e., carbon.

Another important point to be considered in the CVD procedure is the deposition of amorphous carbon (a-C). As a byproduct formed during SWCNT growth, a-C is adsorbed on the surface of growth seeds and the nanotube sidewall. This results in blocking of the active sites of the seeds and shortening of growth lifetime, which decreases the synthesis efficiency [137]. In a metal-catalyzed CNT growth system, to prevent the formation of a-C, some types of oxidants were employed as growth enhancers to etch away a-C. Water (H_2O)-assisted CVD methods helped realize the growth of millimeter-long SWCNTs by maintaining the activity of the metal catalyst by selectively

removing the deposited a-C on its surface [33]. In addition, as the etchant, H_2O exhibited its role in CNT growth kinetics [86, 87]. However, the strong oxidation activity of H_2O limits the supply of the enhancer to the ppm level, while a low concentration results in loss of uniformity of the enhancer in a large-scale reactor [133]. Further, a high concentration of H_2O leads to the possibility of etching of both a-C and CNTs [138]. To date, carbon dioxide (CO_2)—another known growth enhancer with less oxidative activity—has been employed with a higher concentration to induce oxidation reactions [78-85]. A mild etching effect is the advantage of CO_2 in balancing a-C etching and the preservation of CNTs from damage during the mass production of CNTs.

Recently, other enhancing roles of CO_2 in metal-catalyzed CNT growth processes have been found when using acetylene (C_2H_2) [81, 139] or methane (CH_4) [140] as the carbon feedstock. One of its roles is to promote the dehydrogenation reaction of hydrocarbons, which are used as a carbon source in CNT growth. For synthesizing CNTs via CVD, the carbon source is flown into the reactor and the deposition process proceeds with pyrolysis reactions—including the dehydrogenation reaction—to form the intermediate products, which adsorb on the surface of catalysts or growth seeds and are used to construct the CNT structure. When a carbon source such as C_2H_2 was mixed with CO_2 in an equimolar ratio, a dramatic increase in the CNT growth yield and initial growth rate was observed [81]. To prove the occurrence of the CO_2-promoted hydrocarbon dehydrogenation reaction, further evidence was provided through a theoretical calculation. When C_2H_2 was taken as the carbon source, with the injection of CO_2, the calculated energy barrier of the dissociation of the first H atom from C_2H_2 decreased [139].

Despite progress in the use of growth enhancers in metal-catalyzed growth, enhancer effects on SWCNT growth from non-metallic seeds have been scarcely studied, mainly due to the originally low efficiency of SWCNT growth particularly at high temperatures. We recently realized high-temperature SWCNT growth using ND-derived nanoparticles, which we hereafter call carbon nanoparticles (CNPs), as solid growth seeds [141]. The CNPs were prepared by transforming ND at high temperature, as will be described in detail in Method section. To efficiently obtain highly crystalline SWCNTs from the CNPs, we developed a two-step growth process [141]. In this process, the condition of the initial and secondary growth steps was separately adjusted to provide a

suitable growth-driving force for SWCNT cap formation [142] and stationary nanotube elongation, respectively. We also reported a preliminary result on the etching of a-C by H_2O in a CNP-based growth system [141]. A more thorough study on growth enhancers, focusing on a combination with different carbon sources, will be beneficial for understanding the mechanism of SWCNT growth from the unconventional growth seeds and realizing the efficient growth of structure-controlled and high-quality SWCNTs.

In this research, to understand the effects of enhancers on SWCNT growth from the CNPs, we systematically conducted SWCNT growth with the injection of CO_2 and H_2O in C_2H_2- and ethylene (C_2H_4)-supplied SWCNT growth processes at high temperatures. The effects of CO_2 were first examined in a simple one-step growth process with the supply of C_2H_4 or C_2H_2 by changing the concentration and the supply delay of CO_2. The comparison of the results with the previous results on H_2O revealed the similarities and differences in the roles of the two growth enhancers including the oxidation activity. Remarkably, CO_2 in combination with C_2H_2 enhanced a-C deposition as well as SWCNT growth, which revealed the occurrence of the dehydration reaction. We then applied CO_2 and H_2O into the two-step growth process where the efficient growth of high quality SWCNTs was realized [141]. In addition to the concentration dependence of the enhancers, the change in the quality and yield of SWCNTs along the growth steps were investigated with different combinations of the growth enhancers and the carbon sources. We discuss the mechanism of the growth enhancers based on the change in chemical potential considering the dehydrogenation reaction between C_2H_2 and CO_2 as well as the oxidation reaction.

4.2 Experimental Section

4.2.1 Preparation of growth seeds

Figure 4.1 illustrates the entire process of SWCNT growth. As the starting material of growth seeds for SWCNTs, purified ND particles prepared via the detonation method [125] were dispersed in ethanol (2.0 wt%). The diameter of the ND particles was originally 10 nm, which was reduced to a smaller size in the following process and shown in Figure 3.2. The impurity concentration of the ND particles was 2100, 80, and 6–20

ppm for Zr, Fe, and Pd, respectively. The SWCNTs were confirmed to grow from the ND-derived CNPs instead of the metal impurity contained in ND [141].

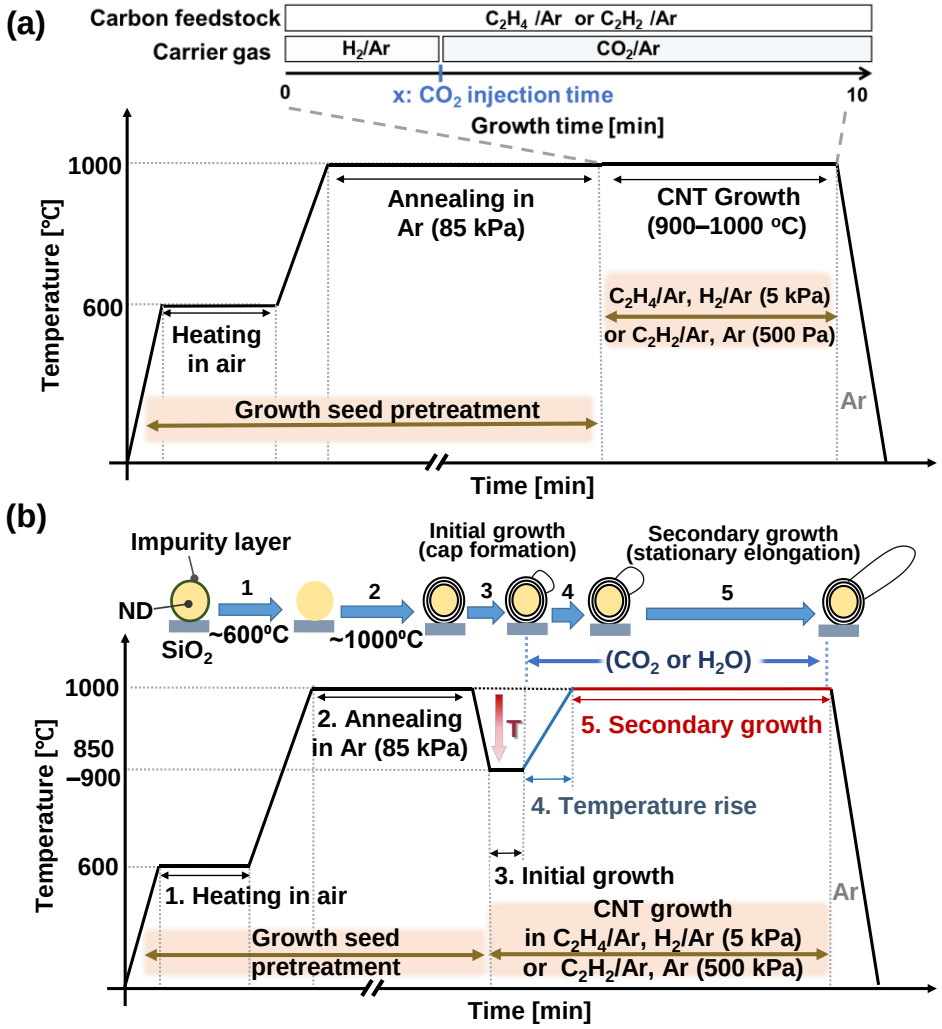

Figure 4.1: (a, b) Temperature profiles of the reaction furnace for (a) one-step growth process and (b) two-step growth process as a function of processing time. (a) The top part shows the gas composition profile during SWCNT growth. In the C_2H_4-supplied case, the variation of the CO_2 injection time (x = 0, 2, 5, 7, and 10 min) during the growth process was included. (b) The top part shows a schematic diagram of the two-step growth process of SWCNTs from the CNP growth seeds.

To support the growth seeds, ~10-mm^2 Si substrates with a 300-nm-thick thermal oxide layer were used. The substrates were cleaned via an ozone treatment process (L-UV253, Japan Electronics Industry) by flowing 6 L/min O_2 for 5 min under ultraviolet light for 60 min, followed by exhausting with 6 L/min N_2 for 5 min. After the cleaning of the Si substrates, 20 μl of the ND solution treated with ultrasonication was dropped on

the surface of the substrates. Additionally, the same cleaned Si substrates without any growth seeds were used as a reference (hereafter called blank samples) to compare the amount of a-C deposited directly on them and on the SWCNT samples.

4.2.2 One-step growth process with CO_2 injection

To transform ND particles into the CNPs which are suitable for the growth seeds, pretreatment was conducted before the one-step and two-step SWCNT growth processes. The pretreatment of the growth seeds and the synthesis of SWCNTs were performed in a tubular CVD furnace (GE-1000, GII Techno) where a quartz tube chamber was used to load the substrates. The quartz tube chamber was designed to have a semicircular cross section with a diameter of 43.6 mm and heating-zone length of 890 mm. The substrates were placed at the center of the quartz tube chamber and treated with the surface-cleaning process in air for 10 min at 600 °C (Figure 4.1 (b), process 1). During this process, the diameter of ND was reduced to 2–3 nm, which is appropriate for SWCNT growth [141]. In the following annealing procedure, the heating temperature was gradually increased to 1000 °C and maintained for 1 h in Ar at 85 kPa with 20-sccm Ar injection. During this step, the surface of ND (sp^3 carbon) changed into more stable graphitic shells (sp^2 carbon), called carbon nano-onion structure [127, 128]. We used the CNPs possessing this structure as the growth seeds.

After the annealing process, SWCNTs were synthesized with two types of carbon feedstocks: C_2H_2 (2%)/Ar and C_2H_4 (2%)/Ar. Considering the difference in the thermal decomposition behaviors of C_2H_2 and C_2H_4 [143, 144], the synthesis condition was adjusted to fit the SWCNT growth from each carbon feedstock.

When using C_2H_4 as the carbon feedstock, SWCNTs were synthesized at 1000 °C for 10 min with a mixture of 2-sccm C_2H_4/Ar and 18-sccm CO_2/Ar while the total pressure was kept at 5 kPa, corresponding to a C_2H_4 partial pressure of 10 Pa. During the growth process, the partial pressure of CO_2 was varied from 0 to 180 Pa by changing the flow rates of CO_2 and Ar individually. When the partial pressure of CO_2 was 0 Pa, the carrier gas was H_2 (3%)/Ar instead of CO_2/Ar, for the usual condition for the SWCNT growth without a growth enhancer. In addition, in C_2H_4-supplied growth, CO_2 injection time was

controlled. Figure 4.1 (a) shows that the start time (x min) for the injection of CO_2 at 140 Pa was varied as 0 (added from the beginning of the growth), 2, 5, 7, and 10 min (no CO_2 addition). Upon completion of the growth process, gas flows were switched to 20-sccm Ar and the temperature was decreased to room temperature while the total pressure was maintained at ~57 Pa.

When using C_2H_2 as the carbon feedstock, SWCNTs were synthesized at 900 °C for 10 min with a mixture of 1-sccm C_2H_2/Ar and 19-sccm CO_2/Ar. Since C_2H_2 is highly active, the total pressure was kept at 500 Pa, corresponding to a C_2H_2 partial pressure of 0.5 Pa, which is lower than the case of C_2H_4. During the growth process, the partial pressure of CO_2 contained in the 19-sccm CO_2/Ar was varied from 0 (0%) to 0.25 Pa (0.05%) by changing the flow rates of CO_2 and Ar individually. When the partial pressure of CO_2 was 0 Pa, the carrier gas was 19-sccm H_2 (3%)/Ar instead of 19-sccm CO_2/Ar.

4.2.3 Two-step growth process with CO_2 or H_2O injection

As reported in the previous study [141], the SWCNT yield for growth at high temperatures is considerably increased by the two-step growth process. Therefore, we employed the two-step growth process in this study as well. As shown in Figure 4.1 (b), before the two-step growth, the pretreatment of the growth seeds is needed (process 1 for heating in air and process 2 for annealing in Ar). Then, the two-step growth process starts, including the initial growth step (process 3 for cap formation), the temperature-rising step (process 4), and the secondary growth step (process 5 for the stationary elongation). After the 1-h annealing process at 1000 °C (process 2 in Figure 4.1 (b)), C_2H_2 (2%)/Ar and C_2H_4 (2%)/Ar were used as the carbon feedstock, and the growth condition was adjusted for each growth step and feedstock. H_2O or CO_2 was added as the growth enhancer after the initial growth stage (process 3 in Figure 4.1 (b)). Because the injection of H_2O in C_2H_2-supplied growth has been studied in our previous work [141], the other three combinations of the feedstocks and enhancers were conducted in this study.

In the C_2H_2-supplied two-step growth process, the initial growth step was held at 850 °C for 1 min with a mixture of 2-sccm C_2H_2/Ar and 18-sccm H_2/Ar while the total pressure was maintained at 500 Pa, corresponding to a C_2H_2 partial pressure of 1 Pa.

When the initial growth step was finished, the growth temperature was set to 1000 °C and the mass flow rate was adjusted to 1-sccm C_2H_2/Ar and 19-sccm CO_2/Ar, where the partial pressure of C_2H_2 was 0.5 Pa. The partial pressure of CO_2 added during the temperature-rising step (process 4 in Figure 4.1 (b)) was optimized to 0.05 Pa. Once the temperature reached 1000 °C, the secondary growth step began. The partial pressure of CO_2 was varied from 0.1 to 0.5 Pa by individually controlling the flow rates of CO_2 and Ar while the mass flow was maintained at 1-sccm C_2H_2/Ar and 19-sccm CO_2/Ar. When choosing H_2O as the growth enhancer, which has been studied in the previous work [141], the partial pressure of injected H_2O during the temperature-rising step was optimized to 0.15 Pa. Once the temperature reached 1000 °C, the secondary growth step commenced. The partial pressure of H_2O was maintained at 0.15 Pa while the mass flow was maintained at 1-sccm C_2H_4/Ar and 19-sccm H_2O/Ar. For comparison, the supply of 19-sccm CO_2/Ar or H_2O/Ar was replaced with that of 19-sccm H_2 (3%)/Ar to realize SWCNT growth without growth enhancers.

In the C_2H_4-supplied two-step growth process, the initial growth step was held at 900 °C for 1 min with a mixture of 4-sccm C_2H_4/Ar and 16-sccm H_2/Ar while the total pressure was kept at 5 kPa, corresponding to a C_2H_4 partial pressure of 20 Pa. When the initial growth step was finished, the growth temperature was set to 1000 °C and the mass flow was adjusted to 1-sccm C_2H_4/Ar and 19-sccm CO_2/Ar, where the partial pressure of C_2H_4 was 5 Pa. Similar to the aforementioned C_2H_2-supplied case, the growth enhancer (H_2O or CO_2) was injected when the initial growth step was finished. The partial pressure of CO_2 added during the temperature-rising step was optimized to 2 Pa. Once the temperature reached 1000 °C, the secondary growth step commenced. The partial pressure of CO_2 was varied from 2 to 62.5 Pa while the mass flow was maintained at 1-sccm C_2H_4/Ar and 19-sccm CO_2/Ar. When choosing H_2O as the growth enhancer, the partial pressure of injected H_2O during the temperature-rising step was optimized to 1 Pa. Once the temperature reached 1000 °C, the secondary growth step started. The partial pressure of H_2O was varied from 0 to 1.5 Pa while the mass flow was maintained at 1-sccm C_2H_4/Ar and 19-sccm H_2O/Ar. For comparison, the injection of 19-sccm CO_2/Ar or H_2O/Ar was replaced with that of 19-sccm H_2 (3%)/Ar to realize SWCNT growth without growth enhancers.

4.2.4 Structure characterization and yield evaluation of synthesized SWCNTs

We analyzed the structure of the synthesized SWCNTs using Raman spectroscopy. A Raman spectrometer (LabRAM HR800, HORIBA Jovin Yvon) was used with an excitation wavelength λ_{ex} of 633 nm. The laser spot size was approximately 0.9 μm, and the laser power was approximately 7 mW at the measurement point. The exposure time of each measurement spot was 1 s for 5 cycles. Raman spectra of 30 randomly selected spots with SWCNT signal were collected from each sample, and the averaged spectra were used for the analysis. The quality of formed SWCNTs was evaluated using the intensity ratio of the G-band (~1590 cm^{-1}) to the D-band (1330–1360 cm^{-1}), which was represented as I_G/I_D [93]. In most of the SWCNT growth situations, the density of SWCNTs was low in the high-temperature synthesis case and the G-band was occasionally not observed. Thus, the growth yield of SWCNTs was evaluated through the G-band observation frequency (GOF), that is, the number of appearances of the G-band in the measured spectra divided by the total number of measurements. Notably, in some growth cases, the density of SWCNTs was high and the GOF was approximately 100%, so that the difference of the growth yield could not be reflected by the changes in the GOF. In such a situation, the SWCNT quantity was evaluated by comparing the intensity ratio of the G-band (~1590 cm^{-1}) with the Raman peak from Si substrates (~520 cm^{-1}), which was represented as I_G/I_{Si}. Typically, Raman spectra of 100 randomly selected spots (with or without SWCNT signal) were collected for the evaluation of the GOF. More measurement spots were used to determine the GOF than that for averaging Raman spectra to ensure the accuracy of the GOF even for samples with low-density SWCNTs. Scanning electron microscopy (SEM) (NVision, Carl Zeiss and S-4800, Hitachi) was used for morphology observations of SWCNTs with an acceleration voltage of 1–5 kV.

4.3 Results and Discussion

4.3.1 Effects of CO_2 on C_2H_4-supplied one-step growth

To investigate the effect of growth enhancers on SWCNT growth without metal catalysts, CO_2 was injected in the high-temperature synthesis process with the CNPs as

the growth seeds and different carbon feedstocks, namely, C_2H_2 and C_2H_4. Figure 4.2 depicts the variation of SWCNT yield and quality for various concentrations of CO_2 input into the C_2H_4-supplied growth processes.

By injecting CO_2 from the beginning of the growth, the SWCNTs were synthesized from C_2H_4 at 10 Pa and 1000 °C for 10 min. The Raman spectra shown in Figure 4.2 (a), which are normalized to the Si peak intensity at ~520 cm^{-1}, show the variation of the D-band and G-band with the injection of CO_2 at different partial pressures (0–180 Pa). The quality (I_G/I_D ratio) and quantity (GOF) of SWCNTs are shown in Figure 4.2 (b). In addition, the I_D/I_{Si} ratio of the SWCNT and blank samples shown in Figure 4.2 (b) helps to distinguish the origin of the D-band: a-C deposited on samples or defects in SWCNT lattices. In the blank samples, since no SWCNTs are grown, the I_D/I_{Si} ratio reflects only the degree of a-C formation under the growth condition. If a-C is deposited on a blank sample, a similar or higher density of a-C should be deposited on an SWCNT sample under the same condition due to the curvature of nanotubes and the increased surface area of the sample. If a-C is not deposited on a blank sample, a-C deposition on an SWCNT sample should be very low or negligible under the same condition. Upon the addition of CO_2, the grown SWCNTs exhibit a decrease in D-band intensity and a slight change in G-band intensity (Figure 4.2 (a)). An improvement in the SWCNT quality is apparently revealed by the increase in the I_G/I_D ratio (Figure 4.2 (b)). The decreasing tendency observed in the I_D/I_{Si} ratio from the blank samples represents the decrease in a-C. A similar tendency is exhibited by the I_D/I_{Si} ratio from the SWCNT samples, and finally the I_D/I_{Si} ratio is close to that of the blank samples. These results prove that the origin of the D-band from the SWCNTs should be mostly from a-C, and with the injection of CO_2, a-C deposition is gradually prevented. The averaged I_G/I_D ratio reached approximately 100 when the partial pressure of CO_2 was adjusted to 160 Pa. With further increase in the partial pressure of CO_2 to an excess value, 180 Pa, the I_D/I_{Si} ratio did not increase in the blank samples but did slightly increase in the SWCNT samples. Thus, the increase in the I_D/I_{Si} ratio in the SWCNT samples reflects the formation of defects. Meanwhile, the yield of SWCNTs shown as the GOF in Figure 4.2 (b) exhibited a small reduction with the injection of CO_2, until an excess amount of CO_2 (180 Pa) was added. The variation in the growth yield indicates that the injection of CO_2 also influences the growth efficiency of

SWCNTs. This growth result indicates the potential of CO_2 in preventing the deposition of a-C at high temperatures. Additionally, the slight formation of defects even with excess CO_2 confirms the mild etching ability of CO_2.

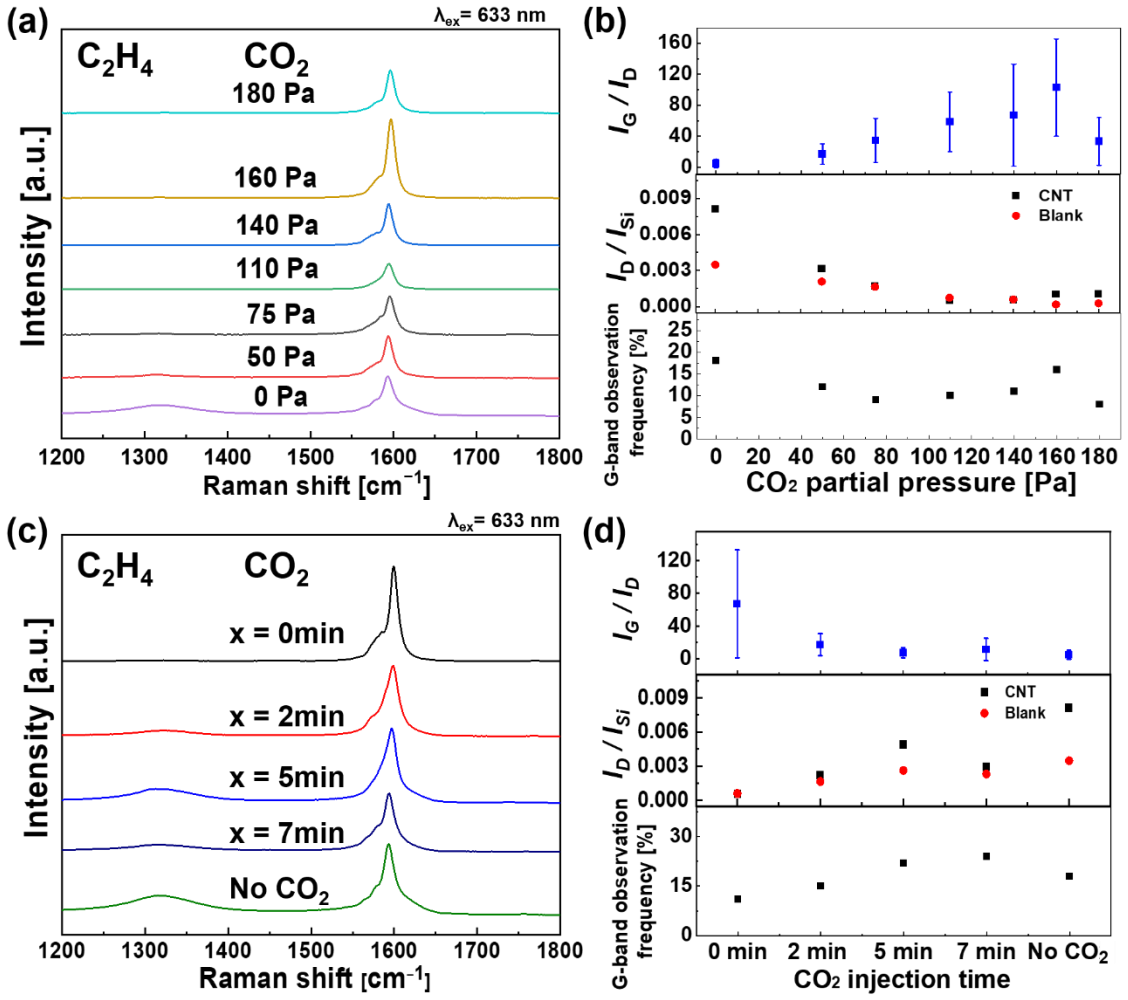

Figure 4.2: (a) Raman spectra of SWCNTs obtained by one-step growth from C_2H_4 with different partial pressures of CO_2 injected from the commencement of growth. (b) GOF, I_D/I_{Si} ratio, and I_G/I_D ratio of the same samples as (a). The error bars presented in the I_G/I_D plot represent the standard deviation of the value from different measurement spots. I_D/I_{Si} was plotted for the blank samples as well. (c) Raman spectra of SWCNTs grown with different delay of CO_2 supply at 140 Pa: 0, 2, 5, and 7 min (indicated as x), and without CO_2 addition (No CO_2). (d) Corresponding GOF, I_D/I_{Si}, and I_G/I_D. Standard deviation was also calculated and presented as the error bars of averaged I_G/I_D.

Next, the etching effect of CO_2 on SWCNT growth was analyzed by delaying the injection time of CO_2 to 2, 5, and 7 min while the partial pressure was maintained at 140 Pa. With the delaying of the injection time, the D-band intensity gradually increased, as shown in Figure 4.2 (c). A decrease in the I_G/I_D ratio can be seen in Figure 4.2 (d), which reflects the reduction in the SWCNT quality. Moreover, the increase in the I_D/I_{Si} ratio of both SWCNTs and the corresponding blank samples, as seen in Figure 4.2 (d), proves that the amount of a-C deposited on the SWCNT samples gradually increases. Even with an increase in the partial pressure of CO_2 to 200 Pa, when delaying the injection time to 5 min, the increase in a-C deposition cannot be prevented perfectly (shown in Figure 4.3). The milder a-C-etching ability of CO_2 has been discussed in previous studies on metal-catalyzed growth systems [79-85, 139, 140]. Moreover, without a metal catalyst, the increase in the D-band intensity along with the delaying of the injection time reflects that the a-C etching rate of CO_2 is limited to be of the same order as the deposition rate of a-C or even slower. Notably, the GOF in Figure 4.2 (d) shows a slightly decreased yield when CO_2 is added from the beginning or after 2 min of growth. Because the initial cap formation is expected to occur in the first few minutes during the synthesis, such a slight decrease in yield implies that CO_2 reduces the growth yield of SWCNTs by influencing the initial growth efficiency. Associating the decrease in the growth yield with the a-C-etching ability, we assume that during SWCNT growth from the CNP growth seeds, CO_2 reduces the density of carbon species adsorbed on the surface of growth seeds via an oxidation reaction. Such a decrease in the density of activated carbon species adsorbed on the growth seeds reduced the carbon supply rate to the growth edge, which explains both the reduction in the growth yield and the deposition of a-C. Thus, in this CO_2-participated SWCNT growth process, the limited deposition of a-C is due to the reduction of the activated carbon species instead of the etching of a-C. Unavoidably, such a decrease in carbon supply also slightly influences the SWCNT growth efficiency, particularly in the nucleation stage, which is more sensitive to the growth condition than is the stationary elongation stage.

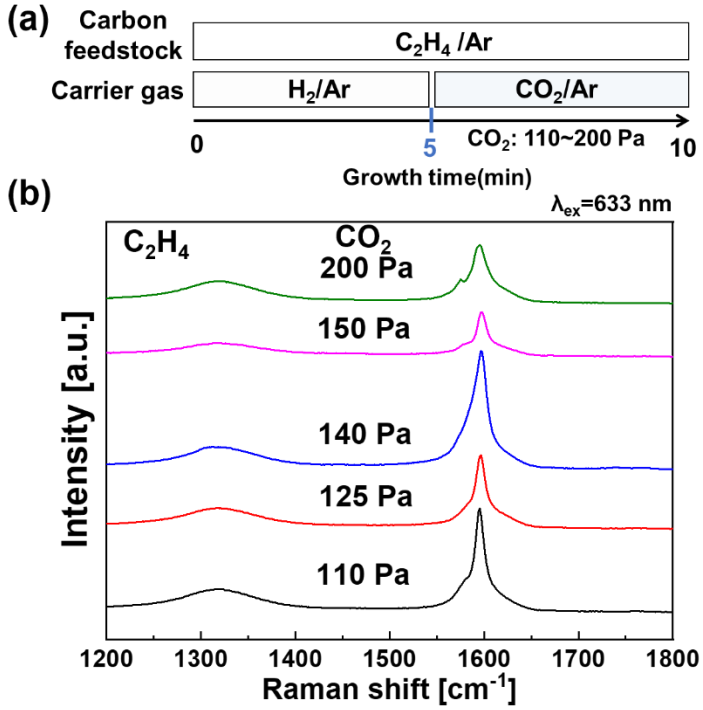

Figure 4.3: (a) Gas composition profile during one-step SWCNT growth process at 1000 ºC for 10 min. In the C_2H_4-supplied case, CO_2 was injected at 5 min after SWCNT growth started, and the partial pressure of CO_2 was varied from 110 Pa to 200 Pa. (b) Raman spectra of SWCNTs obtained by one-step growth from C_2H_4 with the different partial pressure of CO_2 injected at 5 min after the growth starts.

4.3.2 Effects of CO_2 on C_2H_2-supplied one-step growth

We investigated CO_2-assisted SWCNT growth using C_2H_2 at 0.5 Pa as the carbon source at 900 °C for 10 min. CO_2 was added from the beginning of SWCNT growth. As shown in Figure 4.4 (a), the Raman spectra exhibited the difference in the D-band intensity when the partial pressure of CO_2 was changed from 0.025 to 0.25 Pa. In contrast to the D-band suppression in the C_2H_4-supplied case (Figure 4.2), a decrease in the I_D/I_{Si} ratios of the SWCNT samples was not clearly observed, and the I_D/I_{Si} ratios of the blank samples were not negligible even with the highest concentration of CO_2 in this case (Figure 4.4 (b)). This result indicates that the a-C etching by CO_2 in the C_2H_2-supplied SWCNT growth was not evident. A relatively minor improvement in SWCNT quality can be observed in the I_G/I_D shown in Figure 4.4 (b), which is mainly caused by the suspension of a-C deposition.

Compared with less active C_2H_4, the use of highly active C_2H_2 as the carbon source at high growth temperatures resulted in a higher growth yield. The GOF of most samples reached 100% except for the sample with the highest CO_2 pressure under this experiment condition, as shown in Figure 4.4 (a). Thus, I_G/I_{Si} was used to evaluate the yield in this case, which is shown in Figure 4.4 (b). In contrast to the case of C_2H_4, the increased yield was achieved with C_2H_2 when the partial pressure of CO_2 was set to 0.05 and 0.15 Pa. Because a similar I_G/I_D ratio was obtained with and without the assistance of CO_2, the increase in growth yield due to CO_2 is unlikely to be caused by the prevention of a-C deposition, which could prolong the lifetime of the growth seeds. Thus, we need to consider a possible role of CO_2 other than the etching of a-C.

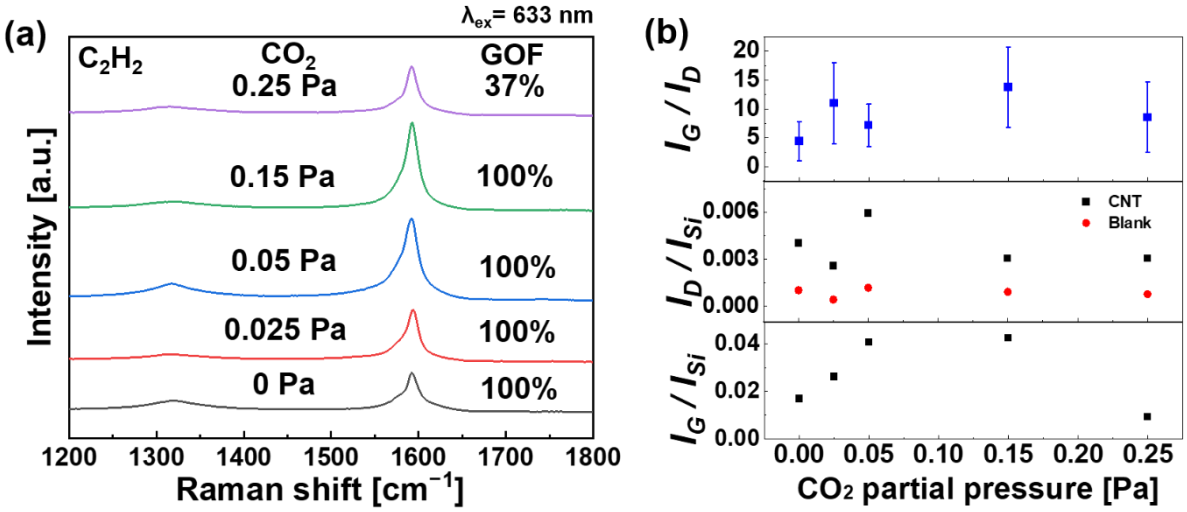

Figure 4.4: (a) Raman spectra of SWCNTs obtained by one-step growth from C_2H_2 with different partial pressures of CO_2 injected from the commencement of growth. The GOF percentage is indicated in the graph. (b) I_G/I_{Si}, I_D/I_{Si}, and I_G/I_D ratios of the same samples as (a). The error bars represent the standard deviation.

In C_2H_2-supplied CNT growth, besides etching ability, CO_2 has been recently proven to exhibit a promoting role in the dehydrogenation reaction of hydrocarbon, which finally increases CNT yield [81]. In the CO_2-enhanced CNT growth process, two chemical reactions are possible between C_2H_2 and CO_2:

$$C_2H_2+CO_2 \leftrightarrow 2C+H_2O+CO, \qquad (1)$$

$$C_2H_2+CO_2 \leftrightarrow C+H_2+2CO. \qquad (2)$$

Based on these reactions, a reduced activation energy barrier (from 5.58 down to 4.97 eV) of the first H dissociation in the C_2H_2 dehydrogenation process with the injection of CO_2 was illustrated through a simulation method [139]. Similar to these studies, we assume that the dehydrogenation reactions between C_2H_2 and CO_2 also occur in the SWCNT growth process from the non-metallic growth seeds. Based on the enhanced dehydrogenation reaction, the formation of activated carbon species on the growth seeds was promoted and caused a higher carbon-source supply, which resulted in an increase in both SWCNT growth yield and a-C deposition.

4.3.3 Effects of enhancers on C_2H_4-supplied two-step growth

Based on the enhancing effect of CO_2 in one-step SWCNT synthesis from the CNP growth seeds, we applied CO_2 to the two-step growth process, which was proven to increase the yield of highly crystalline SWCNTs [141]. In the two-step growth system shown in Figure 4.5 (a), the C_2H_4-supplied growth SWCNTs using H_2O as an enhancer were also conducted for comparison.

Figure 4.5 (b) and (c) present the quality and quantity variation of SWCNTs from the C_2H_4-supplied two-step growth process when using different growth enhancers, namely, H_2O and CO_2. Regarding the injection time of the growth enhancers, we previously found that additional defects were formed if H_2O was injected from the initial growth step [141]. Even when using CO_2 as the growth enhancer, the supply of CO_2 from the initial growth step resulted in a slight decrease in SWCNT yield in the one-step growth from C_2H_4 (Figures 4.2 (c) and (d)). Thus, to maintain the nucleation efficiency during the initial growth step (process 1 in Figure 4.5 (a)), both enhancers were added at the beginning of the temperature-rising step (process 2 in Figure 4.5 (a)). The partial pressure of the growth enhancers during the temperature-rising step was optimized (1 Pa for H_2O or 2 Pa for CO_2) to prevent the deposition of a-C (Figure 4.6). The influence of enhancers was analyzed according to the changes in the yield and quality of SWCNTs when varying the partial pressure of H_2O and CO_2 at the secondary growth step (process 3 in Figure 4.5 (a)). The condition is represented by the partial pressure of enhancers during the three

processes; for example, 0-1-1 Pa means that the partial pressure during the initial growth step, temperature-rising step, and secondary growth step is 0, 1, and 1 Pa, respectively.

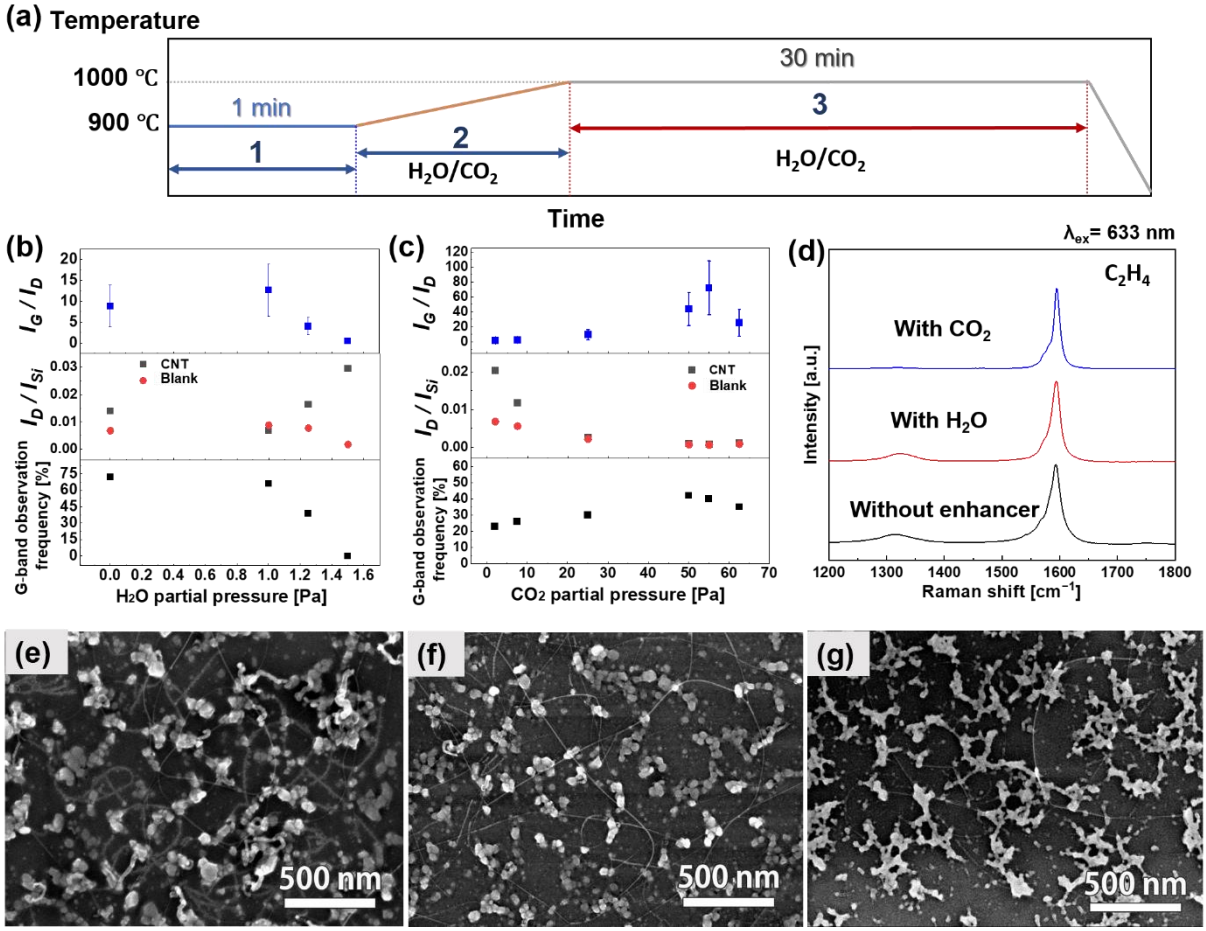

Figure 4.5: (a) Temperature profiles for the C_2H_4-supplied SWCNT two-step growth process with growth enhancers as H_2O or CO_2. Processes 1, 2, and 3 indicated in the profile represent the initial growth step, temperature-rising step, and secondary growth step, respectively. (b, c) GOF, I_D/I_{Si} ratio, and I_G/I_D ratio of the SWCNTs grown from C_2H_4 with different partial pressures of (b) H_2O and (c) CO_2 during the secondary growth step. The partial pressures of H_2O and CO_2 in the secondary growth step were varied from 0 to 1.5 Pa and 2 to 62.5 Pa, respectively. Further, the partial pressures during the temperature-rising step were fixed to 1 and 2 Pa for H_2O and CO_2, respectively. Standard deviation was also calculated and presented as the error bar of averaged I_G/I_D. (d) Raman spectra and (e, f, g) SEM images (acceleration voltage: 5 kV) of SWCNTs synthesized (e) without a growth enhancer, (f) with the injection of H_2O (0-1-1 Pa), and (g) with the injection of CO_2 (0-2-55 Pa).

In Figure 4.5 (b), with increasing H_2O partial pressure at the secondary growth step from 0 to 1.5 Pa (0-1-0, 0-1-1, 0-1-1.25, and 0-1-1.5 Pa), the averaged I_G/I_D ratios exhibit a decreasing tendency, which indicates an increase in a-C or defect formation caused by excess H_2O. The relevant Raman spectra is shown in Figure 4.7 (a). To elucidate the origin of the D-band, we compared the averaged I_D/I_{Si} ratios of the SWCNT samples and the corresponding blank samples. For the growth process in which no H_2O or only 1-Pa H_2O (0-1-0 Pa and 0-1-1 Pa) was supplied during the secondary growth step, slightly higher or similar I_D/I_{Si} ratios were observed for the SWCNT samples compared with the blank samples. The appearance of the D-band in the blank samples originated from the deposition of a-C. Thus, below 1 Pa of H_2O, the appearance of the D-band from SWCNT samples is explained by the deposition of a-C. When the partial pressure of H_2O was increased to 1.5 Pa at the secondary growth step (0-1-1.5 Pa), I_D/I_{Si} decreased in the blank samples, which indicates the removal of a-C. However, a dramatic increase in I_D/I_{Si} was found in the SWCNTs samples. Such a D-band of the SWCNTs samples should originate from the formation of defects. Therefore, we assume that when the partial pressure of H_2O was greater than 1 Pa in this growth system, in addition to a-C, SWCNT structures were partially etched by H_2O, resulting in defect formation. In addition, when the partial pressure of H_2O was increased to 1.25 Pa, the GOF decreased to ~40%. The GOF further decreased to 0% when the partial pressure of H_2O increased to 1.5 Pa. The increase in D-band intensity represents the formation of the sp^3 structure (defects), and the disappearance of the G-band represents the loss of SWCNTs. This dramatic decrease in SWCNT yield also reflects one of the disadvantages of H_2O, which comes from its strong oxidizing ability at high temperatures. Because of this strong oxidizing ability, the oxidizing reaction occurred not only in a-C but also in SWCNTs and activated carbon species, particularly with excess H_2O, which caused a decrease in the SWCNT quality and quantity. The abovementioned growth results indicate that the complete removal of a-C is difficult by adding H_2O without causing damage to SWCNTs and the partial pressure of H_2O needs to be accurately controlled to avoid the destruction of SWCNTs.

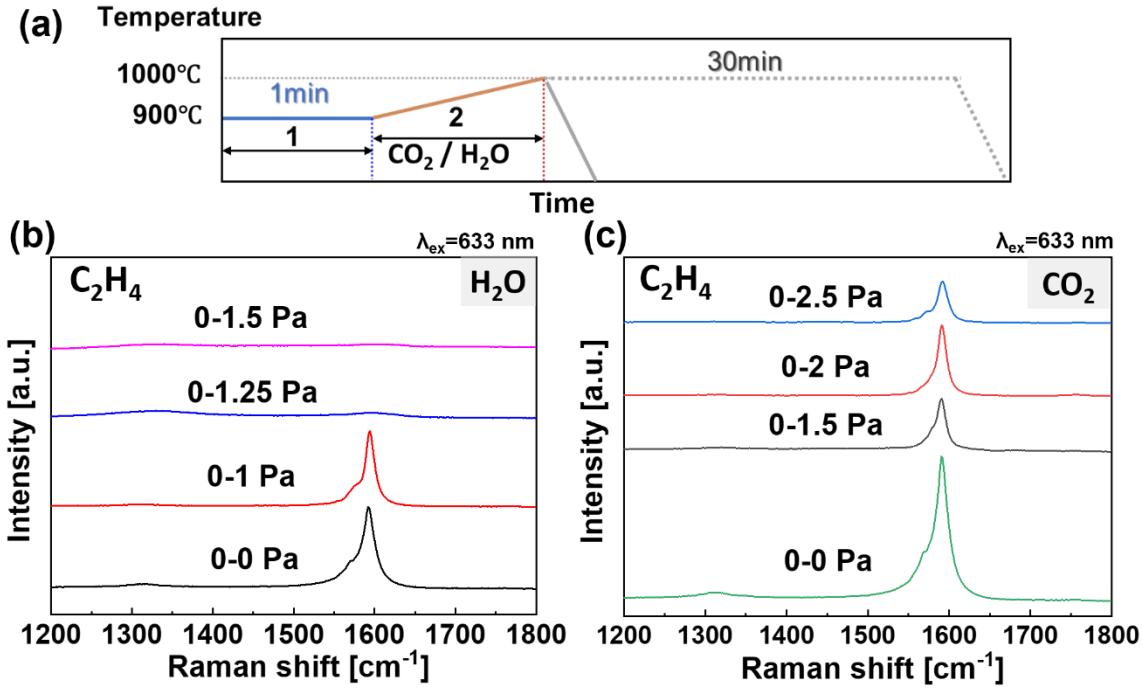

Figure 4.6: (a) Profiles of temperature and growth enhancer partial pressure for the SWCNT two-step growth process with growth enhancer injection. Adjustment of the growth enhancers partial pressure in the temperature rising step (process 2) in the C_2H_4-supplied two-step growth process. The SWCNT samples were collected after the finish of the temperature rising step. (b) Raman spectra of the SWCNT samples grow with the different partial pressure of H_2O (from 0 Pa to 1.5 Pa) in the temperature rising step. (c) Raman spectra of the SWCNT samples grow with the different partial pressure of CO_2 (from 0 Pa to 2.5 Pa) in the temperature rising step.

Moreover, using C_2H_4 as the carbon source, a CO_2-assisted two-step growth was conducted; the corresponding results are summarized in Figure 4.5 (c). Because of its milder oxidizing ability, CO_2 with a partial pressure greater than that of H_2O was used for the secondary growth step. With the same growth condition (carbon-source partial pressure, growth time, and growth temperature) as that using H_2O, CO_2 exhibits a higher effectivity in improving the quality of SWCNTs according to the increase in the averaged I_G/I_D ratios shown in Figure 4.5 (c). Additionally, with an increase in the CO_2 partial pressure from 2 to 62.5 Pa (0-2-2, 0-2-7.5, 0-2-25, c, 0-2-55, and 0-2-62.5 Pa), a decreasing tendency of the averaged I_D/I_{Si} ratio was found in both the SWCNT samples and the blank samples. The relevant Raman spectra is shown in Figure 4.7 (b). Such an increase in the I_G/I_D ratio to ~69 and a decrease of I_D/I_{Si} ratio close to 0 indicates the formation of highly crystalline SWCNTs with negligible deposition of a-C. The lower

deposition of a-C helps to keep the surface of the growth seeds clean and prolongs the growth lifetime, which explains the slight increase in the growth yield. Figure 4.5 (d) depicts the Raman spectra of the SWCNTs grown under optimized growth conditions without growth enhancers, with H_2O (0-1-1 Pa), and with CO_2 (0-2-55 Pa). Because the G-band intensity in the Raman spectra is normalized, the difference in the D-band intensity can be clearly observed. Compared with the growth without growth enhancers or with H_2O, CO_2 presents its advantage in preventing a-C deposition when using C_2H_4 as the carbon source. Figures 4.5 (e), (f), and (g) show the SEM images of the SWCNTs grown without growth enhancers, with H_2O, and with CO_2, respectively. In Figure 4.5 (e), without growth enhancers, SWCNTs with a significantly shorter length (~50 nm) appeared owing to the deposition of a-C, which terminated the growth in a short time. When H_2O is added to the growth process, the decrease in the short SWCNTs shown in Figure 4.5 (f) represents the suppression of a-C deposition, which prolongs the lifetime of the growth seeds. When using CO_2 as the growth enhancer, the formation of a-C was prevented more effectively; longer SWCNTs can be frequently found in Figure 4.5 (g).

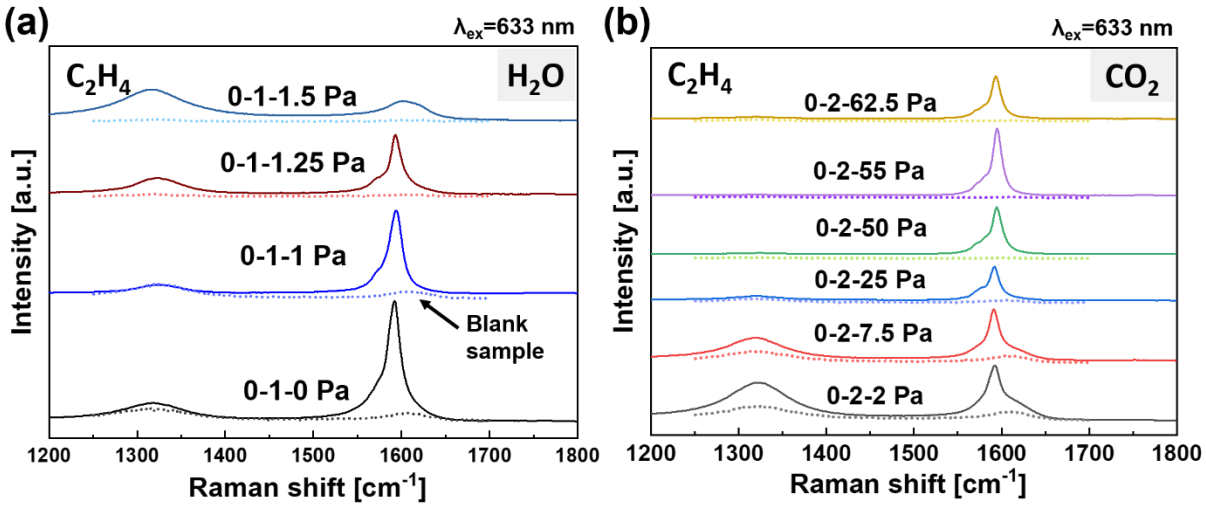

Figure 4.7: (a) Raman spectra of SWCNT samples synthesized by C_2H_4-supplied two-step growth with the injection of H_2O. The partial pressure of H_2O was fixed to 1 Pa in the temperature and varied from 0 Pa to 1.5 Pa (0-1-0 Pa, 0-1-1 Pa, 0-1-1.25 Pa and 0-1-1.5 Pa) in the secondary growth step. (b) Raman spectra of SWCNT samples synthesized by two-step growth with the injection of CO_2. The partial pressure of CO_2 was fixed to 2 Pa in the temperature and varied from 2 Pa to 62.5 Pa (0-2-2 Pa, 0-2-7.5 Pa, 0-2-25 Pa, 0-2-50 Pa, 0-2-55 Pa, and 0-2-62.5 Pa) in the secondary growth step.

We then investigated the changes in growth yield and quality along the process flow of the two-step growth with and without the growth enhancers (0-1-1 Pa of H_2O or 0-2-55 Pa of CO_2). Raman spectra were acquired from the samples immediately after the three steps: the initial growth step, temperature-rising step, and secondary growth step. The changes in GOF and I_G/I_D are shown in Figure 4.8. Even without growth enhancers, the slight increase in the I_G/I_D ratios from the initial growth step to the temperature-rising step proves that the deposition of a-C is still low before the growth temperature rises to 1000 °C. The addition of H_2O or CO_2 with the optimized conditions during the temperature-rising step causes an increase in the I_G/I_D ratios compared with that without growth enhancers. This means that the deposition of a-C is further prevented by H_2O or CO_2. However, according to Figure 4.8 (a), compared to the sample without growth enhancers, the decreased yield of SWCNTs was observed when H_2O or CO_2 was added. Particularly for CO_2, there was almost no increase in yield during the temperature-rising step. Based on the role of CO_2 at high temperatures described in section 4.3.1 (one-step growth), we assume that the prevention of a-C formation is mainly caused by the decrease in carbon species adsorbed on the growth seeds. Such a decrease also caused the decrease in SWCNT yield.

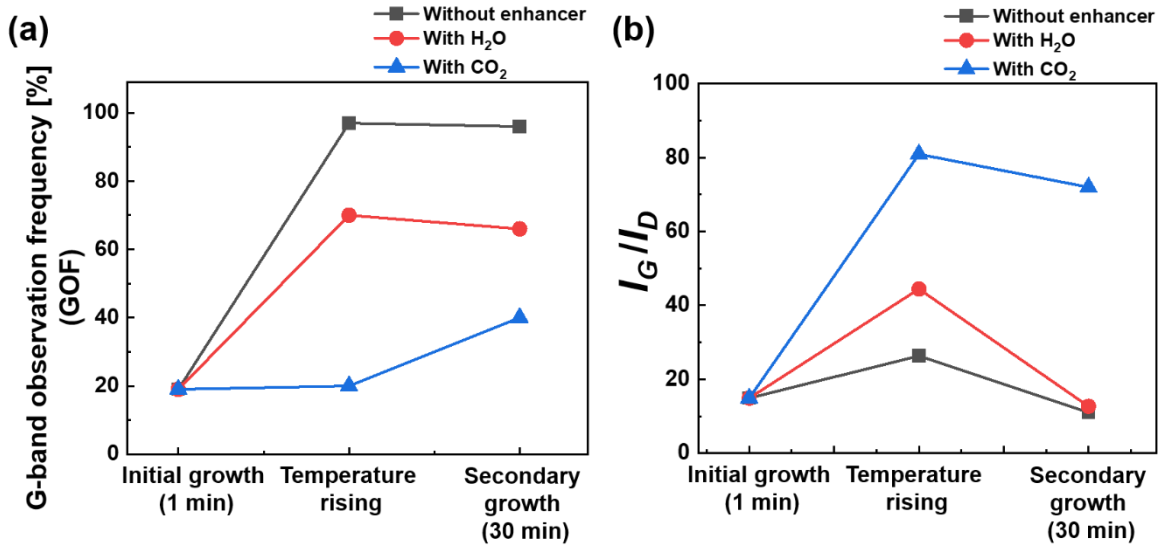

Figure 4.8**:** Changes in (a) yield (GOF) and (b) quality (I_G/I_D ratio) of SWCNTs along the growth steps from C_2H_4 without growth enhancers, with H_2O (0-1-1 Pa), and with CO_2 (0-2-55 Pa).

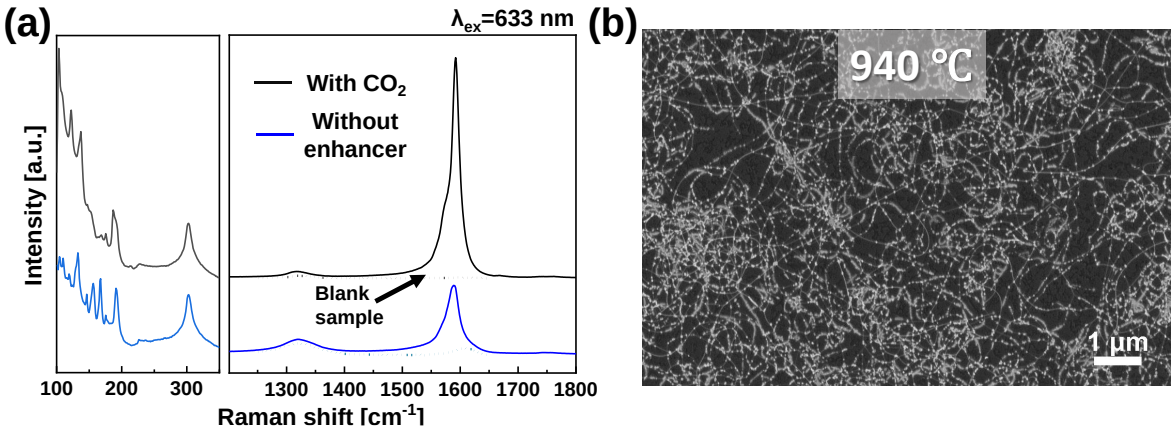

Figure 4.9: (a) Raman spectra of SWCNT samples synthesized by C_2H_4-supplied two-step growth with and without the injection of CO_2. During the growth, the growth temperature was 900 °C in the initial growth step and the temperature rise to 940 °C in the secondary growth step. The partial pressure of C_2H_4 was 20 Pa in the initial growth step, then changed to 5 Pa in the temperature rising step, and varied to 10 Pa when the secondary growth step started. The partial pressure of CO_2 was 2 Pa in the temperature and varied to 400 Pa in the secondary growth step (0-2-400 Pa). (b) SEM image (acceleration voltage: 5 kV) of SWCNTs synthesized with the injection of CO_2 (0-2-400 Pa).

After the temperature-rising step, the secondary growth step was conducted, in which the stationary growth of SWCNTs occurs. Notably, with the temperature rising from 900 °C to 1000 °C, the carbon-source decomposition rate increases, which causes an increase in the supply of activated carbon species [143]. Without the injection of growth enhancers, the deposition of a-C was enhanced, as shown in Figure 4.8 (b). The use of H_2O could not provide SWCNTs with high crystallinity and low a-C simultaneously. The a-C deposition caused the decrease in the I_G/I_D ratio and finally terminated the growth at the beginning of the secondary growth step, which is evidenced by the negligible increase in the GOF from the temperature-rising step to the secondary growth step in Figure 4.8 (a). By contrast, in the case of CO_2 addition, the partial pressure of CO_2 could be largely increased along with the increase in the supplied carbon source without damaging the SWCNTs because of its mild oxidizing ability. The increase in the GOF from the temperature-rising step to the secondary growth step indicates the enhancement effect of CO_2. Based on such enhancement results, CO_2 was further applied to the two-step growth with the supply of higher-partial-pressure C_2H_4 at the secondary growth step. Through the adjustment of the growth temperature at the secondary growth

step, the I_G/I_{Si} ratio was increased to ~0.15 while the GOF was 100%, and the I_G/I_D ratio was kept at ~57 (Figure 4.9). We assume that CO_2 prolongs the lifetime of the growth seeds by keeping their surface clean and maintains the efficient growth of SWCNTs during the secondary growth step.

4.3.4 Effects of enhancers on C_2H_2-supplied two-step growth

We investigated the effect of CO_2 on the C_2H_2-supplied two-step growth process. The growth process is schematically shown in Figure 4.10 (a). Similar to the condition in the C_2H_4-supplied growth described in section 4.3.3, CO_2 was injected after the first growth step and its partial pressure during the temperature-rising step was optimized to 0.05 Pa. Because the growth result with the injection of H_2O has already been discussed in our previous work [141], the growth results with CO_2 injection are mainly discussed in this section.

Figure 4.10 (b) depicts the variation of the quality (I_G/I_D and I_D/I_{Si} ratios) and yield (GOF) of SWCNTs with a change in the partial pressure of CO_2 at the secondary growth step from 0.1 to 0.5 Pa (0-0.05-0.1, 0-0.05-0.25, 0-0.05-0.35, and 0-0.05-0.5 Pa). The relevant Raman spectra are shown in Figure 4.11. Interestingly, contrary to the expected role of CO_2 for a-C deposition prevention, relatively low I_G/I_D ratio were observed. Within the range of CO_2 partial pressure, the growth yield decreased with increasing CO_2. This indicates that the injection of CO_2 cannot prevent the deposition of a-C in the C_2H_2-supplied growth process. Even after the partial pressure of CO_2 was increased to 0.5 Pa (0-0.05-0.5 Pa), the yield decreased while the I_G/I_D ratio did not change significantly, which means that the intensities of both the G-band and D-band decreased. However, as shown in Figure 4.10 (c), the D-band and G-band intensities of the sample with 0.1-Pa CO_2 (0-0.05-0.1 Pa) are higher than those of the sample without growth enhancers. Because the GOF of both samples is already 100% under this condition, the intensity of the G-band reflects the SWCNT yield. Moreover, according to the SEM images shown in Figures 4.10 (d) and (e), a higher density of SWCNTs was observed in the CO_2-injected sample than in the sample without growth enhancers. To analyze the increase of D-band intensity, we compared the change in a-C deposition on the blank samples along the two-

step growth process with and without the injection of CO_2. As shown in Figure 4.12, higher I_D/I_{Si} ratio was found in the CO_2-injected case. The increase of I_D/I_{Si} should be attributed to the a-C deposition since there is no possibility of defect formation on the blank samples, where no SWCNTs were grown. Thus, for the sample grown with a small amount of CO_2, the higher G-band intensity represents a higher yield and the higher D-band intensity could reflect the more intense deposition of a-C. Moreover, the appearance of the radial breathing mode peak at ~180 cm^{-1}, which was not observed in the samples grown without a growth enhancer, indicates that thinner SWCNTs were formed with the injection of CO_2. The formation of the thinner SWCNTs should be due to the increased growth-driving force [71]. Considering that the growth temperature and partial pressure of C_2H_2 were fixed, the increased density of activated carbon species is regarded as the main factor that causes the increase in the growth-driving force. The activated carbon species are formed from the decomposition of C_2H_2. As discussed in section 4.3.2, we assume that CO_2 in C_2H_2-supplied growth mainly works as a growth enhancer, which promotes the dehydrogenation reaction of the carbon source and increases the density of activated carbon species. Such an increase in activated carbon species promotes SWCNT growth but also leads to uncontrolled a-C deposition.

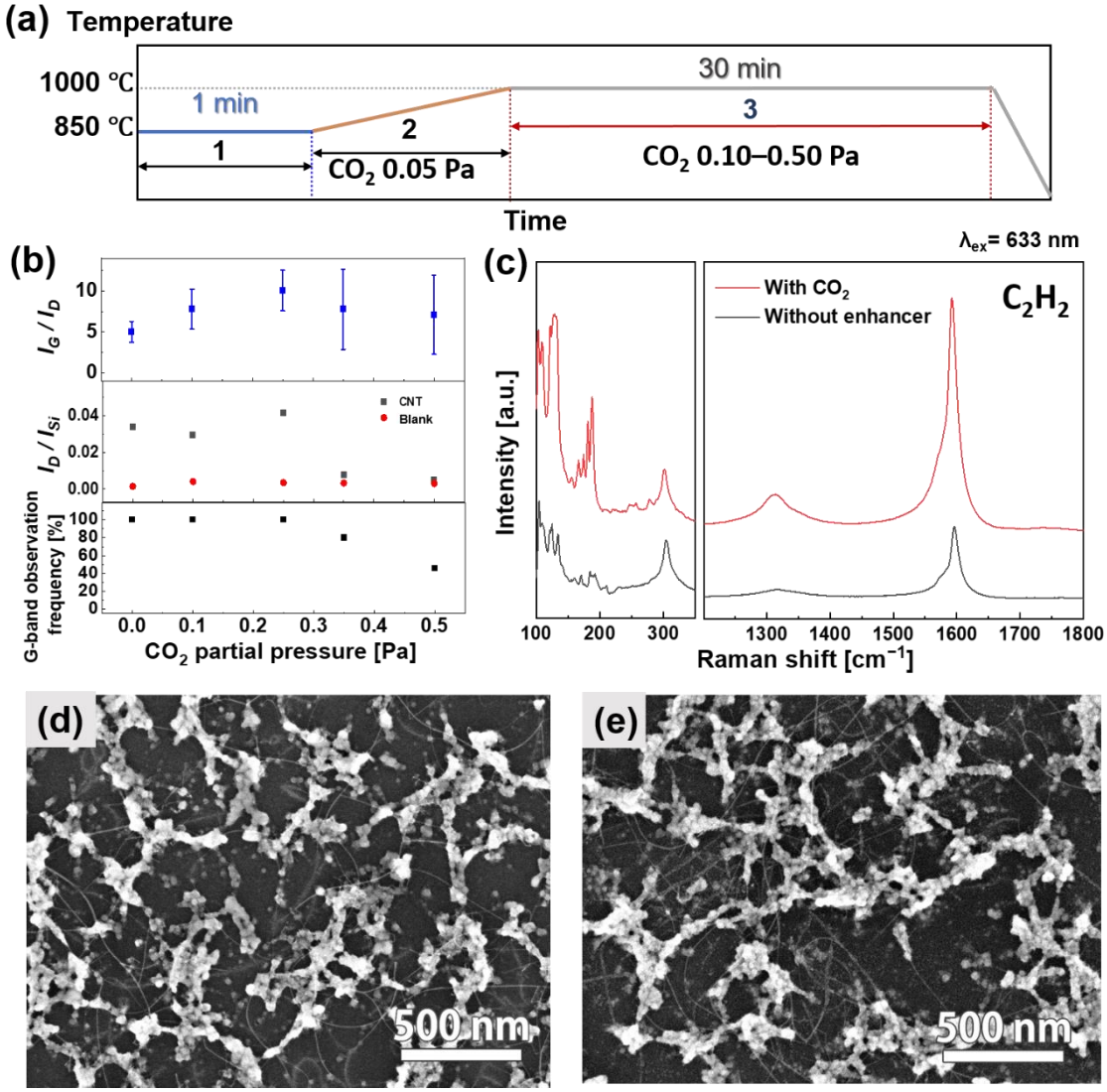

Figure 4.10: (a) Temperature profiles for the C_2H_2-supplied SWCNT two-step growth process with the injection of CO_2. (b) GOF, I_D/I_{Si} ratio, and I_G/I_D ratio of the SWCNTs grown from C_2H_2 with different partial pressures of CO_2 injected since the temperature-rising step. The partial pressure of CO_2 in the secondary growth step was varied from 0 to 0.5 Pa. The partial pressure of CO_2 in the temperature-rising step was fixed to 0.05 Pa. Standard deviation was also calculated and presented as the error bar of averaged I_G/I_D. (c) Raman spectra of the SWCNT samples synthesized with and without the injection of CO_2. The partial pressure of CO_2 was 0.05 and 0.1 Pa during the temperature-rising step and the secondary growth step, respectively (0-0.05-0.1 Pa). (d, e) SEM images (acceleration voltage: 5 kV) of the SWCNT samples synthesized (d) without the injection of a growth enhancer and (e) with the injection of CO_2 (0-0.05-0.1 Pa).

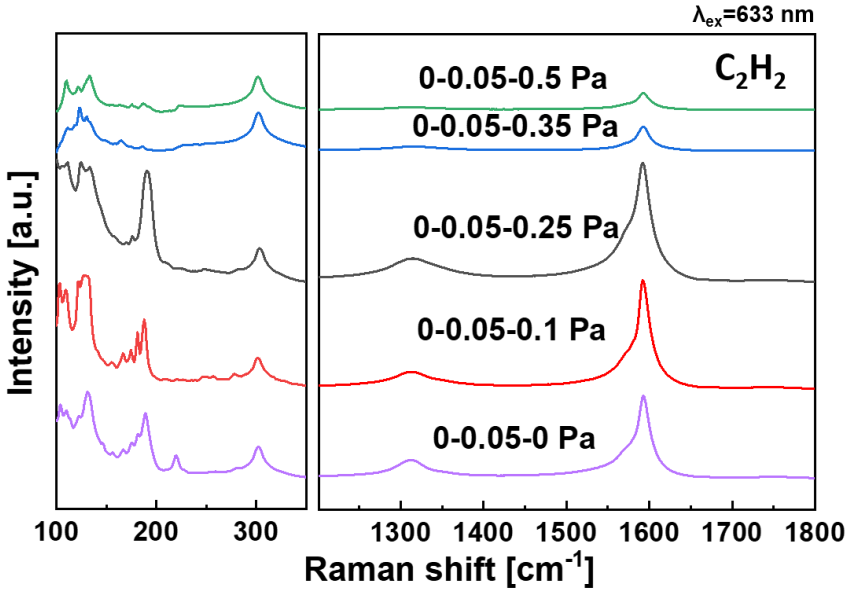

Figure 4.11**:** Raman spectra of SWCNT samples synthesized by C_2H_2 -supplied two-step growth with the injection of CO_2. The partial pressure of CO_2 was fixed to 0.05 Pa in the temperature and varied from 0 Pa to 0.5 Pa (0-0.05-0 Pa, 0-0.05-0.1 Pa, 0-0.05-0.25 Pa, 0-0.05-0.35 Pa, and 0-0.05-0.5 Pa) in the secondary growth step.

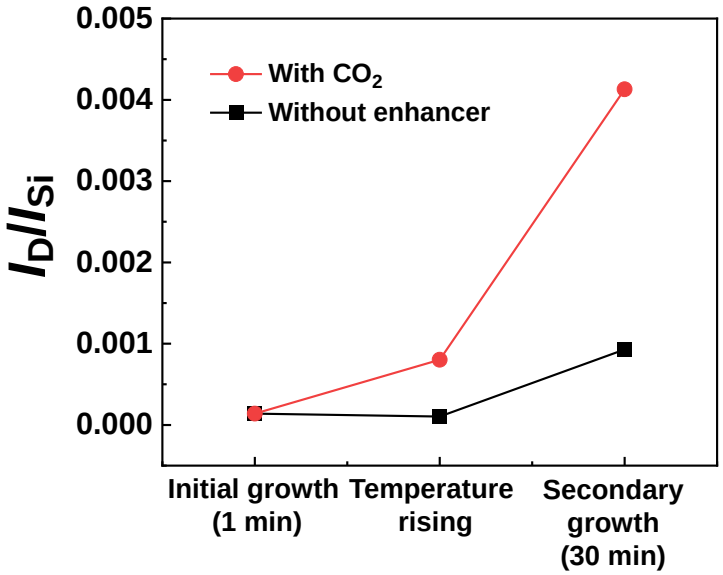

Figure 4.12**:** Changes in a-C deposition (I_D/I_{Si} ratio) of blank sample along the growth steps in C_2H_2-supplied process without growth enhancers and with CO_2 (0-0.05-0.1 Pa).

The changes in the quality and yield of SWCNTs along the growth steps with and without the injection of enhancers are shown in Figure 4.13. The result with H_2O (0-0.15-0.15 Pa) has been taken from our previous work [141]. Raman measurement was conducted after the initial growth, temperature-rising, and secondary growth steps as in the case of C_2H_4. Because of the higher activity of C_2H_2 than C_2H_4, a-C was easily formed during the temperature-rising and secondary growth steps, which caused the decrease in the I_G/I_D ratios when no growth enhancer was injected. As reported in our previous work [141], with accurate control of the H_2O partial pressure (0-0.15-0.15 Pa), a-C was effectively removed and the I_G/I_D ratio increased. At the same time, a part of the activated carbon species was also removed from the growth seed surface by H_2O, which resulted in the decrease in the SWCNT yield compared with the sample without growth enhancers, as shown in Figure 4.13 (a). When using CO_2 as the growth enhancer, contrasting results were obtained. The I_G/I_D ratio decreased while the GOF was increased by CO_2. The dramatic increase in the GOF also supports our assumption that the carbon-source supply is promoted by the injection of CO_2. This promotion effect causes the increase in SWCNT yield as well as the deposition of a-C. Thus, based on the discussion above, we conclude that CO_2 plays more than one role in SWCNT growth from the CNP growth seeds depending on the employed carbon feedstocks.

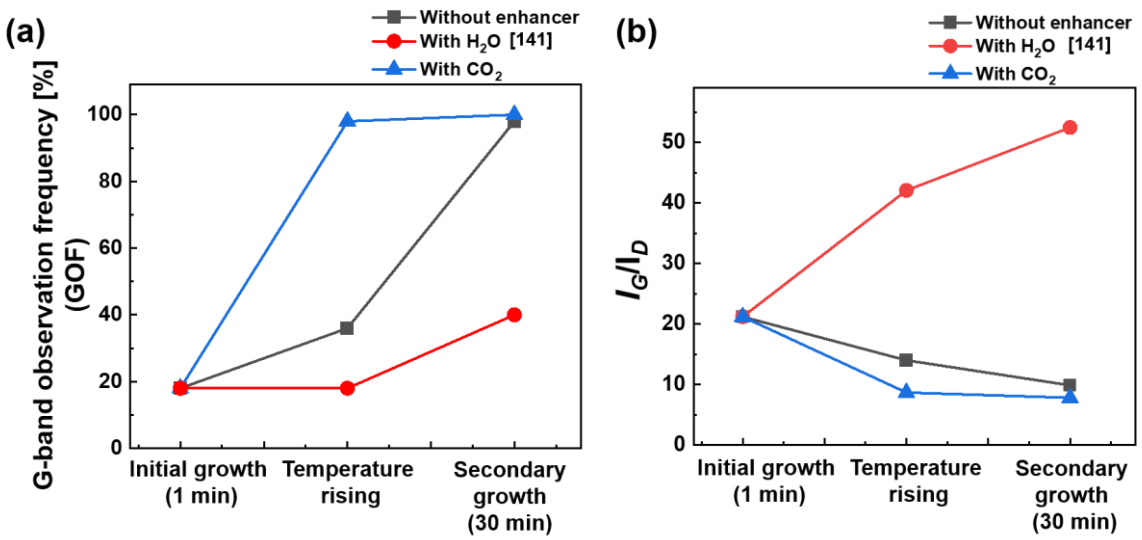

Figure 4.13: Changes in (a) yield (GOF) and (b) quality (I_G/I_D ratio) of SWCNTs along the growth steps from C_2H_2 without growth enhancers, with H_2O (0-0.15-0.15 Pa) [141], and with CO_2 (0-0.05-0.1 Pa).

4.3.5 Mechanism of growth enhancers in combination with carbon sources

The mechanism of the effect of enhancers (H_2O and CO_2) on SWCNT growth behavior is derived from the observed results and is schematically depicted in Figure 4.14. In the SWCNT growth system based on the CNP growth seeds, carbon-source molecules in the gas phase first overcome the energy barrier to proceed with the dehydrogenation reaction, and activated carbon species are adsorbed on the surface of growth seeds. Then, the activated carbon species are attached to the edge of the SWCNT sidewall. Therefore, the conversion process of carbon-source molecules to SWCNTs is divided into two parts: the process in which the carbon-source molecules in the gas phase are transformed into activated carbon species of the adsorbed phase and the subsequent process in which the activated carbon species are transformed into the SWCNT structure. The activation energies (E_A) for these two processes are denoted as E_{A1} and E_{A2}, respectively.

We first discuss the effect of H_2O. In SWCNT growth from both C_2H_2 and C_2H_4 using the CNP growth seeds, H_2O was found to mainly prevent the formation of a-C. We assume that the preventing role is realized through the oxidizing reaction, which is similar to its role in SWCNT growth from a metallic catalyst. With the addition of H_2O, the chemical potential of activated carbon species decreased, which caused the decrease of SWCNT growth efficiency, as shown in Figures 4.14 (a) and (b). In addition to a-C, a part of the activated carbon species on the surface of growth seeds is etched away by H_2O, which decreases the density of the carbon species and accordingly their chemical potential. The decrease in the chemical potential increases the activation energy needed for the formation of SWCNTs (E_{A2}' in Figures 4.14 (a) and (b)), assuming that the transition state is preserved by the addition of H_2O. This change reasonably explains the decrease in the SWCNT growth efficiency in both the C_2H_2- and C_2H_4-supplied system by H_2O.

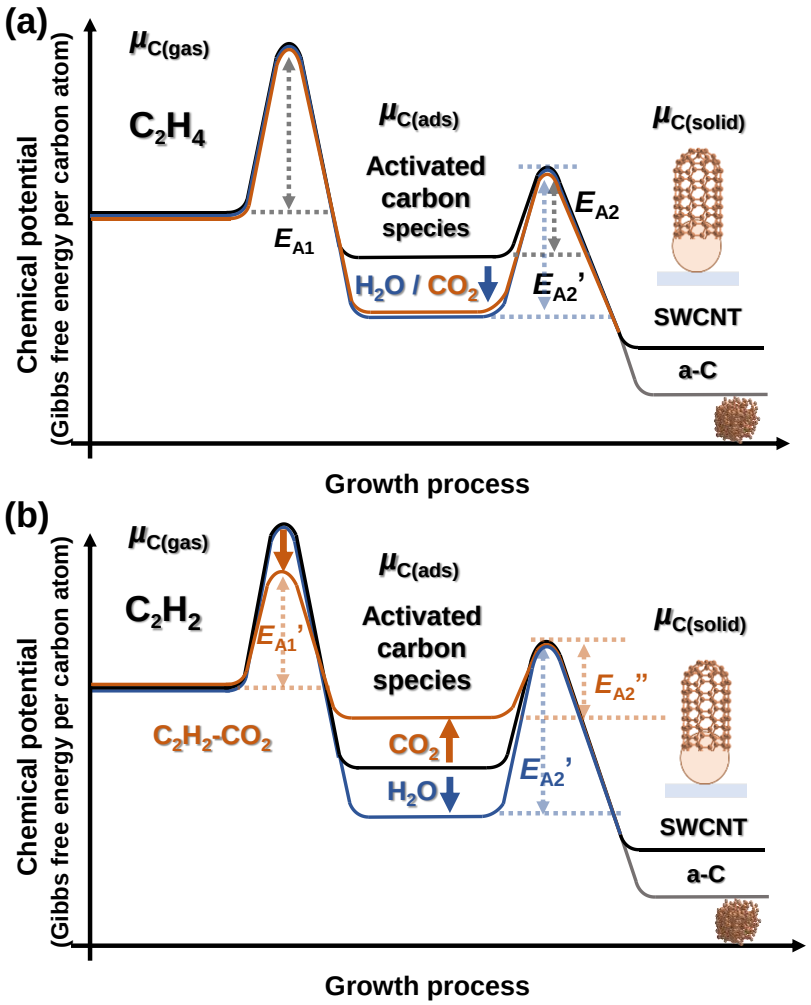

Figure 4.14: Schematic energy diagram of the SWCNT formation process from the CNP growth seeds at a high temperature using (a) C_2H_4 and (b) C_2H_2 as carbon feedstocks with different growth enhancers. Chemical potential variation of carbon in the gas phase, activated carbon species adsorbed on the growth seed, and carbon in an SWCNT is shown. The black, blue, and orange curves denote the chemical potential under the growth conditions without growth enhancers, with H_2O, and with CO_2, respectively.

When using CO_2 as the growth enhancer, the reaction between the carbon source and CO_2 needs to be considered depending on the carbon source. In the case of C_2H_4, as the reaction with CO_2 is not significant, the main role of CO_2 is etching. With the injection of CO_2, the chemical potential of activated carbon species decreased, which caused the decrease of SWCNT growth efficiency, as shown in Figure 4.14 (a). Because the oxidizing ability of CO_2 is lower than that of H_2O, CO_2 mainly etches away activated carbon species on the growth seeds and does not directly react with the formed a-C. The

decrease in the density of the carbon species causes a decrease in chemical potential and increase in activation energy, resulting in the low growth efficiency of SWCNTs. In the case of C_2H_2, a dehydrogenation reaction occurs between CO_2 and C_2H_2. As shown in Figure 4.14 (b), the activation energy of the dehydrogenation reaction of C_2H_2 decreases from E_{A1} (the process without CO_2) to E_{A1}' (the process with CO_2). Such a decrease in the energy barrier helps to increase the rate of carbon feedstock transformation from the gas phase to the adsorbed phase. The increased adsorbed carbon specie density causes the increase in chemical potential of carbon and then the decrease in the activation energy for SWCNT formation (E_{A2}"). This growth condition further promotes the formation of both SWCNTs and a-C. Therefore, the reaction between C_2H_2 and CO_2 significantly affects the enhancement of SWCNT growth not only in the metal-catalyzed SWCNT growth but also in the solid carbon seed-based growth.

4.4 Conclusion

In conclusion, by employing ND-derived CNPs as the growth seeds, we investigated the different roles of growth enhancers (CO_2 and H_2O) in high-temperature SWCNT growth processes using different carbon feedstocks (C_2H_2 and C_2H_4). By comparing two commonly used hydrocarbons, we found that the enhancement role of CO_2 differed depending on the carbon source, while similar etching role of H_2O exhibited in both hydrocarbon-supplied growth. In the C_2H_4-supplied growth, controlling the partial pressure and injection time of CO_2 prevents the formation of a-C without causing the formation of defects and achieves highly crystalline SWCNTs with high purity. However, CO_2 exhibits the enhancement effect in both SWCNT growth and deposition of a-C when using C_2H_2 as the carbon source. About this phenomenon, some works proposed that it is the interaction between the CO_2 and carbon source which promoted the growth of CNTs. This result presents another possible role of the growth enhancers, which enhanced CNT growth through both a-C etching and reacting with carbon source. Moreover, in the two-step growth process, the injection of CO_2 results in a prevention effect of a-C deposition in the C_2H_4-supplied case and the enhancing effect of SWCNT yield and a-C deposition in the C_2H_2 case. Particularly in the C_2H_4-supplied two-step SWCNT growth process, with the use of CO_2, highly crystalline SWCNTs with less a-C deposition were achieved

when the temperature of the secondary growth step was 1000 °C. Furthermore, by tuning the growth condition, the SWCNT yield was highly increased as indicated by the GOF of 100% and the I_G/I_{Si} ratio of ~0.15, while the quality of SWCNTs was preserved compared with previous work (I_G/I_D ratio of ~ 57). Our results demonstrate the different synergetic effects of growth enhancers and carbon sources in high-temperature SWCNT synthesis based on the solid carbon growth seeds, proving that CO_2 can be used as an effective growth enhancer in the C_2H_4-supplied two-step growth process to achieve high-quality SWCNTs with a high yield.

Until now, through the study of the growth driving force and the effects of growth enhancers, the yield of high quality SWCNTs was increased through the high temperature synthesis method. Unfortunately, the yield of high quality SWCNTs achieved through direct synthesis method is still need to be increased for the application. Thus, after developed the high temperature synthesis process, in the next research, I studied the high temperature post-treatment process for increasing the crystallinity level of massive SWCNTs with high defect density.

Chapter 5: Defect healing of single-walled carbon nanotubes via high temperature post-treatment

Thermal defect healing of single-walled carbon nanotubes assisted by supplying carbon-containing reactants

5.1 Background

Single-walled CNTs (SWCNTs) becomes one of the potential materials for application in electronics (transistors, interconnects, memory) [145, 146], sensors (optical, biological, chemical) [11, 147], and so on. However, the defects formed in SWCNTs are challenging to be avoided. The existence of defects dramatically degrades the electrical [101, 103, 104] and thermal transport [105] and mechanical strength [27, 106] of SWCNTs. Such defects, including adatom[148], vacancy[149], pentagon-heptagon pair (5|7) [21, 22], pentagon-heptagon-heptagon-pentagon (5|7/7|5) defects[150], are not favored thermodynamically due to their high formation energy[21, 151], but they can be created in the SWCNT growth process [152-154] and chemical post-treatment step [112]. The defects were observed through structure characterization [155, 156].

High-temperature treatment has been suggested to heal the defects [71]. During the SWCNT growth process, the highly ordered crystalline structure of SWCNTs tends to be found with the increase in the growth temperature [157]. Further theoretical and experimental discussion explained this phenomenon by the temperature-activated catalytic defect healing [158], which mentioned that simple defects with lower healing activation energy would be more readily cured, such as the 5|7 defects [21]. In the meantime, the yield of high crystallinity SWCNTs achieved through high temperature growth is still needs to be increased for further application.

Besides the growth process, high temperature post-treatment was supposed to be another promising method to achieve high quality CNTs through healing massive CNTs with defects formed during growth process or structure measurement. When talking about the defects created by the electron/photon irradiation, unlike the defects formed in the growth process, experimental evidence indicated that the defective SWCNTs could be healed by annealing under a moderate temperature (1000–2000 ^{o}C) and even at room

temperature [159, 160]. Then, the subsequent calculation indicated that, because of the low healing activation energy barrier (~2 eV), the adatom-vacancy defect is a possible candidate of defects generated on the irradiated-nanotubes [161]. Besides, the high temperature was also applied to the post-treatment process to heal the low-temperature synthesized or chemically treated SWCNTs and MWCNTs. For example, treating MWCNTs at 1200–2000 ^{o}C in a high vacuum or at 2000–2800 ^{o}C in an argon (Ar) atmosphere improved crystallinity [162-164]. Similarly, in SWCNT healing, high-temperature treatment (1000–2400 ^{o}C) has also been reported to increase the overall crystallinity by defect aggregation and self-healing of the graphene lattice [165, 166]. Nevertheless, there appears to be a limitation in healing vacancy defects at high temperature. Based on the simulation studies, once the vacancy defects formed and diffused into nanotubes, even if the vacancy defects could proceed with a self-healing via ring isomerization, it is hard to heal entirely unless foreign carbon atoms are added [88]. In previous studies, as one of the carbon-containing reactants, ethanol has been used as the defect healer in the restoration of graphene oxide [167, 168]. Recently, carbon-containing reactants have been considered as the defect healer in the high-temperature annealing process to heal vacancy defects in CNTs. Until now, simulation studies confirmed that the carbon sources (CO, C_2H_2 and C_2H_4) used for CNT growth are good candidates to heal vacancy defects during high-temperature CNT synthesis [88-91]. Unfortunately, there is still no experimental report on the healing effect of such carbon-containing reactants.

In this research, we experimentally present the healing effect of carbon-containing reactants on the defective SWCNTs. As one of the carbon-containing reactants, C_2H_2 is selected for the defect healing because it does not contain oxygen atoms, which lead to spontaneous formation of oxidants during pyrolysis process and might disturb the healing result. To avoid the formation of additional defects induced by metal catalyst impurities during post-treatment, we selected the metal-free carbon solid nanoparticle originating from nanodiamond (ND) as the SWCNT growth seed [69, 70]. By fixing the healing temperature to 1100 ^{o}C, through Raman spectra characterization, we explored the influence of C_2H_2 partial pressure and healing time on the C_2H_2 added annealing results. Compared with the SWCNTs only healed in Ar ambient, higher crystallinity of SWCNTs

is presented with the injection of C_2H_2. Moreover, with the injection of C_2H_2, a significant increase appeared in the healing efficiency of SWCNTs with small diameter. According to these experimental results, we propose that C_2H_2 helps to increase the high-temperature healing efficiency, especially the healing efficiency of thin SWCNTs.

5.2 Experimental section

Relatively defective SWCNTs were prepared by lowering growth temperature from the optimized condition in our previous study [141]. As the starting material of growth seeds, ~10 nm diameter purified ND particles were dropped Si substrates with a 300-nm-thick thermal oxide layer. The substrates were cleaned via an ozone treatment process (L-UV253, Japan Electronics Industry) by flowing 6 L/min O_2 for 5 min under ultraviolet light for 60 min, followed by exhausting with 6 L/min N_2 for 5 min. The ND pretreatment and the SWCNT growth were performed in a quartz tube chamber which is held in a tubular CVD furnace (GE-1000, GII Techno) [141]. As shown in Figure 5.1 (a), before the growth of SWCNTs, the ND was pretreated with the surface-cleaning process (in air for 10 min at 600 °C) and the annealing procedure (in 85 kPa Ar for 1 h with 20-sccm Ar injection at 1000 °C) [141]. After the annealing process, SWCNTs were synthesized for 10 min with a mixture of 10-sccm C_2H_2 (2%)/Ar and 10-sccm Ar. The total pressure was kept at 500 Pa, corresponding to a C_2H_2 partial pressure of 5 Pa. The temperature of the three-zone furnace was set with a gradient, 850-785-750 °C, which corresponds to the temperature of gas mixture preheating, SWCNT growth (substrate temperature), and post heating, respectively.

After the structural characterization of the above synthesized SWCNTs as described later, the heat treatment for the defect healing was proceeded which is shown in Figure 5.1 (b). The annealing temperature was set at 1100 °C to ensure the healing of defects in Ar ambient and the pyrolysis of C_2H_2 [162-164, 169]. The healing time was varied from 0 min to 60 min, where the 0 min represents the healing process stopped once the substrate temperature arrived at 1100°C. During the temperature rising process, 250-sccm Ar was injected into the heating ambient. When the temperature arrived at the annealing temperature, the gas flow was switched to a 250-sccm mixture of Ar (235–250

sccm) and C_2H_2 (2%)/Ar (0–5 sccm). The total pressure was kept at 220 Pa, corresponding to a C_2H_2 partial pressure of 0-0.088 Pa. Keeping the injected C_2H_2 at low partial pressure helped to limit the deposition of a-C. Besides, because such partial pressure is much lower than the value needed for the growth of CNTs (0.5 Pa) [141], we exclude the possibility of CNT nucleation during the annealing process. In addition, the same cleaned Si substrates without any growth seeds and SWCNTs were used as a reference (hereafter called blank samples) to compare the amount of amorphous carbon (a-C) deposited directly on them and on the SWCNT samples.

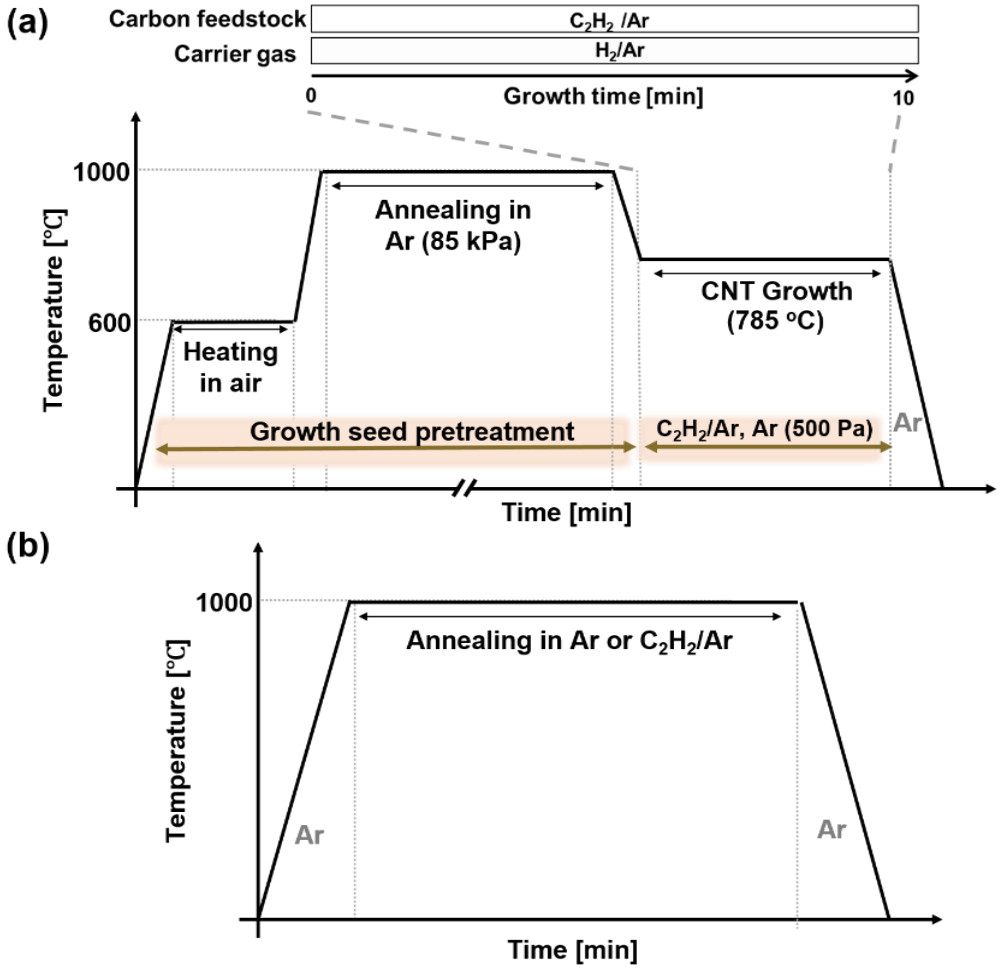

Figure 5.1: (a, b) Temperature profiles of the reaction furnace for (a) one-step growth process and (b) two-step growth process as a function of processing time. (a) The top part shows the gas composition profile during SWCNT growth. In the C_2H_4-supplied case, the variation of the CO_2 injection time (x = 0, 2, 5, 7, and 10 min) during the growth process was included. (b) The top part shows a schematic diagram of the two-step growth process of SWCNTs from the CNP growth seeds.

The structure of the SWCNTs before and after the healing process was analyzed by Raman spectroscopy. A Raman spectrometer (LabRAM HR800, HORIBA Jovin Yvon) was used with an excitation wavelength λex of 633 nm. The laser spot size was approximately 0.9 μm, and the laser power was approximately 9 mW at the measurement point. The exposure time of each measurement spot was 1 s for 5 cycles. Raman spectra of 30 randomly selected spots were collected from each sample, and the averaged spectra were used for the analysis. The quality of formed SWCNTs was evaluated using the intensity ratio of the G-band (~1590 cm^{-1}) to the D-band (1330–1360 cm^{-1}), which was represented as I_G/I_D. The SWCNT quantity was evaluated by comparing the intensity ratio of the G-band (~1590 cm^{-1}) with the Raman peak from Si substrates (~520 cm^{-1}), which was represented as I_G/I_{Si}. Scanning electron microscopy (SEM) (NVision, Carl Zeiss) was used for morphological observation of SWCNTs with an acceleration voltage of 5 kV.

5.3 Results and discussion

To investigate the healing role of C_2H_2, we analyzed the SWCNT samples annealed at 1100 °C with 0, 0.035, 0.088 Pa, 0.176, and 0.264 Pa of C_2H_2 injection. The healing time was varied from 0 to 90 min. Besides, 1000 ^oC and 1100 ^oC was employed to examine the influence of the annealing temperature on the healing. Because of the limitation of the CVD apparatus, the healing temperature should be not higher than 1100 ^oC. Moreover, to exclude the possibility of new growth of SWCNTs with high crystallinity which will affect the defect healing result, the annealing temperature should be 1000 ^oC or higher according to previous study. [141] Therefore, the defect healing temperature was set at 1000 ^oC and 1100 ^oC. A control experiment was conducted to exclude the possibility of new nucleation of CNTs. As shown in Figure 5.2, after the pretreated ND at 1100 ^oC was annealed with C_2H_2 injection, there was no detection of the G-band found on the reference sample, which excluded the possibility of the new growth

of SWCNTs. Thus, the increase in the Raman spectra intensity of the annealed SWCNT samples results from the healing effect.

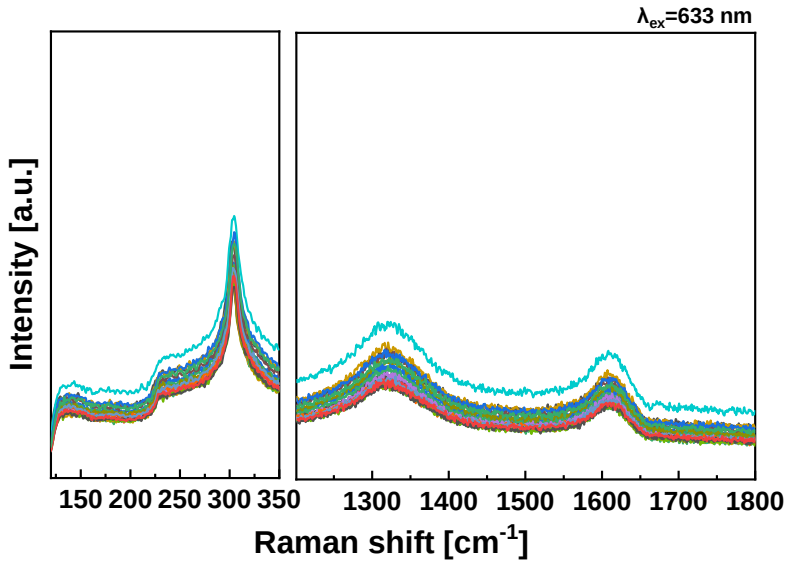

Figure 5.2: Raman spectra of the nanodiamond (ND) sample treated with the same thermal process as SWCNT growth but without the injection of carbon source and then the healing process (heated at 1100 °C for 60 min with 0.088 Pa C_2H_2 injection).

The radial breathing modes (RBMs) of Raman spectra changed with healing time and the partial pressure of C_2H_2 are exhibited in Figure 5.3 (a). As a representative, G-band and D-band Raman spectra of the SWCNT samples annealed with 0.088 Pa C_2H_2 is also shown in Figure 5.3 (b). Compared with the spectra of the pristine SWCNT sample, the RBM, G-band, and D-band intensity first decreases during the temperature rising process (at 0 min). We suppose the decrease of Raman intensity is because SWCNTs are damaged by the interaction between the substrate and the pristine SWCNTs at high temperature [170]. The decrease of G-band and D-band also appeared in a 1000 °C annealing case. The relevant defect healing results are displayed in Figure 5.4. As shown in Figure 5.4 (d), such decrease tendency of G-band intensity even extended from the temperature rising process to the healing process, which affected the analysis of defect healing behavior. Therefore, in this study, we mainly discuss the defect healing results treated at 1100 °C. By prolonging the healing time to 20, 40, and 60 min, as shown in Figures 5.3 (a) and (b), the intensity of RBM spectra and G-band gradually increased both with and without the use of C_2H_2. Additional healing results of SWCNTs treated with 0.035 and 0.088 Pa for 5 and 10 min are shown in Figure 5.5. Without the use of carbon-

containing reactant, such increase of G-band and RBM intensity at high temperature has been discussed and explained by the healing of defects.[165, 166, 171, 172] In the meantime, the use of C_2H_2 caused a more rapid intensity increase of the RBM peaks at around 210 and 280 cm^{-1}.

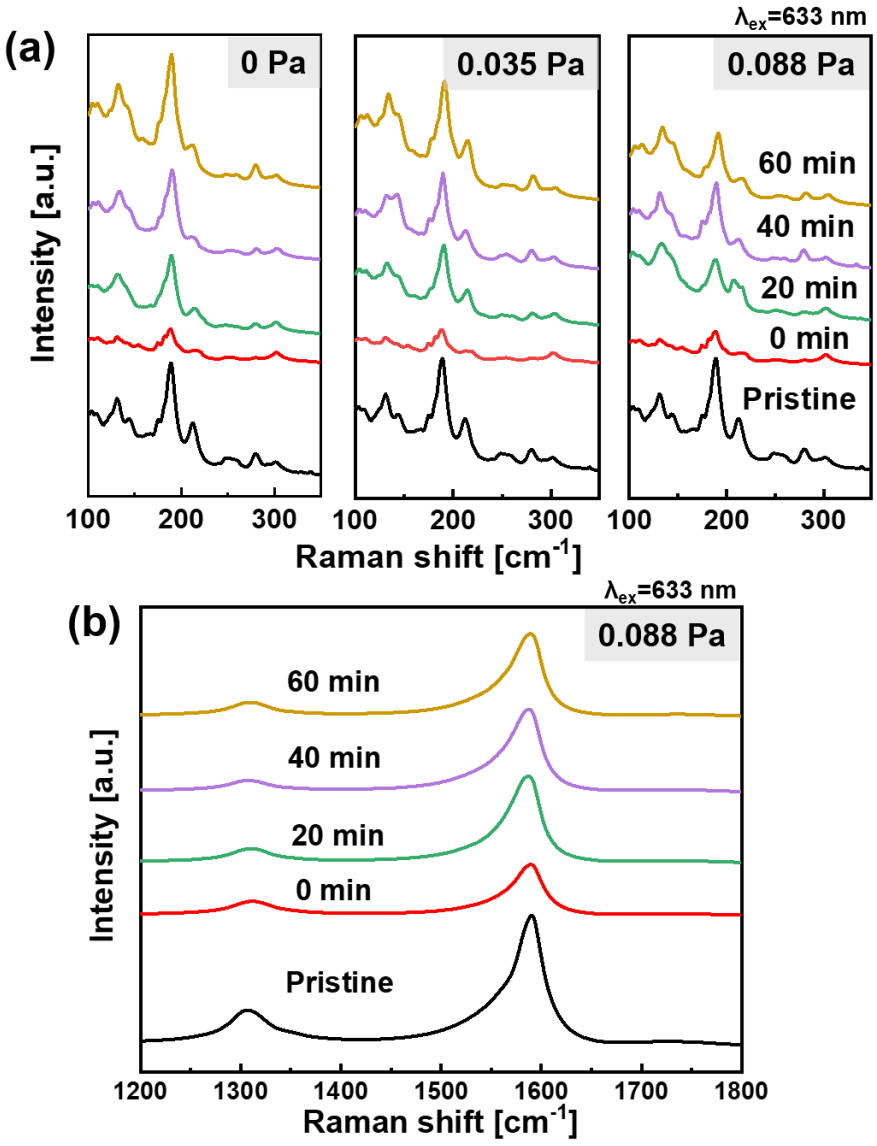

Figure 5.3: (a) RBM spectra of the pristine SWCNTs and the healed SWCNTs treated with 0, 0.035, and 0.088 Pa C_2H_2 for 0, 20, 40, and 60 min at 1100 °C. (b) G-band and D band of the pristine SWCNTs and the SWCNTs annealed with 0.088 Pa C_2H_2 at 1100 °C for 0, 20, 40, and 60 min.

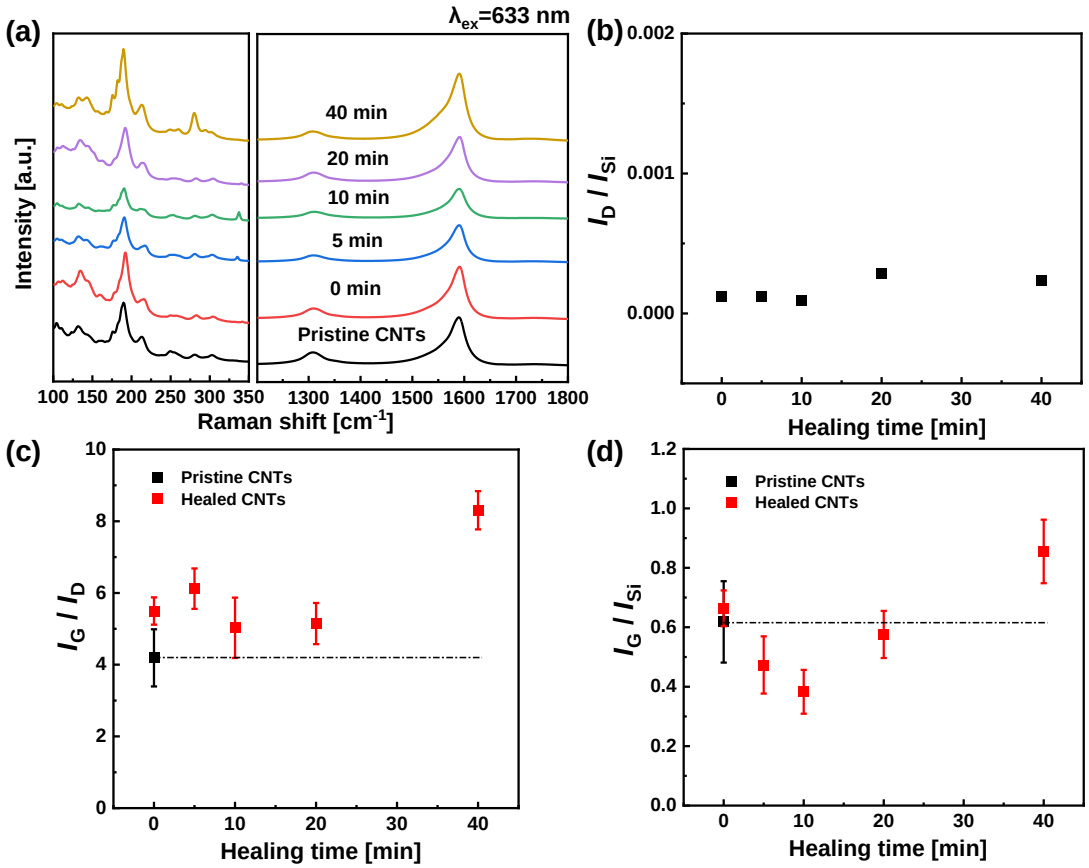

Figure 5.4: Process time dependence of the (a) Raman spectra, (c) I_G/I_D ratio, (d) I_G/I_{Si} ratio of the SWCNTs and (b) the I_D/I_{Si} ratio of the relevant blank sample treated with the C_2H_2-injected healing process (0.088 Pa) at 1000 °C. The I_G/I_D and I_G/I_{Si} ratios of the pristine SWCNTs were plotted as a reference.

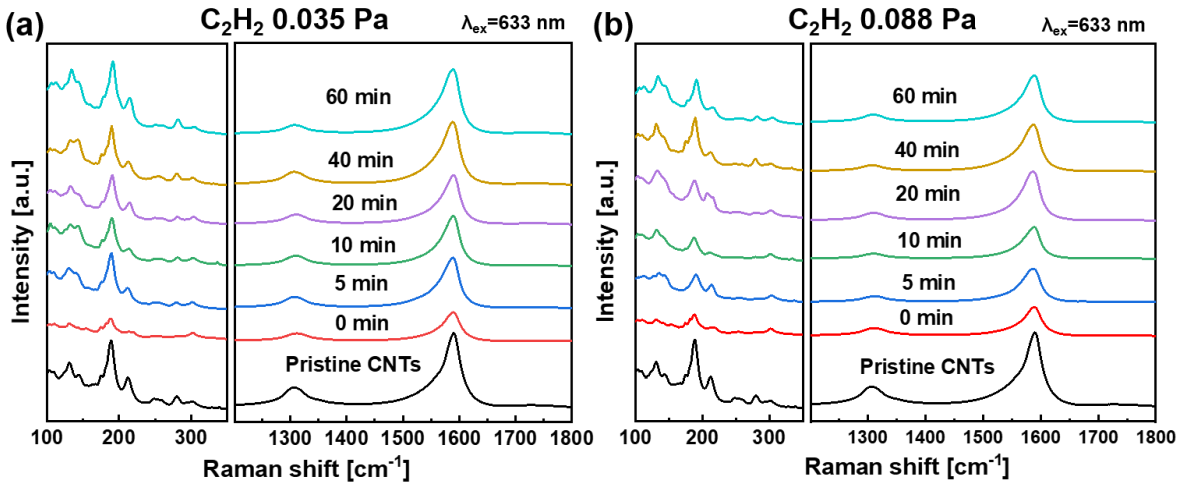

Figure 5.5: Raman spectra of the pristine SWCNTs and the healed SWCNTs treated with (a) 0.035, and (b) 0.088 Pa C_2H_2 for 0, 5, 10, 20, 40, and 60 min at 1100 °C.

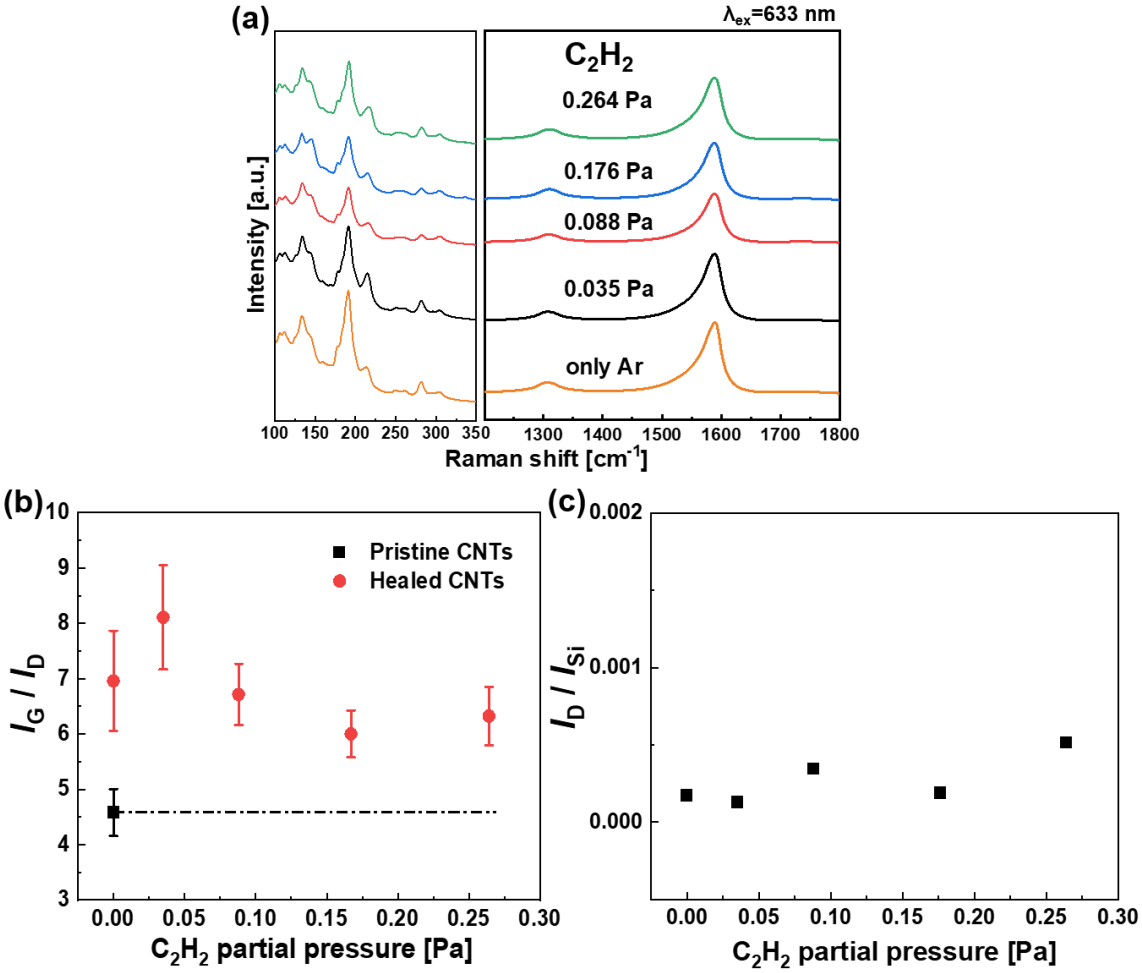

Figure 5.6: C_2H_2 partial pressure dependence of the (a) Raman spectra, (b) I_G/I_D ratio, and (c) the I_D/I_{Si} ratio of the relevant blank sample. The I_G/I_D of the pristine SWCNTs were plotted as a reference.

The Raman spectra of the healed SWCNTs with further changing the injected C_2H_2 partial pressure is exhibited in Figure 5.6. In the annealing process, SWCNTs was treated with higher partial pressure (0.176 and 0.264 Pa) of C_2H_2 at 1100 ^oC for 60 min. The quality of the healed sample was analyzed by I_G/I_D as shown in Figure 5.6 (b). By increasing the partial pressure of C_2H_2 from 0 to 0.035 Pa, the I_G/I_D ratio of SWCNTs increased to ~8. However, as shown in Figure 5.6 (c), compared with the 0.035 Pa-C_2H_2 injection case, 0.088, 0.176, and 0.264 Pa-supplied healing results present higher I_D/I_{Si} ratio of the blank sample, which indicates the increase of a-C deposition in the healing conditions. The SEM images of the pristine and healed SWCNTs are shown in Figure 5.7.

It can be found that there is almost no a-C deposited on the surface of the pristine SWCNTs and the SWCNTs annealed with no Pa-C_2H_2. On the other hand, a-C was observed as ununiformly distributed brighter areas on the SWCNT surface for the higher C_2H_2 partial pressure samples, and the amount of it was increased with increasing the pressure from 0.035 to 0.264 Pa. Thus, the decrease of I_G/I_D ratio of the healed SWCNTs with increasing C_2H_2 partial pressure (Figure 5.6 (b)) is attributed mainly to the increased deposition of a-C.

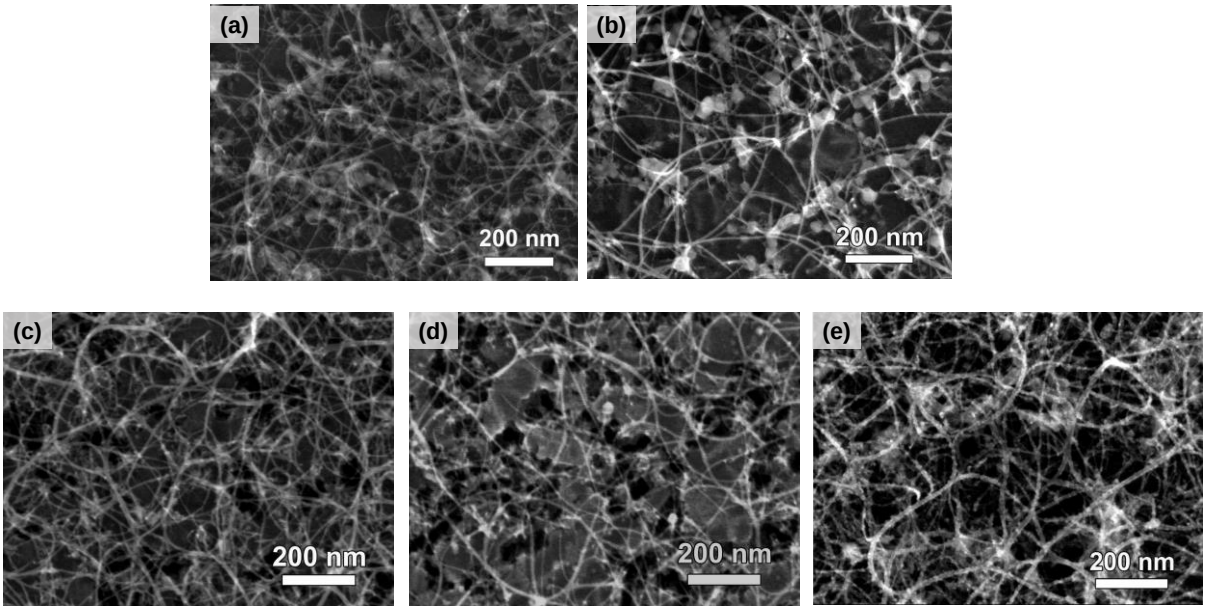

Figure 5.7: SEM images (acceleration voltage: 5 kV) of (a) the pristine SWCNTs and (b–d) the SWCNTs healed at 1100 °C for 60 min with the injection of C_2H_2. The partial pressure of C_2H_2 is (b) 0, (c) 0.035, (d) 0.088, and (e) 0.264 Pa.

To further analyze the change of defect density during the healing process, we calculate the I_G/I_D ratio based on the Raman spectra of the healed samples, and the result is presented in Figure 5.9. The I_G/I_D ratio of the pristine SWCNTs was regarded as the baseline. Compared with the pristine sample, with 0 min healing treatment, the averaged I_G/I_D ratio of the healed SWCNTs did not change much. As the healing time went by, the C_2H_2-injected (0.035 Pa and 0.088 Pa) healing cases gradually expressed higher I_G/I_D ratio than the SWCNTs healed without C_2H_2 injection, which reflects the improvement of SWCNT crystallinity. Moreover, different defect healing rates appeared with changing C_2H_2 partial pressure. According to Figure 5.9, in 0 and 0.035 Pa C_2H_2 injected annealing process, the defect healing rate was similar in first 20 min and the I_G/I_D ratio increased to

around 5.5 in both two cases. After 20 min, the healing rate from 20 min to 60 min gradually decreased in the 0 Pa healing case and finally be almost 0 from 60 to 90 min. Compared with the 0 Pa C_2H_2 injected healing result, although there is a data fluctuation from 20-40 min, a higher overall healing rate from 20 min to 60 min was found in the 0.035 Pa case and the I_G/I_D ratio finally increased to ~8. Further raising the partial pressure of C_2H_2 to 0.088 Pa, a more noticeable increase in healing rate appeared in the first 20 min and the I_G/I_D ratio reached ~8.9 when the healing time was 40 min. Prolonging the healing time to 60 min, we noticed that the I_G/I_D ratio decreased from 40 to 60 min. To analyze this phenomenon, we collected the I_G/I_{Si} ratio of the healed SWCNT samples and the I_D/I_{Si} ratio of the blank samples, shown in Figure 5.8. From Figure 5.8 (b), the I_G/I_{Si} ratio kept stable for 20 min. On the other hand, the I_D/I_{Si} ratio of the blank samples gradually increased from 20 to 60 min, representing the deposition of a-C. Thus, we suppose that the decrease in the I_G/I_D ratio is caused by the deposition of a-C in 0.088 Pa-C_2H_2 supplied healing process. It also explained the decrease of I_G/I_D in the 0.035 Pa case from 60 to 90 min.

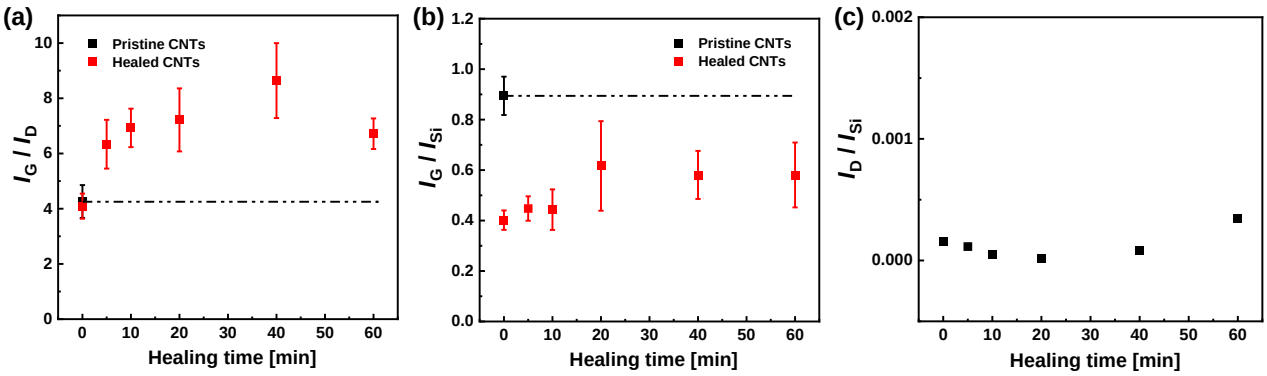

Figure 5.8: Change in the I_G/I_D ratio of the SWCNTs healed with the injection of C_2H_2 (0, 0.035 and 0.088 Pa) along the healing time. The I_G/I_D ratio of the pristine SWCNTs was plotted as a reference. All dotted lines are guide to the eyes.

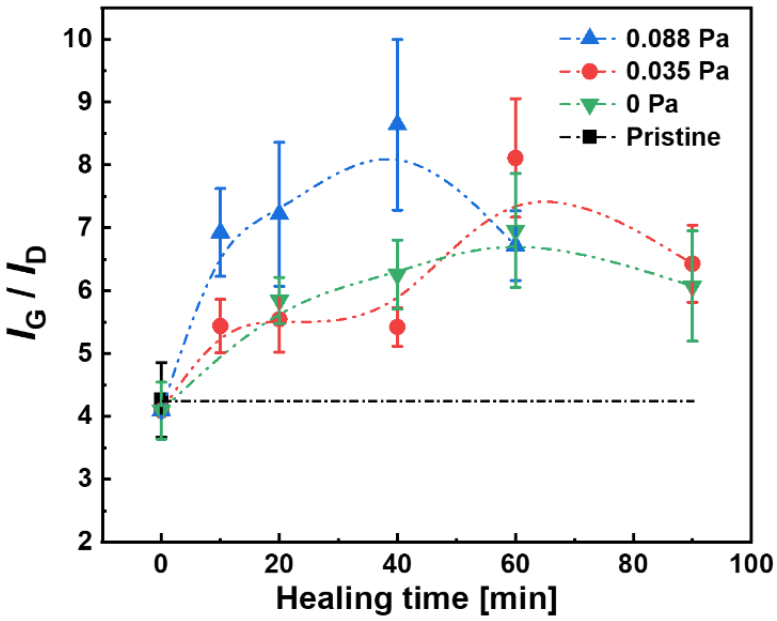

Figure 5.9: Process time dependence of the (a) I_G/I_D ratio and (b) I_G/I_{Si} ratio of the SWCNTs, and (c) the I_D/I_{Si} ratio of the relevant blank sample treated with the C_2H_2-injected healing process (0.088 Pa). The I_G/I_D and I_G/I_{Si} ratios of the pristine SWCNTs were plotted as a reference.

Then, we further discuss the influence of C_2H_2 injection to the healing rate of SWCNTs with different diameters. Based on the previous research, the CNT diameter (d_t) is related to the RBM wavenumber (ω_{RBM}) according to the equation [39]:

$$\omega_{RBM}\ (cm^{-1}) = 223.5\ /d_t\ (nm) + 12.5$$

The relative population of SWCNTs with different diameters can be analyzed based on the peak intensity of the RBM spectra. The high wavenumber (200–300 cm^{-1}) corresponds to the small diameter SWCNTs (<1.1 nm), and the low wavenumber (100–200 cm^{-1}) represents the large diameter SWCNTs (>1.1 nm). Among the RBM spectra shown in Figure 5.3 (a), significant intensity change appears on the four peaks at around 133, 188, 210, and 280 cm^{-1}, which corresponds to the SWCNTs with 1.8, 1.3, 1.1 and 0.8 nm diameter, respectively. Taking the RBM peaks of SWCNTs with the four diameters as the representative, the related details of normalized RBM intensity varied with the healing time are exhibited in Figure 5.10 and the healing rates with or without the injection of C_2H_2 are determined as shown in Figure 5.11. The healing rate was calculated by the changes in the corresponding RBM peak intensity along the healing

time. We divided the intensity change in the RBM peaks from 0 min to 40 min by the duration to exclude the contribution of the a-C deposition in long annealing time, which affects the intensity of Raman spectra. Based on previous works,[21, 173, 174] low formation energy of vacancy and 5|7 defects appears in the SWCNTs with small diameter, which eases the formation of these types of defects in the SWCNTs with small diameter. Healing of thin SWCNTs with higher density of defects, especially the vacancy defect, would take longer time compared with thick SWCNTs. Thus, without the injection of C_2H_2, as shown in Figure 5.11, higher healing rate is found in the SWCNTs with large diameter. When C_2H_2 was added to the healing process, the healing rate of the thick SWCNTs (>1.1 nm) slightly increased. Interestingly, in the SWCNTs with small diameters (<1.1 nm), the healing rate was significantly increased with the use of C_2H_2. These increase in the healing rate confirms that the injection of C_2H_2 during the healing process helped to enhance the defect healing rate, especially to the defects in the SWCNTs with small diameter..

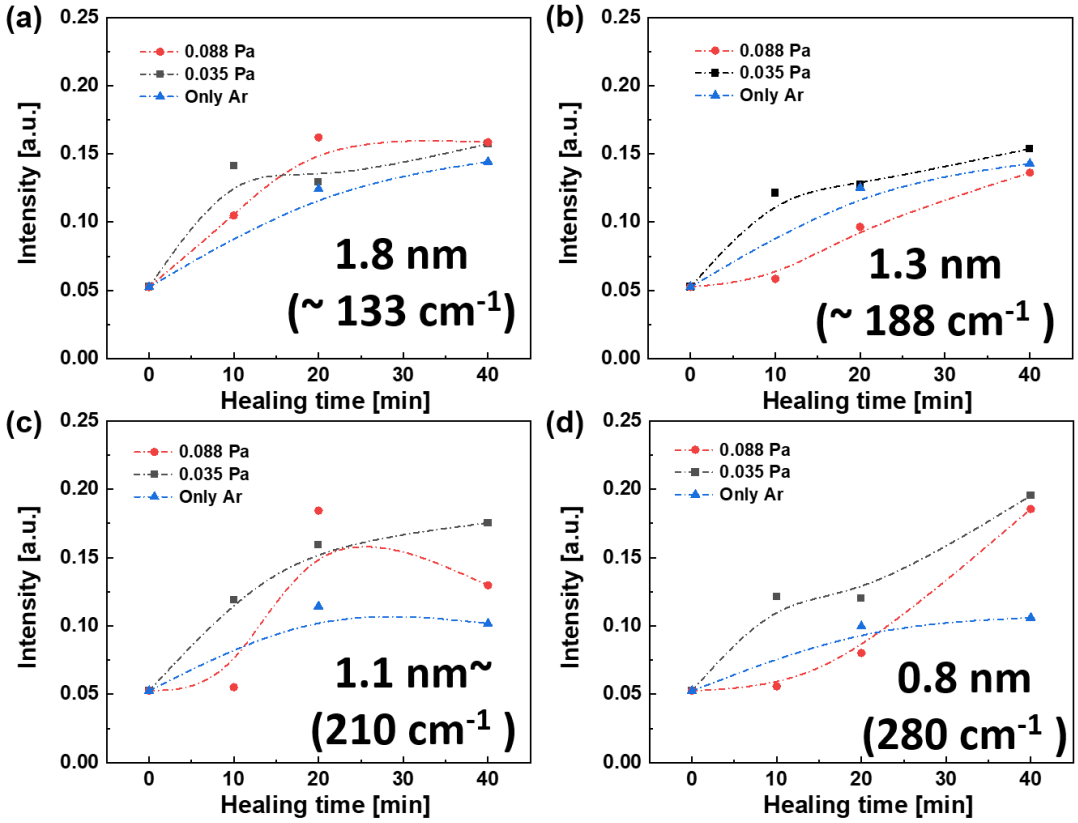

Figure 5.10: The changes in the RBM peak intensity along the healing time (0, 10, 20, and 40 min). The four representative RBM peaks correspond to the SWCNTs with different diameter: (a) 1.8, (b) 1.3, (c) 1.1, and (d) 0.8 nm.

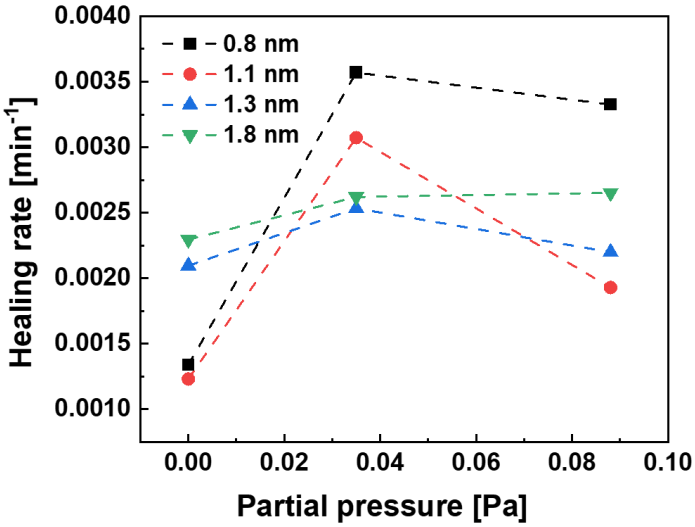

Figure 5.11: Change of the healing rate with the injection of C_2H_2 (0, 0.035 and 0.088 Pa) for the SWCNTs with different diameter (0.8, 1.1, 1.3, and 1.8 nm).

Based on the aforementioned results of C_2H_2 injected defect healing, we derived the healing behavior of C_2H_2 in the high temperature annealing process and schematically depicted it in Figure 5.12. For the pristine SWCNTs synthesized at low temperature, several kinds of defects formed during the growth process, including the adatom, vacancy, 5|7 defects, and so on. During the healing process, with the presence of trace amount of oxidative gas impurities (O_2, H_2O, or CO_2), the adatom defects could be partly healed through etching reaction [175]. However, if there are no carbon atoms injected into the healing process, vacancy defects tend to stay or change to closed lattice structures with pentagon and heptagon defects through Stone-Wales-type transformation [34, 176], which means the difficulty in healing vacancy defects. To heal vacancy defects, the use of carbon-containing reactant is effective because carbon atoms from the reactant are adsorbed on the vacancy defects and incorporated into the lattice of the SWCNTs [88-91]. Thus, in Figure 5.12, we suppose that the adatom defects and the vacancy defects would be the representative defects which can be healed in the C_2H_2-injected healing process.

Among such defects, the low formation energy of adatom defect makes it easy to be constructed [173]. Thus, compared to the adatom defects, the vacancy defects in the pristine SWCNT structure appear with lower density because of their high formation energy [173]. Besides, related to the diameter of SWCNTs, the formation energy of

defects is lower in the SWCNTs with small diameter compared with the one with large diameter [21, 174], which makes vacancy defects easier to form on the thin SWCNTs. Therefore, as shown in Figure 5.12, higher-density vacancy defects appear in the pristine SWCNTs with small diameter.

When only heated in Ar gas with low pressure, the adatom defects tend to be healed while the vacancy defects are more likely to stay. On the other hand, when C_2H_2 was added, the vacancy defects could be better healed, which caused an increase in the healing rate in both thick and thin SWCNTs. In this high temperature treatment, the pyrolysis reaction of C_2H_2 also happens, which produced H_2 and helped to remove adatom defects [175]. Moreover, the high density of defects on the thin tube structure would take longer time and be harder to heal, which brings about the low healing rate in thin SWCNTs with high-density defects. Especially for the thin SWCNTs, the healing rate was more drastically increased compared to the thick tubes.

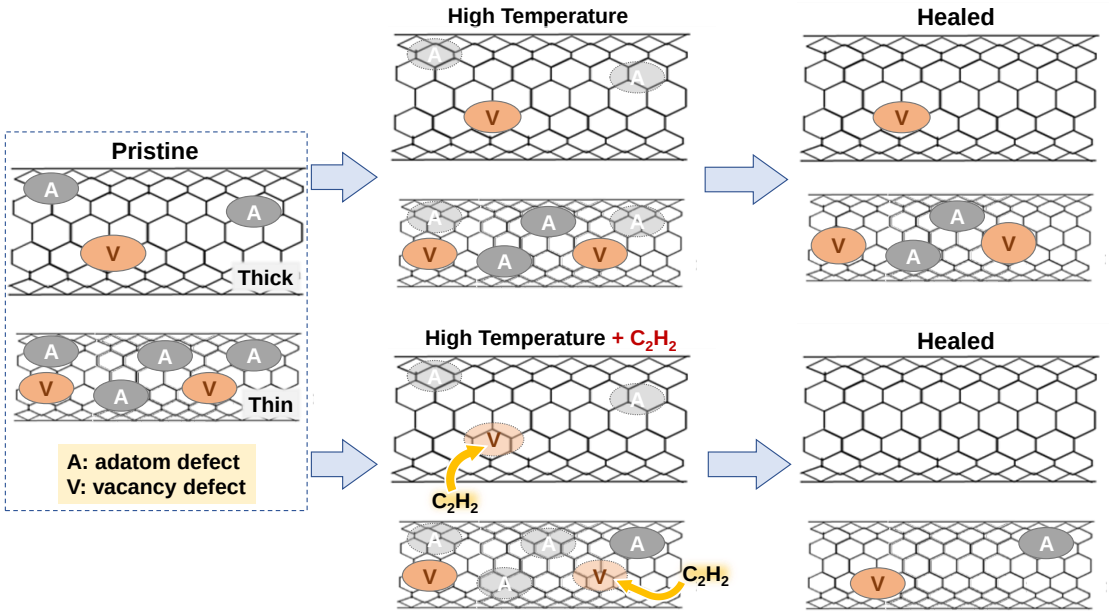

Figure 5.12: Schematic defect healing diagram of the pristine SWCNTs annealed at high temperature (1100 ºC) with or without the injection of C_2H_2. The pristine SWCNTs are divided into thick (>1.1 nm) and thin (<1.1nm) SWCNTs according to their diameter.

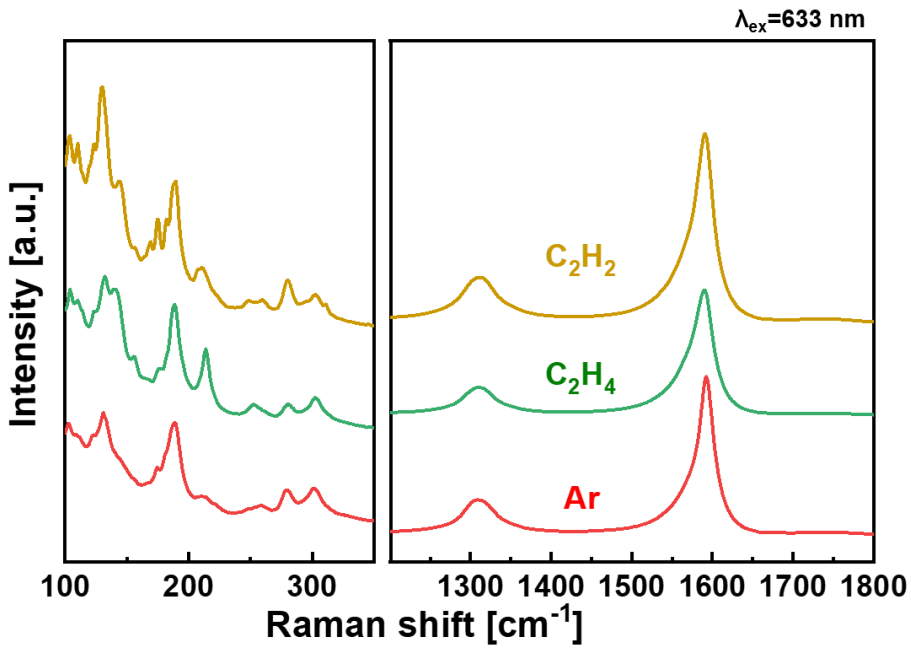

Figure 5.13: Raman spectra of the healed SWCNTs treated with only Ar, 0.352 Pa C_2H_2 and 0.352 Pa C_2H_4 for 60 min at 1100 ^oC.

Besides, we also investigated the healing effect of ethylene (C_2H_4). As shown in Figure 5.13, the injection of C_2H_4 resulted in the efficient healing of SWCNTs similarly to the case of C_2H_2, indicating the general effectiveness of carbon-containing reactants in thermal defect healing.

5.4 Conclusion

In conclusion, with the experimental results, we confirmed the healing behavior of C_2H_2 in the high temperature (1100 ^oC) annealing process, which had been only analyzed through theoretical methods. Compared with the SWCNTs healed only in Ar gas, the SWCNTs healed with C_2H_2 presented higher crystallinity. The defect healing rate was increased with rising the partial pressure of injected C_2H_2 from 0 to 0.088 Pa. On the other hand, with the increase of the injected C_2H_2, the formation of a-C for long process time becomes a problem that needs to be solved in future work. Further, considering the diameter of SWCNTs, we found that the healing effect of C_2H_2 injection was more evident in the SWCNTs with small diameter (<1.1 nm). Combining with the previous simulation research about the healing behavior of C_2H_2, we consider that C_2H_2 helps to

heal the vacancy defects and increased the high temperature healing rate. Moreover, we also found that C_2H_4 exhibited a healing ability which is similar to C_2H_2. These results prove that injecting carbon-containing reactants, like C_2H_2, would be an additional important factor for healing SWCNT defects with high efficiency. With the assistance of such carbon-containing reactants, SWCNTs with higher crystallinity can be achieved by the post treatment process, which would further realize the improvement of SWCNT properties required for electronic, thermal, and mechanical applications.

After finding the promising healing role of carbon-containing reactants, in future, I would like to further prove this result with providing more evidences. Besides, as mentioned in this work, the problem of a-C deposition during the healing process, I would try to inject etchants to prevent it. With these efforts, I suppose that the high temperature defect healing treatment would be more efficient in increasing the quality of SWCNTs and even could be expanded to separated SWCNTs in a large scale.

Chapter 6: Conclusion and future perspective

6.1 Conclusion

Recently, to achieve SWCNTs with high crystallinity, thermal treatment is admitted during SWCNT synthesis process and post-treatment step. One of issues, the aggregation of growth seeds in high temperature synthesis, could be solved by using solid carbon nanoparticles (NDs) because of the high stability of morphology. Moreover, compared to metal nanoparticles, using NDs as the growth seeds brings fewer metal impurities to SWCNTs sample. Thus, in this dissertation, we systematically studied the ND-based high temperature growth process and the effect of growth enhancers injected in such growth. What's more, achieved from ND-based SWCNT growth process, we studied the healing effect of carbon-containing reactants in high temperature annealing post-treatment.

Chapter three describes the efficient synthesis of highly crystalline SWCNTs from unconventional solid carbon nanoparticles derived from NDs as growth seeds. This was enabled by a two-step growth process based on thermodynamic considerations of growth driving force required for different growth stages as well as by an addition of water vapor as the etchant. Systematic experiments revealed that separate control of growth driving force in the cap formation stage and the stationary elongation stage significantly affects the yield and the structural variation of SWCNTs. With the assistance of water vapor, we attained a 10-fold increase in the SWCNT yield from solid carbon nanoparticles while ensuring the high crystallinity of SWCNTs. Instead of metal nanoparticles, in this work, solid carbon nanoparticles (NDs) were employed as the growth seeds, which presents high thermal stability and will not fuse at high growth temperature.

Chapter four discusses the enhancing roles of water (H_2O) and carbon dioxide (CO_2) in the SWCNT growth without metal catalysts. In this research, NDs—one of the non-metallic nanoparticles—was used as the growth seeds to exclude the influence of metal catalysts in the CNT growth process. The enhancing effects of injected H_2O and CO_2 were discussed by analyzing the SWCNT growth results with two types of carbon sources (C_2H_2 and C_2H_4). Systematic experiments revealed that H_2O and CO_2 possess oxidizing ability to prevent the deposition of amorphous carbon (a-C) without the

participation of metal catalysts. In C_2H_4-supplied growth, CO_2 injection presents a better role than H_2O in preventing a-C deposition. Moreover, in the combination of CO_2 and C_2H, we found a unique promotion role of CO_2 by which a-C deposition and SWCNT growth were significantly enhanced. Based on the change in chemical potential, we discuss the effect of the dehydrogenation reaction between C_2H_2 and CO_2, which has been found only in metal-catalyzed SWCNT growth.

Chapter five experimentally investigated the effect of C_2H_2 as the defect healer during the high temperature annealing process. Systematic experiments revealed that C_2H_2 worked as a defect healer and helped to highly improve the crystallinity of the SWCNTs compared with the sample only annealed in Ar ambient. We found the defect healing rate increased with the increase of partial pressure of injected C_2H_2, resulting in sufficient healing which proceeded in a shorter time. Moreover, C_2H_2 exhibited more efficient healing on the SWCNTs with small diameter (<1.1 nm). Based on the experimental results and relevant simulation studies from other groups, we propose that C_2H_2 assists the healing of vacancy defects and provides a higher healing rate. The obtained findings demonstrate the effectiveness of the post-treatment approach to improve SWCNT crystallinity, leading to highly crystalline and structure-controlled SWCNTs which are demanded for their vast applications.

6.2 Future perspective

In this thesis, through the ND-based two-step growth process, we increased the yield of high quality SWCNTs, an uncontrolled mixture of metallic and semiconducting SWCNTs. Because of the difference in electric transport properties of SWCNTs with different chirality, developing a chirality-selective synthesis process would be more recommended. It needs to be noticed that the cap structure will influence the chirality of SWCNTs, but the nucleation behavior of SWCNTs still needs to be clarified in VSSS growth mode. Thus, in the ND-based growth process, we would like to further study the nucleation behavior of SWCNTs on the surface of solid carbon growth seeds and modify the growth condition to achieve SWCNTs with high chirality purity.

Moreover, through this study, we achieved SWCNTs randomly arranged on the SiO_2/Si substrates. However, the appearance of crosslinks and the difference in the orientation of SWCNTs reduce its electronic properties and influences their applications, especially in the application of thin film transistors (TFTs). Therefore, we suppose to apply this high temperature growth system into the formation of horizontally well-aligned SWCNTs arrays and study the related properties.

Besides, the study about the effect of carbon-containing reactants will continue to illustrate their healing behavior at high temperature. Considering about the deposition of a-C in the annealing process, growth enhancers, such as CO_2, will be added to prevent the formation of such carbon impurity.

References

[1] Kroto, H. W.;Heath, J. R.;O'Brien, S. C.;Curl, R. F.; Smalley, R. E. C60: Buckminsterfullerene. *Nature* **1985**, *318*, 162-163.

[2] Krätschmer, W.;Lamb, L. D.;Fostiropoulos, K.; Huffman, D. R. Solid C60: a new form of carbon. *Nature* **1990**, *347*, 354-358.

[3] Novoselov, K. S.;Geim, A. K.;Morozov, S. V.;Jiang, D.;Zhang, Y.;Dubonos, S. V.;Grigorieva, I. V.; Firsov, A. A. Electric Field Effect in Atomically Thin Carbon Films. *Science* **2004**, *306*, 666-669.

[4] Iijima, S.; Ichihashi, T. Single-shell carbon nanotubes of 1-nm diameter. *Nature* **1993**, *363*, 603-605.

[5] Iijima, S. Helical microtubules of graphitic carbon. *Nature* **1991**, *354*, 56-58.

[6] Collins, P. G.;Arnold, M. S.; Avouris, P. Engineering Carbon Nanotubes and Nanotube Circuits Using Electrical Breakdown. *Science* **2001**, *292*, 706-709.

[7] Yu, M.-F.;Files, B. S.;Arepalli, S.; Ruoff, R. S. Tensile Loading of Ropes of Single Wall Carbon Nanotubes and their Mechanical Properties. *Physical Review Letters* **2000**, *84*, 5552-5555.

[8] Krishnan, A.;Dujardin, E.;Ebbesen, T. W.;Yianilos, P. N.; Treacy, M. M. J. Young's modulus of single-walled nanotubes. *Physical Review B* **1998**, *58*, 14013-14019.

[9] Pop, E.;Mann, D.;Wang, Q.;Goodson, K.; Dai, H. Thermal Conductance of an Individual Single-Wall Carbon Nanotube above Room Temperature. *Nano Letters* **2006**, *6*, 96-100.

[10] Yu, C.;Shi, L.;Yao, Z.;Li, D.; Majumdar, A. Thermal Conductance and Thermopower of an Individual Single-Wall Carbon Nanotube. *Nano Letters* **2005**, *5*, 1842-1846.

[11] Kong, J.;Franklin, N. R.;Zhou, C.;Chapline, M. G.;Peng, S.;Cho, K.; Dai, H. Nanotube Molecular Wires as Chemical Sensors. *Science* **2000**, *287*, 622-625.

[12] Collins, P. G.;Bradley, K.;Ishigami, M.; Zettl, A. Extreme Oxygen Sensitivity of Electronic Properties of Carbon Nanotubes. *Science* **2000**, *287*, 1801-1804.

[13] Landi, B. J.;Ganter, M. J.;Cress, C. D.;DiLeo, R. A.; Raffaelle, R. P. Carbon nanotubes for lithium ion batteries. *Energy & Environmental Science* **2009**, *2*, 638-654.

[14] Kaempgen, M.;Chan, C. K.;Ma, J.;Cui, Y.; Gruner, G. Printable Thin Film Supercapacitors Using Single-Walled Carbon Nanotubes. *Nano Letters* **2009**, *9*, 1872-1876.

[15] Picó, F.;Rojo, J. M.;Sanjuán, M. L.;Ansón, A.;Benito, A. M.;Callejas, M. A.;Maser, W. K.; Martínez, M. T. Single-Walled Carbon Nanotubes as Electrodes in Supercapacitors. *Journal of The Electrochemical Society* **2004**, *151*, A831.

[16] Odom, T. W.;Huang, J.-L.;Kim, P.; Lieber, C. M. Atomic structure and electronic properties of single-walled carbon nanotubes. *Nature* **1998**, *391*, 62-64.

[17] Baughman, R. H.;Zakhidov, A. A.; de Heer, W. A. Carbon Nanotubes--the Route Toward Applications. *Science* **2002**, *297*, 787-792.

[18] Bati, A. S. R.;Yu, L.;Batmunkh, M.; Shapter, J. G. Synthesis, purification, properties and characterization of sorted single-walled carbon nanotubes. *Nanoscale* **2018**, *10*, 22087-22139.

[19] Kharlamova, M. V. Advances in tailoring the electronic properties of single-walled carbon nanotubes. *Progress in Materials Science* **2016**, *77*, 125-211.

[20] Charlier, J.-C.;Blase, X.; Roche, S. Electronic and transport properties of nanotubes. *Reviews of Modern Physics* **2007**, *79*, 677-732.

[21] Yuan, Q.;Xu, Z.;Yakobson, B. I.; Ding, F. Efficient Defect Healing in Catalytic Carbon Nanotube Growth. *Physical Review Letters* **2012**, *108*, 245505.

[22] Vicarelli, L.;Heerema, S. J.;Dekker, C.; Zandbergen, H. W. Controlling Defects in Graphene for Optimizing the Electrical Properties of Graphene Nanodevices. *ACS Nano* **2015**, *9*, 3428-3435.

[23] Yousefi, F.; Khoeini, F. Impact of topological line defects on wall roughness and thermal conductivity of carbon nanotubes: A molecular dynamics study. *AIP Advances* **2019**, *9*, 025024.

[24] Khalap, V. R.;Sheps, T.;Kane, A. A.; Collins, P. G. Hydrogen Sensing and Sensitivity of Palladium-Decorated Single-Walled Carbon Nanotubes with Defects. *Nano Letters* **2010**, *10*, 896-901.

[25] Robinson, J. A.;Snow, E. S.;Bădescu, Ş. C.;Reinecke, T. L.; Perkins, F. K. Role of Defects in Single-Walled Carbon Nanotube Chemical Sensors. *Nano Letters* **2006**, *6*, 1747-1751.

[26] Jhon, Y. I.;Kim, C.;Seo, M.;Cho, W. J.;Lee, S.; Jhon, Y. M. Tensile Characterization of Single-Walled Carbon Nanotubes with Helical Structural Defects. *Scientific Reports* **2016**, *6*, 20324.

[27] Shi, X.;He, X.;Sun, L.; Liu, X. Influence of Defect Number, Distribution Continuity and Orientation on Tensile Strengths of the CNT-Based Networks: A Molecular Dynamics Study. *Nanoscale Research Letters* **2022**, *17*, 15.

[28] Yakobson, B. I. Mechanical relaxation and "intramolecular plasticity" in carbon nanotubes. *Applied Physics Letters* **1998**, *72*, 918-920.

[29] Neyts, E. C.;van Duin, A. C. T.; Bogaerts, A. Changing Chirality during Single-Walled Carbon Nanotube Growth: A Reactive Molecular Dynamics/Monte Carlo Study. *Journal of the American Chemical Society* **2011**, *133*, 17225-17231.

[30] Tong, T.;Zhao, Y.;Delzeit, L.;Kashani, A.;Meyyappan, M.; Majumdar, A. Dense Vertically Aligned Multiwalled Carbon Nanotube Arrays as Thermal Interface Materials. *IEEE Transactions on Components and Packaging Technologies* **2007**, *30*, 92-100.

[31] Qin, C.; Peng, L. M. Measurement accuracy of the diameter of a carbon nanotube from TEM images. *Physical Review B* **2002**, *65*, 155431.

[32] Zhang, Y.;Shi, Z.;Gu, Z.; Iijima, S. Structure modification of single-wall carbon nanotubes. *Carbon* **2000**, *38*, 2055-2059.

[33] Hata, K.;Futaba, D. N.;Mizuno, K.;Namai, T.;Yumura, M.; Iijima, S. Water-Assisted Highly Efficient Synthesis of Impurity-Free Single-Walled Carbon Nanotubes. *Science* **2004**, *306*, 1362-1364.

[34] Börrnert, F.;Gorantla, S.;Bachmatiuk, A.;Warner, J. H.;Ibrahim, I.;Thomas, J.;Gemming, T.;Eckert, J.;Cuniberti, G.;Büchner, B.; Rümmeli, M. H. In situ observations of self-repairing single-walled carbon nanotubes. *Physical Review B* **2010**, *81*, 201401.

[35] Yoshida, H.;Takeda, S.;Uchiyama, T.;Kohno, H.; Homma, Y. Atomic-Scale In-situ Observation of Carbon Nanotube Growth from Solid State Iron Carbide Nanoparticles. *Nano Letters* **2008**, *8*, 2082-2086.

[36] Campbell, J. F.;Tessmer, I.;Thorp, H. H.; Erie, D. A. Atomic Force Microscopy Studies of DNA-Wrapped Carbon Nanotube Structure and Binding to Quantum Dots. *Journal of the American Chemical Society* **2008**, *130*, 10648-10655.

[37] Samir, K.;Prabhat, K.;Anamika, D.; Chandra Shakher, P. Surface-Enhanced Raman Scattering: Introduction and Applications. In *Recent Advances in Nanophotonics*. K. Mojtaba; A. S. Parsoua, Eds.; IntechOpen; Rijeka, 2020; pp Ch. 8.

[38] Belin, T.; Epron, F. Characterization methods of carbon nanotubes: a review. *Materials Science and Engineering: B* **2005**, *119*, 105-118.

[39] Bachilo, S. M.;Strano, M. S.;Kittrell, C.;Hauge, R. H.;Smalley, R. E.; Weisman, R. B. Structure-Assigned Optical Spectra of Single-Walled Carbon Nanotubes. *Science* **2002**, *298*, 2361-2366.

[40] Ishizaki, F.; Kim, M. Near-Infrared Attenuated Total Reflection Raman Spectroscopy for Polymer Surface Observation. *Japanese Journal of Applied Physics* **2008**, *47*, 1621.

[41] Arora, N.; Sharma, N. N. Arc discharge synthesis of carbon nanotubes: Comprehensive review. *Diamond and Related Materials* **2014**, *50*, 135-150.

[42] Thess, A.;Lee, R.;Nikolaev, P.;Dai, H.;Petit, P.;Robert, J.;Xu, C.;Lee, Y. H.;Kim, S. G.;Rinzler, A. G.;Colbert, D. T.;Scuseria, G. E.;Tománek, D.;Fischer, J. E.; Smalley, R. E. Crystalline Ropes of Metallic Carbon Nanotubes. *Science* **1996**, *273*, 483.

[43] Dai, H.;Rinzler, A. G.;Nikolaev, P.;Thess, A.;Colbert, D. T.; Smalley, R. E. Single-wall nanotubes produced by metal-catalyzed disproportionation of carbon monoxide. *Chemical Physics Letters* **1996**, *260*, 471-475.

[44] Szabó, A.;Perri, C.;Csató, A.;Giordano, G.;Vuono, D.; Nagy, J. B. Synthesis Methods of Carbon Nanotubes and Related Materials. *Materials* **2010**, *3*, 3092-3140.

[45] Santangelo, S.;Messina, G.;Faggio, G.;Lanza, M.;Pistone, A.; Milone, C. Calibration of reaction parameters for the improvement of thermal stability and crystalline quality of multi-walled carbon nanotubes. *Journal of Materials Science* **2010**, *45*, 783-792.

[46] Hernadi, K.;Fonseca, A.;Nagy, J. B.;Bernaerts, D.; Lucas, A. A. Fe-catalyzed carbon nanotube formation. *Carbon* **1996**, *34*, 1249-1257.

[47] He, D.;Li, H.;Li, W.;Haghi-Ashtiani, P.;Lejay, P.; Bai, J. Growth of carbon nanotubes in six orthogonal directions on spherical alumina microparticles. *Carbon* **2011**, *49*, 2273-2286.

[48] Kong, J.;Cassell, A. M.; Dai, H. Chemical vapor deposition of methane for single-walled carbon nanotubes. *Chemical Physics Letters* **1998**, *292*, 567-574.

[49] Shirazi, Y.;Tofighy, M. A.;Mohammadi, T.; Pak, A. Effects of different carbon precursors on synthesis of multiwall carbon nanotubes: Purification and Functionalization. *Applied Surface Science* **2011**, *257*, 7359-7367.

[50] Rinzler, A. G.;Hafner, J. H.;Nikolaev, P.;Nordlander, P.;Colbert, D. T.;Smalley, R. E.;Lou, L.;Kim, S. G.; Tománek, D. Unraveling Nanotubes: Field Emission from an Atomic Wire. *Science* **1995**, *269*, 1550-1553.

[51] Satishkumar, B. C.;Govindaraj, A.; Rao, C. N. R. Bundles of aligned carbon nanotubes obtained by the pyrolysis of ferrocene–hydrocarbon mixtures: role of the metal nanoparticles produced in situ. *Chemical Physics Letters* **1999**, *307*, 158-162.

[52] Tomie, T.;Inoue, S.;Kohno, M.; Matsumura, Y. Prospective growth region for chemical vapor deposition synthesis of carbon nanotube on C–H–O ternary diagram. *Diamond and Related Materials* **2010**, *19*, 1401-1404.

[53] Li, W. Z.;Xie, S. S.;Qian, L. X.;Chang, B. H.;Zou, B. S.;Zhou, W. Y.;Zhao, R. A.; Wang, G. Large-Scale Synthesis of Aligned Carbon Nanotubes. *Science* **1996**, *274*, 1701-1703.

[54] Parthasarathy, R. V.;Phani, K. L. N.; Martin, C. R. Template synthesis of graphitic nanotubules*. *Adv. Mater.* **1995**, *7*, 896-897.

[55] Yong, Z.;Fang, L.; Zhi-hua, Z. Synthesis of heterostructured helical carbon nanotubes by iron-catalyzed ethanol decomposition. *Micron* **2011**, *42*, 547-552.

[56] Hillert, M.; Lange, N. The structure of graphite filaments. *Zeitschrift für Kristallographie - Crystalline Materials* **1959**, *111*, 24-34.

[57] Han, S.;Liu, X.; Zhou, C. Template-Free Directional Growth of Single-Walled Carbon Nanotubes on a- and r-Plane Sapphire. *Journal of the American Chemical Society* **2005**, *127*, 5294-5295.

[58] Kocabas, C.;Hur, S.-H.;Gaur, A.;Meitl, M. A.;Shim, M.; Rogers, J. A. Guided Growth of Large-Scale, Horizontally Aligned Arrays of Single-Walled Carbon Nanotubes and Their Use in Thin-Film Transistors. *Small* **2005**, *1*, 1110-1116.

[59] Kocabas, C.;Shim, M.; Rogers, J. A. Spatially Selective Guided Growth of High-Coverage Arrays and Random Networks of Single-Walled Carbon Nanotubes and Their Integration into Electronic Devices. *Journal of the American Chemical Society* **2006**, *128*, 4540-4541.

[60] Seidel, R.;Duesberg, G. S.;Unger, E.;Graham, A. P.;Liebau, M.; Kreupl, F. Chemical Vapor Deposition Growth of Single-Walled Carbon Nanotubes at 600 °C and a Simple Growth Model. *The Journal of Physical Chemistry B* **2004**, *108*, 1888-1893.

[61] Esconjauregui, S.;Whelan, C. M.; Maex, K. The reasons why metals catalyze the nucleation and growth of carbon nanotubes and other carbon nanomorphologies. *Carbon* **2009**, *47*, 659-669.

[62] Li, Y.;Cui, R.;Ding, L.;Liu, Y.;Zhou, W.;Zhang, Y.;Jin, Z.;Peng, F.; Liu, J. How Catalysts Affect the Growth of Single-Walled Carbon Nanotubes on Substrates. *Advanced Materials* **2010**, *22*, 1508-1515.

[63] Everhart, B. M.;Rao, R.;Nikolaev, P.;Liu, T.-W.;Gómez-Gualdrón, D. A.;Maruyama, B.; Amama, P. B. High-Throughput Experimentation for Selective Growth of Small-Diameter Single-Wall Carbon Nanotubes Using Ru-Promoted Co Catalysts. *Chemistry of Materials* **2022**, *34*, 4548-4559.

[64] Sugime, H.;Noda, S.;Maruyama, S.; Yamaguchi, Y. Multiple “optimum” conditions for Co–Mo catalyzed growth of vertically aligned single-walled carbon nanotube forests. *Carbon* **2009**, *47*, 234-241.

[65] Homma, Y.;Kobayashi, Y.;Ogino, T.;Takagi, D.;Ito, R.;Jung, Y. J.; Ajayan, P. M. Role of Transition Metal Catalysts in Single-Walled Carbon Nanotube Growth in Chemical Vapor Deposition. *J. Phys. Chem. B* **2003**, *107*, 12161-12164.

[66] Wagner, R. S.; Ellis, W. C. Vapor-Liquid-Solid Mechanism of Single Crystal Growth. *Appl. Phys. Lett.* **1964**, *4*, 89-90.

[67] Feng, X.;Chee, S. W.;Sharma, R.;Liu, K.;Xie, X.;Li, Q.;Fan, S.; Jiang, K. In Situ TEM observation of the gasification and growth of carbon nanotubes using iron catalysts. *Nano Research* **2011**, *4*, 767.

[68] Li, M.;Liu, X.;Zhao, X.;Yang, F.;Wang, X.; Li, Y. Metallic Catalysts for Structure-Controlled Growth of Single-Walled Carbon Nanotubes. *Topics in Current Chemistry* **2017**, *375*, 29.

[69] Takagi, D.;Kobayashi, Y.; Homma, Y. Carbon Nanotube Growth from Diamond. *Journal of the American Chemical Society* **2009**, *131*, 6922-6923.

[70] Homma, Y.;Liu, H.;Takagi, D.; Kobayashi, Y. Single-walled carbon nanotube growth with non-iron-group “catalysts” by chemical vapor deposition. *Nano Research* **2009**, *2*, 793.

[71] Vinten, P.;Marshall, P.;Lefebvre, J.; Finnie, P. Thermodynamic and Energetic Effects on the Diameter and Defect Density in Single-Walled Carbon Nanotube Synthesis. *The Journal of Physical Chemistry C* **2013**, *117*, 3527-3536.

[72] Oberlin, A. Carbonization and graphitization. *Carbon* **1984**, *22*, 521-541.

[73] Saito, Y. *Statistical physics of crystal growth*; World Scientific, 1996.

[74] Wagg, L. M.;Hornyak, G. L.;Grigorian, L.;Dillon, A. C.;Jones, K. M.;Blackburn, J.;Parilla, P. A.; Heben, M. J. Experimental Gibbs Free Energy Considerations in the Nucleation and Growth of Single-Walled Carbon Nanotubes. *J. Phys. Chem. B* **2005**, *109*, 10435-10440.

[75] Kim, S. M.;Pint, C. L.;Amama, P. B.;Zakharov, D. N.;Hauge, R. H.;Maruyama, B.; Stach, E. A. Evolution in Catalyst Morphology Leads to Carbon Nanotube Growth Termination. *J. Phys. Chem. Lett.* **2010**, *1*, 918-922.

[76] Yoshida, H.; Takeda, S. Elucidation of the origin of grown-in defects in carbon nanotubes. *Carbon* **2014**, *70*, 266-272.

[77] Kase, H.;Negishi, R.;Arifuku, M.;Kiyoyanagi, N.; Kobayashi, Y. Biosensor response from target molecules with inhomogeneous charge localization. *J. Appl. Phys.* **2018**, *124*, 064502.

[78] Futaba, D. N.;Goto, J.;Yasuda, S.;Yamada, T.;Yumura, M.; Hata, K. General Rules Governing the Highly Efficient Growth of Carbon Nanotubes. *Advanced Materials* **2009**, *21*, 4811-4815.

[79] Nasibulin, A. G.;Brown, D. P.;Queipo, P.;Gonzalez, D.;Jiang, H.; Kauppinen, E. I. An essential role of CO2 and H2O during single-walled CNT synthesis from carbon monoxide. *Chemical Physics Letters* **2006**, *417*, 179-184.

[80] Wen, Q.;Qian, W.;Wei, F.;Liu, Y.;Ning, G.; Zhang, Q. CO2-Assisted SWNT Growth on Porous Catalysts. *Chemistry of Materials* **2007**, *19*, 1226-1230.

[81] Magrez, A.;Seo, J. W.;Kuznetsov, V. L.; Forró, L. Evidence of an equimolar C2H2–CO2 reaction in the synthesis of carbon nanotubes. *Angewandte Chemie* **2007**, *119*, 445-448.

[82] Huang, J.;Zhang, Q.;Zhao, M.; Wei, F. Process intensification by CO2 for high quality carbon nanotube forest growth: Double-walled carbon nanotube convexity or single-walled carbon nanotube bowls? *Nano Research* **2009**, *2*, 872.

[83] Qu, J.;Zhao, Z.;Wang, Z.;Wang, X.; Qiu, J. Carbon dioxide-assisted fabrication of self-organized tubular carbon micropatterns on silicon substrates. *Carbon* **2010**, *48*, 1465-1472.

[84] Magrez, A.;Seo, J. W.;Smajda, R.;Korbely, B.;Andresen, J. C.;Mionić, M.;Casimirius, S.; Forró, L. Low-Temperature, Highly Efficient Growth of Carbon Nanotubes on Functional Materials by an Oxidative Dehydrogenation Reaction. *ACS Nano* **2010**, *4*, 3702-3708.

[85] Sato, T.;Sugime, H.; Noda, S. CO2-assisted growth of millimeter-tall single-wall carbon nanotube arrays and its advantage against H2O for large-scale and uniform synthesis. *Carbon* **2018**, *136*, 143-149.

[86] Otsuka, K.;Ishimaru, R.;Kobayashi, A.;Inoue, T.;Xiang, R.;Chiashi, S.;Kato, Y. K.; Maruyama, S. Universal Map of Gas-Dependent Kinetic Selectivity in Carbon Nanotube Growth. *ACS Nano* **2022**, *16*, 5627-5635.

[87] Wen, Q.;Zhang, R.;Qian, W.;Wang, Y.;Tan, P.;Nie, J.; Wei, F. Growing 20 cm Long DWNTs/TWNTs at a Rapid Growth Rate of 80−90 μm/s. *Chemistry of Materials* **2010**, *22*, 1294-1296.

[88] Nongnual, T.; Limtrakul, J. Healing of a Vacancy Defect in a Single-Walled Carbon Nanotube by Carbon Monoxide Disproportionation. *The Journal of Physical Chemistry C* **2011**, *115*, 4649-4655.

[89] Xiao, B.;Zhao, J.-x.;Ding, Y.-h.; Sun, C.-c. Theoretical Investigation of the Interaction between Carbon Monoxide and Carbon Nanotubes with Single-Vacancy Defects. *ChemPhysChem* **2010**, *11*, 3505-3510.

[90] Xiao, B.;Yu, X.-f.; Ding, Y.-h. Theoretical investigation on the healing mechanism of divacancy defect in CNT growth by C2H2 and C2H4. *Journal of Molecular Modeling* **2014**, *20*, 2125.

[91] Zhou, R. L.;He, H. Y.; Pan, B. C. Enhancing the topological structures of defected carbon nanotubes with adsorbed hydrocarbon radicals at low temperatures. *Physical Review B* **2007**, *75*, 113401.

[92] 郡山翔二 ナノダイヤモンドを核としたカーボンナノチューブに関する研究. *大阪大学大学院平成 23 年度修士論文* **2012**.

[93] Belin, T.; Epron, F. Characterization methods of carbon nanotubes: a review. *Mater. Sci. Eng., B* **2005**, *119*, 105-118.

[94] Hills, G.;Lau, C.;Wright, A.;Fuller, S.;Bishop, M. D.;Srimani, T.;Kanhaiya, P.;Ho, R.;Amer, A.;Stein, Y.;Murphy, D.;Arvind;Chandrakasan, A.; Shulaker, M. M. Modern microprocessor built from complementary carbon nanotube transistors. *Nature* **2019**, *572*, 595-602.

[95] Kong, J.;Franklin, N. R.;Zhou, C.;Chapline, M. G.;Peng, S.;Cho, K.; Dai, H. Nanotube Molecular Wires as Chemical Sensors. *Science* **2000**, *287*, 622.

[96] He, X.;Htoon, H.;Doorn, S. K.;Pernice, W. H. P.;Pyatkov, F.;Krupke, R.;Jeantet, A.;Chassagneux, Y.; Voisin, C. Carbon nanotubes as emerging quantum-light sources. *Nature Materials* **2018**, *17*, 663-670.

[97] Saito, R.;Fujita, M.;Dresselhaus, G.; Dresselhaus, M. S. Electronic structure of chiral graphene tubules. *Applied Physics Letters* **1992**, *60*, 2204-2206.

[98] Nikolaev, P.;Bronikowski, M. J.;Bradley, R. K.;Rohmund, F.;Colbert, D. T.;Smith, K. A.; Smalley, R. E. Gas-phase catalytic growth of single-walled carbon nanotubes from carbon monoxide. *Chem. Phys. Lett.* **1999**, *313*, 91-97.

[99] Yang, F.;Wang, X.;Zhang, D.;Yang, J.;Luo, D.;Xu, Z.;Wei, J.;Wang, J.-Q.;Xu, Z.;Peng, F.;Li, X.;Li, R.;Li, Y.;Li, M.;Bai, X.;Ding, F.; Li, Y. Chirality-specific growth of single-walled carbon nanotubes on solid alloy catalysts. *Nature* **2014**, *510*, 522-524.

[100] He, M.;Wang, X.;Zhang, S.;Jiang, H.;Cavalca, F.;Cui, H.;Wagner, J. B.;Hansen, T. W.;Kauppinen, E.;Zhang, J.; Ding, F. Growth kinetics of single-walled carbon nanotubes with a (2*n*,*n*) chirality selection. *Sci. Adv.* **2019**, *5*, eaav9668.

[101] Charlier, J. C.;Ebbesen, T. W.; Lambin, P. Structural and electronic properties of pentagon-heptagon pair defects in carbon nanotubes. *Phys. Rev. B* **1996**, *53*, 11108-11113.

[102] Senga, R.;Pichler, T.;Yomogida, Y.;Tanaka, T.;Kataura, H.; Suenaga, K. Direct Proof of a Defect-Modulated Gap Transition in Semiconducting Nanotubes. *Nano Lett.* **2018**, *18*, 3920-3925.

[103] Choi, H. J.;Ihm, J.;Louie, S. G.; Cohen, M. L. Defects, quasibound states, and quantum conductance in metallic carbon nanotubes. *Phys. Rev. Lett.* **2000**, *84*, 2917.

[104] Suzuki, S.; Kobayashi, Y. Conductivity decrease in carbon nanotubes caused by low-acceleration-voltage electron irradiation. *Jpn. J. Appl. Phys.* **2005**, *44*, L1498.

[105] Yamamoto, T.; Watanabe, K. Nonequilibrium Green's Function Approach to Phonon Transport in Defective Carbon Nanotubes. *Phys. Rev. Lett.* **2006**, *96*, 255503.

[106] Sammalkorpi, M.;Krasheninnikov, A.;Kuronen, A.;Nordlund, K.; Kaski, K. Mechanical properties of carbon nanotubes with vacancies and related defects. *Phys. Rev. B* **2004**, *70*, 245416.

[107] Tibbetts, G. G. Vapor-grown carbon fibers: Status and prospects. *Carbon* **1989**, *27*, 745-747.

[108] Harutyunyan, A. R.;Pradhan, B. K.;Kim, U. J.;Chen, G.; Eklund, P. C. CVD Synthesis of Single Wall Carbon Nanotubes under "Soft" Conditions. *Nano Lett.* **2002**, *2*, 525-530.

[109] Altay, M. C.; Eroglu, S. Synthesis of multi-walled C nanotubes by Fe–Ni (70wt.%) catalyzed chemical vapor deposition from pre-heated CH4. *Materials Letters* **2012**, *67*, 124-127.

[110] Bethune, D. S.;Kiang, C. H.;de Vries, M. S.;Gorman, G.;Savoy, R.;Vazquez, J.; Beyers, R. Cobalt-catalysed growth of carbon nanotubes with single-atomic-layer walls. *Nature* **1993**, *363*, 605-607.

[111] Chiang, W.-H.; Mohan Sankaran, R. Linking catalyst composition to chirality distributions of as-grown single-walled carbon nanotubes by tuning NixFe1−x nanoparticles. *Nat. Mater.* **2009**, *8*, 882-886.

[112] Hersam, M. C. Progress towards monodisperse single-walled carbon nanotubes. *Nat. Nanotechnol.* **2008**, *3*, 387-394.

[113] Takagi, D.;Hibino, H.;Suzuki, S.;Kobayashi, Y.; Homma, Y. Carbon Nanotube Growth from Semiconductor Nanoparticles. *Nano Letters* **2007**, *7*, 2272-2275.

[114] Zhang, S.;Kang, L.;Wang, X.;Tong, L.;Yang, L.;Wang, Z.;Qi, K.;Deng, S.;Li, Q.;Bai, X.;Ding, F.; Zhang, J. Arrays of horizontal carbon nanotubes of controlled chirality grown using designed catalysts. *Nature* **2017**, *543*, 234-238.

[115] Liu, H.;Takagi, D.;Ohno, H.;Chiashi, S.;Chokan, T.; Homma, Y. Growth of Single-Walled Carbon Nanotubes from Ceramic Particles by Alcohol Chemical Vapor Deposition. *Applied Physics Express* **2008**, *1*, 014001.

[116] Qian, L.;Xie, Y.;Yu, Y.;Wang, S.;Zhang, S.; Zhang, J. Growth of Single‐Walled Carbon Nanotubes with Controlled Structure: Floating Carbide Solid Catalysts. *Angew. Chem. Int. Ed.* **2020**, *59*, 10884-10887.

[117] K. Nakamura et al., Synthesis of defect-free single-walled carbon nanotube from solid nanoparticles by high temperature process, submitted

[118] Efremov, V. P.;Zakatilova, E. I.;Maklashova, I. V.; Shevchenko, N. V. Thermal stability of detonation-produced micro and nanodiamonds. *Journal of Physics: Conference Series* **2018**, *946*, 012107.

[119] Vinten, P.;Marshall, P.;Lefebvre, J.; Finnie, P. Thermodynamic and Energetic Effects on the Diameter and Defect Density in Single-Walled Carbon Nanotube Synthesis. *J. Phys. Chem. C* **2013**, *117*, 3527-3536.

[120] Qi, H.;Yuan, D.; Liu, J. Two-Stage Growth of Single-Walled Carbon Nanotubes. *The Journal of Physical Chemistry C* **2007**, *111*, 6158-6160.

[121] Yamada, T.;Maigne, A.;Yudasaka, M.;Mizuno, K.;Futaba, D. N.;Yumura, M.;Iijima, S.; Hata, K. Revealing the Secret of Water-Assisted Carbon Nanotube Synthesis by Microscopic Observation of the Interaction of Water on the Catalysts. *Nano Lett.* **2008**, *8*, 4288-4292.

[122] Smajda, R.;Andresen, J. C.;Duchamp, M.;Meunier, R.;Casimirius, S.;Hernádi, K.;Forró, L.; Magrez, A. Synthesis and mechanical properties of carbon nanotubes produced by the water assisted CVD process. *Phys. Status Solidi B* **2009**, *246*, 2457-2460.

[123] Wyss, R. M.;Klare, J. E.;Park, H. G.;Noy, A.;Bakajin, O.; Lulevich, V. Water-Assisted Growth of Uniform 100 mm Diameter SWCNT Arrays. *ACS Appl. Mater. Interfaces* **2014**, *6*, 21019-21025.

[124] Hasegawa, K.; Noda, S. Millimeter-Tall Single-Walled Carbon Nanotubes Rapidly Grown with and without Water. *ACS Nano* **2011**, *5*, 975-984.

[125] Shenderova, O. A.; Gruen, D. M. *Ultrananocrystalline diamond: synthesis, properties and applications*; William Andrew, 2012.

[126] Gruen, D. M.;Shenderova, O. A.; Vul, A. Y. *Synthesis, Properties and Applications of Ultrananocrystalline Diamond: Proceedings of the NATO ARW on Synthesis, Properties and Applications of Ultrananocrystalline Diamond, St. Petersburg, Russia, from 7 to 10 June 2004*; Springer Science & Business Media, 2006.

[127] Kuznetsov, V. L.;Chuvilin, A. L.;Butenko, Y. V.;Mal'kov, I. Y.; Titov, V. M. Onion-like carbon from ultra-disperse diamond. *Chem. Phys. Lett.* **1994**, *222*, 343-348.

[128] Kovalenko, I.;Bucknall, D. G.; Yushin, G. Detonation Nanodiamond and Onion-Like-Carbon-Embedded Polyaniline for Supercapacitors. *Adv. Funct. Mater.* **2010**, *20*, 3979-3986.

[129] 中村圭介 固体成長核からの無欠陥核スピン制御されたカーボンナノチューブの合成. *In 大阪大学大学院平成 30 年度修士論文* **2018**.

[130] Homma, Y.;Suzuki, S.;Kobayashi, Y.;Nagase, M.; Takagi, D. Mechanism of bright selective imaging of single-walled carbon nanotubes on insulators by scanning electron microscopy. *Applied Physics Letters* **2004**, *84*, 1750-1752.

[131] Milani, A.;Tommasini, M.;Russo, V.;Bassi, A. L.;Lucotti, A.;Cataldo, F.; Casari, C. S. Raman spectroscopy as a tool to investigate the structure and electronic properties of carbon-atom wires. *Beilstein J. Nanotechnol.* **2015**, *6*, 480-491.

[132] Ajayan, P. M.;Ebbesen, T. W.;Ichihashi, T.;Iijima, S.;Tanigaki, K.; Hiura, H. Opening carbon nanotubes with oxygen and implications for filling. *Nature* **1993**, *362*, 522-525.

[133] Kimura, H.;Futaba, D. N.;Yumura, M.; Hata, K. Mutual Exclusivity in the Synthesis of High Crystallinity and High Yield Single-Walled Carbon Nanotubes. *Journal of the American Chemical Society* **2012**, *134*, 9219-9224.

[134] Homma, Y.;Kobayashi, Y.;Ogino, T.;Takagi, D.;Ito, R.;Jung, Y. J.; Ajayan, P. M. Role of Transition Metal Catalysts in Single-Walled Carbon Nanotube Growth in Chemical Vapor Deposition. *The Journal of Physical Chemistry B* **2003**, *107*, 12161-12164.

[135] Zhang, X.;Graves, B.;Volder, M. D.;Yang, W.;Johnson, T.;Wen, B.;Su, W.;Nishida, R.;Xie, S.; Boies, A. High-precision solid catalysts for investigation of carbon nanotube synthesis and structure. *Science Advances* **2020**, *6*, eabb6010.

[136] Qian, L.;Xie, Y.;Yu, Y.;Wang, S.;Zhang, S.; Zhang, J. Growth of Single-Walled Carbon Nanotubes with Controlled Structure: Floating Carbide Solid Catalysts. *Angewandte Chemie International Edition* **2020**, *59*, 10884-10887.

[137] Reilly, P. T. A.; Whitten, W. B. The role of free radical condensates in the production of carbon nanotubes during the hydrocarbon CVD process. *Carbon* **2006**, *44*, 1653-1660.

[138] Xie, K.;Muhler, M.; Xia, W. Influence of Water on the Initial Growth Rate of Carbon Nanotubes from Ethylene over a Cobalt-Based Catalyst. *Industrial & Engineering Chemistry Research* **2013**, *52*, 14081-14088.

[139] Shi, W.;Peng, Y.;Steiner III, S. A.;Li, J.; Plata, D. L. Carbon Dioxide Promotes Dehydrogenation in the Equimolar C2H2-CO2 Reaction to Synthesize Carbon Nanotubes. *Small* **2018**, *14*, 1703482.

[140] Li, Z.;Xu, Y.;Ma, X.;Dervishi, E.;Saini, V.;Biris, A. R.;Lupu, D.; Biris, A. S. CO2 enhanced carbon nanotube synthesis from pyrolysis of hydrocarbons. *Chemical Communications* **2008**, 10.1039/B803465F, 3260-3262.

[141] Wang, M.;Nakamura, K.;Arifuku, M.;Kiyoyanagi, N.;Inoue, T.; Kobayashi, Y. Growth of Single-Walled Carbon Nanotubes from Solid Carbon Nanoparticle Seeds via Cap Formation Engineering with a Two-Step Growth Process and Water Vapor Supply. *ACS Omega* **2022**, *7*, 3639-3648.

[142] Ding, L. P.;McLean, B.;Xu, Z.;Kong, X.;Hedman, D.;Qiu, L.;Page, A. J.; Ding, F. Why Carbon Nanotubes Grow. *Journal of the American Chemical Society* **2022**, *144*, 5606-5613.

[143] Norinaga, K.;Janardhanan, V. M.; Deutschmann, O. Detailed chemical kinetic modeling of pyrolysis of ethylene, acetylene, and propylene at 1073–1373 K with a plug-flow reactor model. *International Journal of Chemical Kinetics* **2008**, *40*, 199-208.

[144] Norinaga, K.; Deutschmann, O. Detailed Kinetic Modeling of Gas-Phase Reactions in the Chemical Vapor Deposition of Carbon from Light Hydrocarbons. *Industrial & Engineering Chemistry Research* **2007**, *46*, 3547-3557.

[145] Franklin, A. D.;Luisier, M.;Han, S.-J.;Tulevski, G.;Breslin, C. M.;Gignac, L.;Lundstrom, M. S.; Haensch, W. Sub-10 nm Carbon Nanotube Transistor. *Nano Letters* **2012**, *12*, 758-762.

[146] Seidel, R.;Graham, A. P.;Unger, E.;Duesberg, G. S.;Liebau, M.;Steinhoegl, W.;Kreupl, F.;Hoenlein, W.; Pompe, W. High-Current Nanotube Transistors. *Nano Letters* **2004**, *4*, 831-834.

[147] Yamada, T.;Hayamizu, Y.;Yamamoto, Y.;Yomogida, Y.;Izadi-Najafabadi, A.;Futaba, D. N.; Hata, K. A stretchable carbon nanotube strain sensor for human-motion detection. *Nature Nanotechnology* **2011**, *6*, 296-301.

[148] Tsetseris, L.; Pantelides, S. T. Adatom complexes and self-healing mechanisms on graphene and single-wall carbon nanotubes. *Carbon* **2009**, *47*, 901-908.

[149] Huang, J. Y.;Ding, F.; Yakobson, B. I. Vacancy-hole and vacancy-tube migration in multiwall carbon nanotubes. *Physical Review B* **2008**, *78*, 155436.

[150] Ertekin, E.;Chrzan, D. C.; Daw, M. S. Topological description of the Stone-Wales defect formation energy in carbon nanotubes and graphene. *Physical Review B* **2009**, *79*, 155421.

[151] Zhou, L. G.; Shi, S.-Q. Formation energy of Stone–Wales defects in carbon nanotubes. *Applied Physics Letters* **2003**, *83*, 1222-1224.

[152] Xia, Y.;Ma, Y.;Xing, Y.;Mu, Y.;Tan, C.; Mei, L. Growth and defect formation of single-wall carbon nanotubes. *Physical Review B* **2000**, *61*, 11088-11092.

[153] Burgos, J. C.;Jones, E.; Balbuena, P. B. Dynamics of Topological Defects in Single-Walled Carbon Nanotubes during Catalytic Growth. *The Journal of Physical Chemistry C* **2014**, *118*, 4808-4817.

[154] Qian, W.;Liu, T.;Wei, F.;Wang, Z.;Luo, G.;Yu, H.; Li, Z. The evaluation of the gross defects of carbon nanotubes in a continuous CVD process. *Carbon* **2003**, *41*, 2613-2617.

[155] Krasheninnikov, A. V.; Banhart, F. Engineering of nanostructured carbon materials with electron or ion beams. *Nature Materials* **2007**, *6*, 723-733.

[156] Suenaga, K.;Wakabayashi, H.;Koshino, M.;Sato, Y.;Urita, K.; Iijima, S. Imaging active topological defects in carbon nanotubes. *Nature Nanotechnology* **2007**, *2*, 358-360.

[157] Lee, C. J.;Park, J.;Huh, Y.; Yong Lee, J. Temperature effect on the growth of carbon nanotubes using thermal chemical vapor deposition. *Chemical Physics Letters* **2001**, *343*, 33-38.

[158] Zhang, R.;Zhang, Y.; Wei, F. Controlled Synthesis of Ultralong Carbon Nanotubes with Perfect Structures and Extraordinary Properties. *Accounts of Chemical Research* **2017**, *50*, 179-189.

[159] Suzuki, S.; Kobayashi, Y. Healing of Low-Energy Irradiation-Induced Defects in Single-Walled Carbon Nanotubes at Room Temperature. *The Journal of Physical Chemistry C* **2007**, *111*, 4524-4528.

[160] Suzuki, S.;Yamaya, K.;Homma, Y.; Kobayashi, Y. Activation energy of healing of low-energy irradiation-induced defects in single-wall carbon nanotubes. *Carbon* **2010**, *48*, 3211-3217.

[161] Okada, S. Energetics and electronic structures of carbon nanotubes with adatom–vacancy defects. *Chemical Physics Letters* **2007**, *447*, 263-267.

[162] Mattia, D.;Rossi, M. P.;Kim, B. M.;Korneva, G.;Bau, H. H.; Gogotsi, Y. Effect of Graphitization on the Wettability and Electrical Conductivity of CVD-Carbon Nanotubes and Films. *The Journal of Physical Chemistry B* **2006**, *110*, 9850-9855.

[163] Jin, R.;Zhou, Z. X.;Mandrus, D.;Ivanov, I. N.;Eres, G.;Howe, J. Y.;Puretzky, A. A.; Geohegan, D. B. The effect of annealing on the electrical and thermal transport properties of macroscopic bundles of long multi-wall carbon nanotubes. *Phys. B* **2007**, *388*, 326-330.

[164] Zhao, J.;Zhang, Y.;Su, Y.;Huang, X.;Wei, L.;Kong, E. S.-W.; Zhang, Y. Structural improvement of CVD multi-walled carbon nanotubes by a rapid annealing process. *Diamond and Related Materials* **2012**, *25*, 24-28.

[165] Yudasaka, M.;Kataura, H.;Ichihashi, T.;Qin, L. C.;Kar, S.; Iijima, S. Diameter Enlargement of HiPco Single-Wall Carbon Nanotubes by Heat Treatment. *Nano Letters* **2001**, *1*, 487-489.

[166] Yudasaka, M.;Ichihashi, T.;Kasuya, D.;Kataura, H.; Iijima, S. Structure changes of single-wall carbon nanotubes and single-wall carbon nanohorns caused by heat treatment. *Carbon* **2003**, *41*, 1273-1280.

[167] De Silva, K. K. H.;Huang, H.-H.;Suzuki, S.;Badam, R.; Yoshimura, M. Ethanol-assisted restoration of graphitic structure with simultaneous thermal reduction of graphene oxide. *Japanese Journal of Applied Physics* **2018**, *57*, 08NB03.

[168] Su, C.-Y.;Xu, Y.;Zhang, W.;Zhao, J.;Liu, A.;Tang, X.;Tsai, C.-H.;Huang, Y.; Li, L.-J. Highly Efficient Restoration of Graphitic Structure in Graphene Oxide Using Alcohol Vapors. *ACS Nano* **2010**, *4*, 5285-5292.

[169] Matsumoto, N.;Oshima, A.;Chen, G.;Yudasaka, M.;Yumura, M.;Hata, K.; Futaba, D. N. Elucidating the effect of heating induced structural change on electrical and thermal property improvement of single wall carbon nanotube. *Carbon* **2015**, *87*, 239-245.

[170] Nemes-Incze, P.;Magda, G.;Kamarás, K.; Biró, L. P. Crystallographically selective nanopatterning of graphene on SiO2. *Nano Res.* **2010**, *3*, 110-116.

[171] Cançado, L. G.;Jorio, A.;Ferreira, E. H. M.;Stavale, F.;Achete, C. A.;Capaz, R. B.;Moutinho, M. V. O.;Lombardo, A.;Kulmala, T. S.; Ferrari, A. C. Quantifying Defects in Graphene via Raman Spectroscopy at Different Excitation Energies. *Nano Letters* **2011**, *11*, 3190-3196.

[172] Yang, Y.;Ramirez, C.;Wang, X.;Guo, Z.;Tokranov, A.;Zhao, R.;Szlufarska, I.;Lou, J.; Sheldon, B. W. Impact of carbon nanotube defects on fracture mechanisms in ceramic nanocomposites. *Carbon* **2017**, *115*, 402-408.

[173] Ding, F. Theoretical study of the stability of defects in single-walled carbon nanotubes as a function of their distance from the nanotube end. *Phys. Rev. B* **2005**, *72*, 245409.

[174] Lu, A. J.; Pan, B. C. Nature of Single Vacancy in Achiral Carbon Nanotubes. *Physical Review Letters* **2004**, *92*, 105504.

[175] Tsetseris, L.; Pantelides, S. T. Adsorbate-Induced Defect Formation and Annihilation on Graphene and Single-Walled Carbon Nanotubes. *The Journal of Physical Chemistry B* **2009**, *113*, 941-944.

[176] Lee, G.-D.;Wang, C. Z.;Yoon, E.;Hwang, N.-M.;Kim, D.-Y.; Ho, K. M. Diffusion, Coalescence, and Reconstruction of Vacancy Defects in Graphene Layers. *Physical Review Letters* **2005**, *95*, 205501.

List of Publications

1. M. Wang, K. Nakamura, M. Arifuku, N. Kiyoyanagi, T. Inoue, Y. Kobayashi, Growth of Single-Walled Carbon Nanotubes from Solid Carbon Nanoparticle Seeds via Cap Formation Engineering with a Two-Step Growth Process and Water Vapor Supply. ACS Omega, 7 (2022) 3639-3648.
2. M. Wang, Y. Liu, M. Maekawa, M. Arifuku, N. Kiyoyanagi, T. Inoue, Y. Kobayashi, Combination effect of growth enhancers and carbon sources on synthesis of single-walled carbon nanotubes from solid carbon growth seeds. Diamond and Related Materials **2022**, *130*, 109516.
3. M. Wang, M. Maekawa, M. Shen, Y. Liu, M. Arifuku, N. Kiyoyanagi, T. Inoue, Y. Kobayashi, Thermal defect healing of single-walled carbon nanotubes assisted by supplying carbon-containing reactants. Appl. Phys. Express **2023**, *16*, 015002.

List of Conferences

International conferences:

1. M. Wang, Y. Liu, M. Maekawa, M. Arifuku, N. Kiyoyanagi, M. Satake, T. Inoue, Y. Kobayashi, "Effect of CO_2 in high temperature SWCNT growth from solid carbon growth seeds", The 22nd Int. Conf. on the Science and Applications of Nanotubes and Low-Dimensional Materials (NT-22), June 19-24, 2022, online. (Poster)
2. M. Wang, K. Nakamura, H. Semba, M. Arifuku, N. Kiyoyanagi, Y. Kobayashi, "Efficient synthesis of defect-free single-walled carbon nanotube from solid nanoparticles by chemical vapor deposition at high-temperature", The 22nd Int. Conf. on the Science and Applications of Nanotubes and Low-Dimensional Materials (NT19), July, 21-26, 2019. (Poster)

Domestic conferences:

1. M. Wang, M. Arifuku, N. Kiyoyanagi, M. Satake, T. Inoue, Y. Kobayashi, "Influence of carbon source pyrolysis on high-temperature CNT growth from

solid carbon growth seeds", 2021年第61回フラーレン・ナノチューブ･グラフェン総合シンポジウム,1P-14, September 1, 2021, online. (Poster)

2. M. Wang, M. Arifuku, N. Kiyoyanagi, M. Satake, T. Inoue, Y. Kobayashi, "Influence of carbon source decomposition process to CNT growth from carbon solid seeds at high temperature", 2021年第68回応用物理学会春季学術講演会, 19p-P02-4, March 16-19, 2021, online. (Poster)
3. M. Wang, K. Nakamura, M. Arifuku, N. Kiyoyanagi, M. Ikeda, Y. Kobayashi, "Etching effect of carbon dioxide on carbon nanotube growth at high temperature", 2020年第81回応用物理学会秋季学術講演会, 8p-Z29-1, September 8-11, 2020, online. (Oral)
4. M. Wang, K. Nakamura, M. Arifuku, N. Kiyoyanagi, Y. Kobayashi, "High temperature growth of highly crystalline carbon nanotube from carbon nano-onion seed using ethylene as carbon feedstock", 2020年第67回応用物理学会春季講演会, 13a-A404-9, March 12-15, 2020, online. (Poster)
5. M. Wang, K. Nakamura, M. Arifuku, N. Kiyoyanagi, Y. Kobayashi, "Efficient synthesis of low-defect carbon nanotube from carbon nano-onion at high temperature through balancing gas phase conditions in two-stage growth", 2019年第80回応用物理学会秋季学術講演会, 21a-PB1-1, September 18-21, 2019. (Poster)

Co-author:

1. M. Maekawa, M. Wang, T. Inoue, Y. Kobayashi, "High-temperature stability of carbon nanotubes on SiO_2 substrate", 第63回フラーレン・ナノチューブ･グラフェン総合シンポジウム, August 31-September 2, 2022. (Poster)
2. 前川愛佳、王梦玥(Wang Mengyue)、周詠凱、井ノ上泰輝、根岸良太、小林慶裕:"バイオセンサ応用に向けたカーボンナノチューブ電界効果トランジスタの動作安定性におけるグラフェン被覆効果", P-31、応用物理学

会関西支部2021年度第2回講演会、2021年10月5日.（オンライン Poster）

3. 中村圭介、仙波弘樹、王梦玥(Wang Mengyue)、有福達治、清柳典子、小林慶裕:“二段階温度成長法によるカーボンナノオニオンからの 極低欠陥カーボンナノチューブ成長量増大効果”,11p-W621-7、２０１９年第66回応用物理学会春季学術講演会、2019年3月9日-12日. (Oral)

Acknowledgement

During these years of study, I have received a lot of care and help from my teachers, lab mates and friends. As my dissertation is about to be completed, I would like to express my most sincere thanks to all the people who have supported, helped and encouraged me during this period.

First and foremost, I would like to thank my supervisor, Professor Kobayashi Yoshihiro. During my doctor study, he provided me many precious opportunities and constant support. From the selection of the topic, the conception, the completion of the experiment, the writing of the thesis to the final draft, Professor Kobayashi gave me rigorous and careful guidance to help me complete my thesis successfully.

I also wish to express a similar gratitude to Assistant Professor Inoue Taiki, who leads by example to encourage me a lot in my daily studies and provided me many precious advices on the experimental design. Besides, I wish to thank him for his extreme patience and responsibility in helping me with my research articles.

I also want to thank Professor Negishi Ryota, who taught me volumes of knowledge and techniques when I began my study as a doctoral course student.

At the same time, I would like to thank my thesis reviewer and my defense teacher for their valuable comments on my thesis revision, which improved it.

I would like to express my gratitude to Noriko Kiyoyanagi and Michiharu Arifuku (from the Research and Development Division of Nippon Kayaku Company) for providing us high purity nanodiamonds, which are necessary for the research.

My special thanks also go to Professor Chen Qiang, who supervised me when I was a master student in Xi'an Jiaotong University. I appreciate that I have had a chance to study in his laboratory.

I would like to thank all the members in the Kobayashi laboratory. I wish to express my thanks to Xu Zizhao and Ishiguro (Sasaki) Chikako. As my tutors, they help me a lot in handling various procedures when I came to Osaka University, and help me adapt to the life in Japan. I also would like to give my thanks to Nakamura Keisuke, who

made efforts to teach me basic knowledge about CNT synthesis and several experimental operations, including, most importantly, the operation of CVD equipment. Moreover, I would give my thanks to Yura Shingo, Liu Yuanjia, Maekawa Manaka, Chou Yungkai, Shen Man, and Li Shaoxian, for their kind help in the research works. I also greatly appreciate our Women's club (Chikako-san, Manaka-san, Yuna-san, and Yao-san). It brings me so many happy memories. I would like to thank my landlady, Tsuzuki-san, who has provided me with so much warm help in my daily life.

Last, I am deeply indebted to my beloved parents, who always supported me and offered me help. I feel so happy being their daughter.